

34

Two Topics in Non-Perturbative Lattice Field Theories: The U(1) Quantum Link Model and Perfect Actions for Scalar Theories

by

Antonios S. Tsapalis

B.S. in Physics, National and Kapodistrian University of Athens, Greece (1993)

Submitted to the Department of Physics
in partial fulfillment of the requirements for the degree of

Doctor of Philosophy

at the

MASSACHUSETTS INSTITUTE OF TECHNOLOGY

September 1998

© Massachusetts Institute of Technology 1998. All rights reserved.

1

Author

Department of Physics

August 7, 1998

Certified by

Uwe-Jens Wiese

Assistant Professor of Physics

Thesis Supervisor

Accepted by

Thomas J. Greytak

Associate Department Head for Education

MASSACHUSETTS INSTITUTE
OF TECHNOLOGY

OCT 09 1998

LIBRARIES

Science

Two Topics in Non-Perturbative Lattice Field Theories: The $U(1)$ Quantum Link Model and Perfect Actions for Scalar Theories

by

Antonios S. Tsapalis

Submitted to the Department of Physics
on August 7, 1998, in partial fulfillment of the
requirements for the degree of
Doctor of Philosophy

Abstract

This thesis deals with two topics in lattice field theories. In the first part we discuss aspects of renormalization group flow and non-perturbative improvement of actions for scalar theories regularized on a lattice. We construct a perfect action, an action which is free of lattice artifacts, for a given theory. It is shown how a good approximation to the perfect action — referred to as classically perfect — can be constructed based on a well-defined blocking scheme for the $O(3)$ non-linear σ -model. We study the $O(N)$ non-linear σ -model in the large- N limit and derive analytically its perfect action. This action is applied to the $O(3)$ model on a square lattice. The Wolff cluster algorithm is used to simulate numerically the system. We perform scaling tests and discuss the scaling properties of the large- N inspired perfect action as opposed to the standard and the classically perfect action.

In the second part we present a new formulation for a quantum field theory with Abelian gauge symmetry. A Hamiltonian is constructed on a four-dimensional Euclidean space-time lattice which is invariant under local transformations. The model is formulated as a 5-dimensional path integral of discrete variables. We argue that dimensional reduction will allow us to study the behavior of the standard compact $U(1)$ gauge theory in 4-d. Based on the idea of the loop-cluster algorithm for quantum spins, we present the construction of a flux-cluster algorithm for the $U(1)$ quantum link model for the spin-1/2 quantization of the electric flux. It is shown how improved estimators for Wilson loop expectation values can be defined. This is important because the Wilson loops are traditionally used to identify confining and Coulomb phases in gauge theories. Our study indicates that the spin-1/2 $U(1)$ quantum link model is strongly coupled for all bare coupling values we examined.

Thesis Supervisor: Uwe-Jens Wiese
Title: Assistant Professor of Physics

Acknowledgments

I wish to express my gratitude to Uwe-Jens Wiese for supervising my thesis research and giving me the opportunity to work on some of the most interesting ideas in lattice field theory. It has been an extremely enjoyable collaboration in the process of which I have been taught a great deal of physics. Uwe has the combined gift of a great teacher and a genuine field theorist who is able to convey to the uninitiated the deepest ideas in physics with the outmost clarity, enthusiasm and patience. His friendly, caring and understanding behavior has been very helpful through the sometimes frustrating stages of graduate studies.

I wish to thank Profs. John Negele and Ed Bertschinger for reading my thesis and providing valuable comments and criticism. I wish to thank John Negele also for providing me with constant financial support during my five-year stay at the CTP.

I thank also all the people that I had the opportunity to collaborate with during various stages of my work. Especially I thank Bernard Beard, Wolfgang Bietenholz, Rich Brower, Schailesh Chandrasekharan, Victor Chudnovsky, Juergen Cox, Kieran Holland and Ben Scarlet for all the discussions from which I have benefited a lot.

I wish to thank also the following gentlemen: Pavlos Glicofridis, Leonidas Pantelidis, Jiannis Pachos, Nikos Prezas, Apostolos Rizos and Yiorgos Zonios for their invaluable friendship.

Finally, I wish to thank my family, Theodora and Sotirios Tsapalis and Dimitra and Panayiotis Panagopoulos for their infinite love and support.

*Αφιερώνεται στους γονείς μου,
Θεοδώρα και Σωτήριο Τσάπαλη.*

Contents

1	Introduction and Outline	8
1.1	Introduction	8
1.2	Outline	10
2	The Two-Dimensional Non-Linear σ-Model	14
2.1	The Model in the Continuum	14
2.2	The Lattice Regularization	18
2.3	Mass-gap at Large N	21
3	The Classically Perfect Action for $O(3)$ Spins	25
3.1	Seeking Improvement	25
3.2	The Classically Perfect Action	29
3.3	A Scaling Test	33
4	The Large N Quantum Perfect Action for $O(N)$ Spins	38
4.1	Quantum Perfect Action for a Free Massive Scalar	39
4.2	The Large N Quantum Perfect Action	43
4.3	Scaling in the $O(3)$ Non-Linear σ -Model	45
4.4	Final Comments	46
5	The Cluster Algorithm for Classical $O(N)$ Spins	49
5.1	The Monte Carlo Method	49
5.2	The Metropolis Algorithm	51
5.3	The Cluster Algorithm for Classical Spins	55

6	Classical $O(3)$ Spins and Quantum Antiferromagnets	60
6.1	Introduction	60
6.2	The 2-d Heisenberg Antiferromagnet	61
7	Non-Abelian Gauge Theories on a Lattice: Classical and Quantum	
	Links	67
7.1	Introduction	67
7.2	Wilson Formulation of Non-Abelian Gauge Theories	71
7.3	Phases and Order Parameters for Gauge Theories	75
7.4	Quantum Link Formulation of Non-Abelian Gauge Theory	81
7.5	Dimensional reduction and the Gauss Law	86
7.6	Rishon formulation of Quantum Link Models	89
8	Classical and Quantum Spins with Global $U(1)$ Symmetry	93
8.1	The 2-d Classical XY Model	93
8.2	The 2-d Quantum XY Model	96
8.3	Dimensional Reduction to the Classical XY Model	98
9	Abelian Gauge Theory in the Wilson and Quantum Link Formulation	100
9.1	The Wilson Formulation	100
9.2	Phases of the Wilson Theory	104
9.3	The $U(1)$ Quantum Link Model	106
9.4	Dimensional Reduction	109
10	Strong Coupling Expansions in $U(1)$ Gauge Theory	112
10.1	Confinement at Strong Coupling	112
10.2	Some Comments	117
10.3	A Constraint on the Critical Coupling	119
11	The Cluster Algorithm for Quantum Spins	121
11.1	Introduction	121

11.2	The Suzuki-Trotter decomposition	122
11.3	Clustering the XY model	125
11.4	Basis-Independence of the Clusters	129
11.5	Measurement of Green's Functions	130
12	The Flux-Cluster Algorithm	135
12.1	Introduction	135
12.2	Suzuki-Trotter decomposition	135
12.3	The Discrete Time Algorithm	138
12.4	Measuring Wilson Loops	144
12.5	The Continuous Time Algorithm	146
13	The Winding Number	151
13.1	Winding number in the XY model	151
13.2	Winding number in the $U(1)$ gauge theory	155
14	Simulations of the $U(1)$ Quantum Link Model	161
14.1	Local Observables	161
14.2	Higgsing the $U(1)$ Theory	166
14.3	Final Comments	168
A	An Ultralocal Perfect Action in One Dimension	172

Chapter 1

Introduction and Outline

1.1 Introduction

Gauge symmetry is at the heart of our attempt to understand the fundamental interactions we observe in Nature. The axioms of quantum field theory provide us with the framework for a consistent description of the various particles that we observe and constitute what we traditionally call matter and light. A few sacred principles form the core of this framework: First, the axioms of special relativity which dictate that we live in a four dimensional space-time continuum structured such that there is a maximal velocity — the speed of light — and covariance of the physical laws within it. The Lorentzian structure of space-time and the Poincaré group of transformations within it assign discrete spin and continuous mass labels to particle states.

Second, the principles of quantum mechanics which deprive us from knowing exactly the whereabouts of the particles in the sense that classical mechanics allowed us to. In fact they raise an uncertainty curtain when one tries to pinpoint the energy and momentum of a particle in arbitrarily small space-time intervals, an uncertainty controlled by Planck's constant. Further, they congeal particles and waves into a quantum field, an object which displays, when properly probed, either matter or wave behavior. Particles of the same identity become truly indistinguishable, something with profound consequences if one remembers that it is the Pauli exclusion principle that allows an atom to be built.

Third, locality of the interactions between the various quantum fields that we have identified is an imperative principle. Surprisingly enough, these local interaction rules, besides respecting the relativistic invariance, are restricted in such a way that arbitrary transformations of the quantum fields at different space-time points leave the physical laws unaltered. This symmetry, the gauge symmetry, is the principle which dictates the interactions.

The final ingredient in our approach is the renormalizability of the interaction terms. In that sense, we have seen that the interaction of these quantum fields in arbitrarily short distances — and correspondingly when they carry large momentum — is structurally similar to the interaction at large distances. All that happens is that the strength of the couplings between the fermions and the gauge bosons — the spin-1 particles that carry the force — becomes dependent on the momentum scale of the interaction.

The above principles led to the Standard Model for fundamental interactions which has so far passed all experimental tests. It incorporates three types of gauge symmetry; a $U(1)$ group which acts on the weak hypercharge assigned to the fermions and is mediated by a gauge boson, an $SU(2)$ group which acts on the left handed weak isospin doublets of the fermions and is mediated by a triplet of gauge bosons, and an $SU(3)$ group which acts on the color charge of the quarks and is mediated by eight gauge bosons, the gluons. The $SU(2) \times U(1)$ symmetry is spontaneously broken at low energy and experiments indicate that this happens at an energy scale of 250 GeV, resulting in an extremely short-ranged weak interaction between the leptons and the quarks. The Abelian symmetry that appears at low energy is no other than the one of electromagnetism; the exchange of photons between electrically charged particles. It appears as a weak force which according to the renormalization analysis becomes stronger as the charges come closer and closer. Exactly the opposite behavior appears in QCD —the quark and gluon sector of the Standard Model. There, the self-interaction of gluons, which is due to the non-Abelian character of the gauge symmetry, antiscreens the color charge as the distance becomes smaller and the interaction weakens. As a result, experiments done with high energy beams of

colliding particles are well understood within the framework of perturbative quantum field theory of quarks and gluons. On the other hand, at low energies quarks and gluons do not appear as free particles in Nature. Their interaction becomes stronger as the energy is lowered and all we see in Nature is the nucleons and the short-lived mesons.

An understanding of this effect, the confinement of the color charge in hadrons has not been achieved despite the 25-year efforts on the subject. The leading proposal for a non-perturbative understanding of QCD was developed by K. Wilson as early as 1974. The space-time continuum is replaced by a four-dimensional hypercubic lattice which is regulating the infinities that plague continuum field theory. As will be shown in Chapter 7, quark and gluon fields are defined naturally on the sites and the links of the lattice. The problem becomes one of statistical mechanics. One has to generate configurations with the weight $\exp(-\frac{1}{g^2}S)$ where S is the Euclidean action of the configuration and measure the correlation functions of interest. Unfortunately, it turns out that the amount of computing power that is needed in order to manipulate large lattices and extract physical results is immense. While patient extraction of results and anticipation of superior computers guarantee progress in lattice QCD, the search for different approaches, less dependent on computer technology is definitely well justified.

1.2 Outline

This thesis presents two approaches for a non-perturbative treatment of lattice field theories. In part I we investigate the perfect action approach for scalar 2-d theories. This is well motivated, given that the naive actions used in numerical simulations have strong finite lattice spacing effects and the extraction of physical values is difficult. This is especially true for QCD and, in fact, the quest for actions with improved behavior has become a major frontline of research in the last years. In chapter 2 we introduce the 2-d $O(N)$ non-linear σ -model and demonstrate some of the properties that make it an interesting model to study.

In chapter 3 we present the lattice regularization scheme and discuss how the notion of a perfect action arises based on a renormalization group flow study. We then present the construction of the classically perfect action for the $O(3)$ spins by Hasenfratz and Niedermayer and its amazing scaling properties.

In chapter 4 the quantum perfect action for $O(N)$ spins in the large- N limit is constructed. We demonstrate how this action can be applied to the $O(3)$ model. Finally, we present our comparative study of the scaling properties of the naive, the classically perfect and the large- N perfect action.

In chapter 5 we introduce the Monte Carlo method in the study of field theory. We present the Wolff cluster algorithm for the $O(N)$ spins, an algorithm that has revolutionized the traditional Monte Carlo approach.

In part II we present a new class of Hamiltonian models with gauge symmetry. This approach is motivated by the relation between classical and quantum spin physics. In chapter 6 we present the physics of the 2-d quantum Heisenberg antiferromagnet (AF) and its relation with the 2-d classical $O(3)$ spin model. The dimensional reduction of a system with large correlation length is the key to this correspondence. This correspondence will be our paradigm for *D-theory*, the general framework using *discrete* variables and *dimensional* reduction to represent theories with continuous symmetry.

In chapter 7 we start with a presentation of the Wilson formulation for gauge theories, the leading proposal for a non-perturbative understanding of QCD. We proceed to construct the non-Abelian quantum link models, and demonstrate how a continuous gauge symmetry can be represented exactly even if one works with discrete variables, by properly using the existence of a Coulomb phase in 5-d non-Abelian models. This formulation may turn out to be especially useful since theories with discrete variables can be approached numerically with the powerful cluster algorithms. Such algorithms have already been constructed for the quantum spin models and proved very efficient tools for their study. We actually present a study of the Abelian gauge theory with a cluster algorithm and it is likely that cluster algorithms can be constructed for the non-Abelian theories also.

We start chapter 8 with a discussion of the XY model — a spin model with global Abelian symmetry — in two dimensions. We then proceed to the 2-d quantum XY model and show how their connections can be understood within D-theory.

Chapter 9 repeats the study for the Abelian gauge theory in 4-d. The compact $U(1)$ gauge theory as constructed by Wilson, can be promoted to a 4-d Hamiltonian model with the $U(1)$ symmetry represented exactly. We discuss features of the classical theory which based on D-Theory we would anticipate for the Abelian quantum link model also.

Chapter 10 deals with the strong coupling limit of $U(1)$ gauge theory. We show that confinement occurs in the strong coupling limit of the quantum link models in complete similarity to the Wilson theory.

In chapter 11 we show how the partition function of a quantum spin model can be sampled efficiently with a cluster algorithm. We examine the XY model as a concrete example. We further show that improved estimators for non-diagonal correlation functions can be defined for the loop-cluster algorithm.

In chapter 12 it is shown how a flux-cluster algorithm can be naturally introduced to sample the Abelian quantum link model. We further show how improved estimators for Wilson loops can be defined for the flux-cluster algorithm. Due to the discrete character of the variables, the evolution can be simulated in continuous time. We discuss how a continuous time algorithm can be constructed making the sampling more efficient from a practical point a view.

In chapter 13 we demonstrate the existence of a topological number — the winding number — that can be defined in the finite volume Abelian spin and Abelian gauge theory. The winding number is sensitive to the boundary conditions of the system if there are infinite correlations in the theory. It is therefore a good probe for the deconfinement transition of the 4-d $U(1)$ gauge theory which can be measured very efficiently from the flux-cluster algorithm.

Finally, in chapter 14 we present results from our numerical study of the $U(1)$ quantum link model. We discuss conclusions that can be drawn from measurements of local quantities and the cluster area. We also study the effects of Higgsing the

gauge symmetry and the influence of short correlations on the cluster area. We close with final remarks about the efficiency of the study through the existing algorithm and future directions.

Chapter 2

The Two-Dimensional Non-Linear σ -Model

2.1 The Model in the Continuum

There are very few models in theoretical physics that have received the constant attention over decades that the non-linear σ -model has received. The reason for this attention is the simplicity of the model in conjunction to the very interesting properties it possesses. Especially the model in two space-time dimensions has been established as a classic testground for various ideas in perturbative, non-perturbative and lattice formulations. The $O(N)$ non-linear σ -model is formulated in the (Euclidean) continuum as an N -vector of scalar fields $\vec{e}(\mathbf{x})$ with action

$$S[\vec{e}] = \frac{1}{2} \int d^2x \partial_\mu \vec{e} \cdot \partial_\mu \vec{e} \quad (2.1)$$

and the fields constrained to take values on the N -sphere

$$\vec{e}(\mathbf{x}) \cdot \vec{e}(\mathbf{x}) = 1. \quad (2.2)$$

The scalar fields are dimensionless in two dimensions. The theory is invariant under global $O(N)$ rotations of the fields $\vec{e}(\mathbf{x}) \rightarrow R\vec{e}(\mathbf{x})$ where R is an $N \times N$ orthogonal

matrix. The configurations that minimize the action (2.1) have a constant N -vector $\vec{e}(\mathbf{x})$ throughout space-time. The classical ground state therefore breaks the $O(N)$ symmetry down to an $O(N - 1)$ symmetry of rotations around the constant vector. Based on standard knowledge on the spontaneous breaking of continuous symmetries, we would expect a number of massless particles — the Goldstone bosons — in the theory. Their number equals the number of generators of the coset group $O(N)/O(N - 1)$ which is $N(N - 1)/2 - (N - 1)(N - 2)/2 = N - 1$. We would therefore expect that (2.1) is a theory of Goldstone bosons and this is indeed true for more than two dimensions. As we will explain in a while, quantum mechanics changes this picture in two dimensions. The model can be quantized through the path integral

$$Z = \int \mathcal{D}\vec{e} \delta(\vec{e}^2(\mathbf{x}) - 1) \exp\left(-\frac{1}{g}S[\vec{e}]\right) \quad (2.3)$$

with the dimensionless coupling constant g . Based on Wilson's renormalization group ideas Polyakov argued [1] that the model is asymptotically free, i.e. the coupling g is getting smaller as the momentum scale is getting larger. The constraint (2.2) is responsible for a non-trivial interaction between the fields. One way to see the interaction is to solve the constraint for one of the fields and replace it in the action (2.1). Let us name the first $N - 1$ fields $\vec{\pi}(\mathbf{x})$ and the N -th field $\sigma(\mathbf{x})$ and solve the constraint

$$\sigma(\mathbf{x}) = \sqrt{1 - \vec{\pi}^2(\mathbf{x})}. \quad (2.4)$$

Replacing σ in the action we get the form of the theory for the $N - 1$ unconstrained fields

$$S[\vec{\pi}] = \frac{1}{2} \int d^2\mathbf{x} \left[\partial_\mu \vec{\pi} \cdot \partial_\mu \vec{\pi} + \frac{(\vec{\pi} \cdot \partial_\mu \vec{\pi})^2}{1 - \vec{\pi}^2} \right] \quad (2.5)$$

For weakly fluctuating fields $|\vec{\pi}| \ll 1$ the dominant interaction is a four-point vertex. For general configurations an expansion of the denominator in (2.5) generates an infinite series of even-point vertices. Since the fields are dimensionless, the model is perturbatively renormalizable. A detailed perturbative study can be found in [2]. In particular, we mention that although in this form the theory seems to retain only

an $O(N - 1)$ symmetry, the correlation functions of the model respect the full $O(N)$ symmetry. To one-loop order of perturbation theory the β -function that governs the running of the coupling with the momentum scale is given by [2]

$$\beta(g) \equiv \frac{d}{d \ln \frac{\Lambda}{M}} g(\Lambda) = -\frac{N - 2}{2\pi} g^2. \quad (2.6)$$

We therefore meet the first interesting property of the model, the *asymptotic freedom*, which is also a main feature of non-Abelian gauge theories. Notice that for $N = 2$ the β -function vanishes. This should not surprise us since the $O(2)$ action is easily seen to be the free theory of a massless angular variable.

Integrating equation (2.6) in the small g regime where it is valid, we get the scaling of the mass scale with the coupling

$$M = \Lambda \exp \left[-\frac{2\pi}{(N - 2)g} \right]. \quad (2.7)$$

We see that although we started with an action which has no dimensionfull parameters in it and therefore no scale, still a mass scale appears already in one-loop perturbation theory. This is the effect of *dimensional transmutation*, the appearance of a mass scale Λ which breaks the classical scale invariance of the model, typically denoted as $\Lambda_{\overline{MS}}$ in the modified minimal subtraction scheme. This effect also appears in pure Yang-Mills theory which is classically a scale invariant theory.

The third interesting property of the model in 2-d is the effect of *dynamical mass generation*. This is based on the Coleman-Mermin-Wagner theorem [3] which states that there is no continuous symmetry breaking in two-dimensions and therefore no two-dimensional Goldstone boson. The theorem is based on an examination of the infrared properties of the 'would-be' Goldstone bosons which turn out to be strong enough in 2-d so that the continuous symmetry does not break. Instead, the particles get a mass whose evaluation requires non-perturbative methods. An equivalent statement in the language of statistical mechanics is that the theory cannot get ordered in 2-d and the correlation length — which is the inverse of the particle mass — is kept finite at all couplings. The dynamical generation of mass also appears in

the Yang-Mills theory. In that case there is Coleman-Mermin-Wagner theorem, but instead the color confinement is responsible for the non-perturbative generation of massive states, the glueballs.

A special property of the $O(3)$ model is the existence of *instantons* [4]. Instantons are solutions to the Euclidean classical equations of motion with finite action and characterized by a topological charge. Their existence is due to topological reasons, in particular these configurations are approaching a constant at infinity so that their action remains finite. This requires the existence of smooth mappings with non-trivial homotopy from the compactified 2-d space-time which is a sphere, to the internal $O(3)$ space which is also a sphere. In mathematical terminology these maps have “integer second homotopy group” $\Pi_2(S^2) = \mathbb{Z}$. Since $\Pi_2(S^N)$ is trivial for $N > 2$ we understand the uniqueness of instantons in the $O(3)$ case. The Yang-Mills theory in 4-d also possesses instantons and their role in the non-perturbative mechanism of confinement is under continuous investigation.

All these properties shared between Yang-Mills theory and the $O(3)$ model make it a unique testground for the phenomena of Nature’s strong interactions. Non-perturbative results have become available through analytical techniques in the $O(N)$ models. It has been shown [5] that the models possess an infinite set of conserved quantities. Based on the existence of these infinitely many charges the exact construction of the S-matrix of the theory was also possible [6]. Furthermore, the authors of [7], using the thermodynamic Bethe’s ansatz and the exact S-matrix, managed to connect the mass-gap of the theory to the $\Lambda_{\overline{MS}}$ scale through the exact formula

$$m = \left(\frac{8}{e}\right)^{1/(N-2)} \frac{1}{\Gamma(1 + 1/(N-2))} \Lambda_{\overline{MS}}. \quad (2.8)$$

Finally, the model admits $1/N$ expansion for large N [8] which goes beyond the ordinary perturbative expansions and at infinite N provides an equation for the mass-gap of the theory (section 1.3).

2.2 The Lattice Regularization

Formulating a field theory in the continuum is going to introduce infinities in every physical quantity due to the infinite number of degrees of freedom. One way out is to regularize the perturbative expansion of the theory in Feynman diagrams by cutting-off the number of momentum modes. The diverging parts are then isolated and the physical quantities are renormalized to momentum-scale dependent finite values. A non-perturbative regularization of field theories is the lattice regularization which replaces space-time with (in most cases) a hypercubic lattice of spacing a . The scalar fields, for example the N -vector fields \vec{E}_x of the $O(N)$ models are defined on the sites x of the lattice. In order to describe the theory on the lattice we need some regularized definition of the derivatives. A first approximation is to use the nearest-neighbor difference $\partial_\mu \vec{E} \rightarrow (\vec{E}_{x+\hat{\mu}} - \vec{E}_x)/a$ and write a lattice action

$$S[\vec{E}] = \frac{1}{2} \sum_{x, \hat{\mu}=1,2} a^2 \left(\frac{\vec{E}_{x+\hat{\mu}} - \vec{E}_x}{a} \right)^2 = \sum_{x, \hat{\mu}=1,2} \left(1 - \vec{E}_x \cdot \vec{E}_{x+\hat{\mu}} \right). \quad (2.9)$$

The path integral expressions for the model become ordinary integrations over the field space defined on each site. For example, we can write

$$Z = \prod_x \int d\vec{E}_x \delta(\vec{E}_x^2 - 1) \exp \left(-\frac{1}{g} S[\vec{E}] \right) \quad (2.10)$$

and design methods (chapter 5) to simulate this path integral. The finite lattice spacing a introduces a momentum cut-off to the modes of the theory. A plane wave on the lattice becomes $\exp(ipna)$ with $n = (n_1, n_2) \in \mathbb{Z}^2$ and therefore the momentum is taking values in the first Brillouin zone $B =] - \pi/a, \pi/a]^2$. The lattice field is represented in momentum space

$$\vec{E}_x = \int_B \frac{d^2 p}{(2\pi)^2} \vec{E}(p) \exp(ipx) \quad (2.11)$$

with inverse Fourier transform

$$\vec{E}(p) = a^2 \sum_{n \in \mathbb{Z}^2} \vec{E}_{na} \exp(-ipna). \quad (2.12)$$

The Dirac $\delta(x - y)$ in configuration space becomes the Kronecker- δ on the lattice

$$\delta_{n,m} = a^2 \int_B \frac{d^2p}{(2\pi)^2} \exp(ip(n - m)a) \quad (2.13)$$

while the δ -function in momentum space becomes periodically identified in the first Brillouin zone

$$\delta_P(p) = \frac{a^2}{(2\pi)^2} \sum_{n \in \mathbb{Z}^2} \exp(-ipna). \quad (2.14)$$

It is very common to set the lattice spacing to 1 and restore it at the end using dimensionality arguments. Using the tools above, we can deduce the form of the action in momentum space

$$\begin{aligned} S[\vec{E}] &= \sum_{\mathbf{x}, \hat{\mu}=1,2} \left(1 - \vec{E}_{\mathbf{x}} \cdot \vec{E}_{\mathbf{x}+\hat{\mu}}\right) = \frac{1}{2} \sum_{\mathbf{x}, \hat{\mu}=1,2} \vec{E}_{\mathbf{x}} \cdot \left(2\vec{E}_{\mathbf{x}} - \vec{E}_{\mathbf{x}+\hat{\mu}} - \vec{E}_{\mathbf{x}-\hat{\mu}}\right) \quad (2.15) \\ &= \frac{1}{2} \int_B \frac{d^2p}{(2\pi)^2} \vec{E}(p) \cdot \sum_{\hat{\mu}=1,2} [2 - \exp(-ip_{\mu}) - \exp(ip_{\mu})] \vec{E}(-p) \\ &= \frac{1}{2} \int_B \frac{d^2p}{(2\pi)^2} \vec{E}(p) \cdot \sum_{\hat{\mu}=1,2} 4 \sin^2(p_{\mu}/2) \vec{E}(-p) \\ &\equiv \frac{1}{2} \int_B \frac{d^2p}{(2\pi)^2} \vec{E}(p) \cdot \tilde{\rho}_{ST}(p) \vec{E}(-p). \end{aligned}$$

Forgetting the constraint for a moment, we learn that the massless free field with the standard nearest-neighbor coupling has the lattice propagator $\Delta_{ST}(p)$

$$\Delta_{ST}(p) = \tilde{\rho}_{ST}^{-1}(p) = \left[\sum_{\hat{\mu}=1,2} \frac{4}{a} \sin^2(p_{\mu}a/2) \right]^{-1}. \quad (2.16)$$

The dispersion relation of the free particle with spatial momentum p_1 is then extracted from the poles of the propagator with the identification $(p_1, p_2) \rightarrow (p_1, iE(p_1))$ as

$$\sinh^2(E(p_1)a/2) = \sin^2(p_1a/2) \quad (2.17)$$

which agrees with the continuum result $E(p_1) = |p_1|$ only for small momenta $|p_1| \ll \pi/a$. We see that our naive discretization of the action has already introduced severe deviations from the continuum physics. The premise is that if we manage to make a infinitesimally small, our results will converge to the continuum results. This is in fact the main strategy in lattice field theory. We introduce the lattice and inevitably break the Poincaré symmetry down to the symmetries of the hypercubic lattice. We nevertheless try to keep the other symmetries intact. We are going to show in chapter 7 how the gauge symmetry can be represented exactly on the lattice. The main effort is to extrapolate results which are collected on finite lattices to the continuum. For example, if we want to measure the mass m of a particle, we measure its two-point function at zero spatial momentum and extract the mass from the exponential decay with the distance (more in section 4.1). The continuum limit is reached by tuning the bare coupling g such that $ma \rightarrow 0$. The physical mass m is held fixed in this limit as the spacing $a \rightarrow 0$.

One should note the similarity of the lattice formulation of the Euclidean field theory with the statistical physics approach which studies the behavior of a large number of degrees of freedom defined on a physical crystal lattice. In the second case though, the spacing a is physical and is not removed. In statistical mechanics language, the Euclidean action becomes the classical Hamilton function of the system. For example, the action (2.9) becomes the Hamilton function of the *classical* $O(N)$ *Heisenberg ferromagnet* giving the energy associated with the configuration $[\vec{E}]$ of classical spins on the crystal lattice. The lattice path integral (2.10) becomes the partition function of the spin system with the bare coupling g identified with the physical temperature T of the system. The weight of each path $\exp(-S[\vec{E}]/g)$, which accounts for the contribution of quantum fluctuations, becomes the Boltzmann weight of thermal fluctuations. One of the goals of the statistical physics study of the crystal lattice is to explain the long-range properties of the system. One generally models the complicated realistic interactions with a simpler theory and looks for the critical range of parameters that can explain the long-range properties of the model. Therefore one looks for a *universal behavior* of the model at long distances which requires

that the correlation length of some physical quantities becomes very large. The correlation length ξ is generally identified as the inverse mass of a particle in the field-theoretic picture. The *criticality* that one looks here therefore requires taking $\xi/a \rightarrow \infty$ while keeping the crystal spacing a finite. This approach is therefore very similar to Euclidean field theory although the interpretation of the limit is different.

With the above translation between field theory and statistical physics language it is common to apply the terminology from both fields to a lattice system.

2.3 Mass-gap at Large N

It might appear surprising at first, but the $O(N)$ model actually simplifies very much when the number of components N goes to infinity. The partition function for the nearest-neighbor lattice action is

$$Z = \prod_{\mathbf{x}} \int d\vec{E}_{\mathbf{x}} \delta(\vec{E}_{\mathbf{x}}^2 - 1) \exp \left(\frac{1}{g} \sum_{\mathbf{x}, \hat{\mu}=1,2} \vec{E}_{\mathbf{x}} \cdot \vec{E}_{\mathbf{x}+\hat{\mu}} \right). \quad (2.18)$$

The constraint can be replaced by the integration over the auxiliary field λ (the coupling g is introduced for later convenience)

$$Z = \prod_{\mathbf{x}} \int d\vec{E}_{\mathbf{x}} d\lambda_{\mathbf{x}} \exp \left(\frac{1}{g} \sum_{\mathbf{x}, \hat{\mu}=1,2} \vec{E}_{\mathbf{x}} \cdot \vec{E}_{\mathbf{x}+\hat{\mu}} + \frac{i}{2g} \sum_{\mathbf{x}} \lambda_{\mathbf{x}} (\vec{E}_{\mathbf{x}}^2 - 1) \right). \quad (2.19)$$

Going to momentum space, we obtain

$$Z = \int \mathcal{D}\vec{E} \mathcal{D}\tilde{\lambda} \exp \left\{ -\frac{1}{2g} \int_B \frac{d^2 p}{(2\pi)^2} \vec{E}(p) \cdot \tilde{\rho}_{ST}(p) \vec{E}(-p) \right. \\ \left. + \frac{i}{2g} \int_B \frac{d^2 p}{(2\pi)^2} \int_B \frac{d^2 q}{(2\pi)^2} \vec{E}(p) \cdot \vec{E}(-p-q) \tilde{\lambda}(q) - \frac{i}{2g} \int_B d^2 q \tilde{\lambda}(q) \delta_P(q) \right\}. \quad (2.20)$$

We can now understand that the leading contribution to the path integral at large N comes from an expansion around the zero momentum mode of the auxiliary field $\tilde{\lambda}(q) \sim \lambda_0 (2\pi)^2 \delta_P(q)$. This is because the zero mode makes the action N times a Gaussian term for each of the N components. At large N therefore, this behavior

is going to dominate the path integral. A zero momentum mode for the auxiliary field corresponds to a constant field $\lambda_x = \lambda_0$ over all space-time. Notice that the zero mode effectively acts as a mass term for the scalars $m^2 = -i\lambda_0$. In this limit, the partition function can be approximated by the saddle point and the integration over the N -vector can be performed trivially

$$\begin{aligned}
Z &= \int \mathcal{D}\vec{E} d\lambda_0 \exp \left\{ -\frac{1}{2g} \int_B \frac{d^2p}{(2\pi)^2} [\vec{E}(p) \cdot (\tilde{\rho}_{ST}(p) - i\lambda_0)\vec{E}(-p)] - \frac{i}{2g} \lambda_0 V \right\} \\
&= \int d\lambda_0 \text{Det}[\tilde{\rho}_{ST} - i\lambda_0]^{-N/2} \exp(-\frac{i}{2g} \lambda_0 V) \\
&= \int d\lambda_0 \exp \left\{ -\frac{N}{2} \text{Tr} \ln[\tilde{\rho}_{ST} - i\lambda_0] - \frac{i}{2g} \lambda_0 V \right\},
\end{aligned} \tag{2.21}$$

where V is the space-time volume of the system. An effective potential for the zero mode can be defined (with the momentum trace $\text{Tr} \rightarrow V/(2\pi)^2 \int_B d^2p$)

$$\exp(-V_{\text{eff}}(\lambda_0)V) = \exp \left\{ -\frac{N}{2} V \int_B \frac{d^2p}{(2\pi)^2} \ln [\tilde{\rho}_{ST}(p) - i\lambda_0] - \frac{i}{2g} \lambda_0 V \right\}. \tag{2.22}$$

Since the first term of the effective potential is proportional to N , in order for the saddle point approximation to be valid, the second term should also be proportional to N and therefore the coupling must behave such that gN is fixed with $gN = \mathcal{O}(1)$. The saddle point value for λ_0 can now be computed from a direct minimization of the effective potential

$$\frac{dV_{\text{eff}}(\lambda_0)}{d\lambda_0} = -\frac{N}{2} V \int_B \frac{d^2p}{(2\pi)^2} \frac{1}{\tilde{\rho}_{ST}(p) - i\lambda_0} + \frac{1}{2g} V = 0. \tag{2.23}$$

This equation is real and therefore accepts only a positive imaginary solution $\lambda_0 = im^2$. Notice that a negative imaginary λ_0 would create a pole and therefore give an imaginary contribution to the equation. Therefore the zero mode of the constraint that survives the large N limit is indeed responsible for a mass generation. We finally arrive at the *gap equation*, which determines the non-perturbative mass-gap of the

theory in the large N limit

$$\int_B \frac{d^2 p}{(2\pi)^2} \frac{1}{\tilde{\rho}_{ST}(p) + m^2} = \frac{1}{gN}. \quad (2.24)$$

We should note that there is nothing special in this derivation about the use of the standard action couplings. The gap equation is valid for any two-spin couplings with Fourier transform $\tilde{\rho}(p)$.

Having the gap equation (2.24), we can also demonstrate the asymptotic freedom of the model at large N . Consider a small lattice cut-off a which corresponds to a large momentum cut-off $\Lambda \sim \pi/a$. The standard action for relatively small momenta becomes $\tilde{\rho}_{ST}(p) \approx p^2$ and therefore we can perform the momentum integration up to the cut-off

$$2\pi \int_0^\Lambda \frac{p dp}{(2\pi)^2} \frac{1}{p^2 + m^2} = \frac{1}{4\pi} \int_0^\Lambda dp^2 \frac{1}{p^2 + m^2} \approx \frac{1}{4\pi} \ln(\Lambda^2/m^2). \quad (2.25)$$

We therefore arrive to the cut-off dependent coupling

$$\frac{1}{g(\Lambda)} = \frac{N}{2\pi} \ln(\Lambda/m) \quad (2.26)$$

and renormalization can be performed by a redefinition of the coupling at an arbitrary scale M through

$$\frac{1}{g(\Lambda)} = \frac{1}{g(M)} + \frac{N}{2\pi} \ln(\Lambda/M). \quad (2.27)$$

The large N β -function which describes the running of the coupling with the scales is (Λ is now an intermediate scale)

$$\beta(g) \equiv \frac{d}{d \ln \frac{\Lambda}{M}} g(\Lambda) = -g^2(\Lambda) \frac{d}{d \ln \frac{\Lambda}{M}} \frac{1}{g(\Lambda)} = -\frac{N}{2\pi} g^2 \quad (2.28)$$

and indeed agrees with the large N limit of the exact result.

The *asymptotic scaling* of the mass-gap at large N , based on the one-loop β -

function and therefore valid for small gN is

$$m \sim M \exp \left[-\frac{2\pi}{gN} \right]. \quad (2.29)$$

It can be shown [8] that the non-zero modes of the auxiliary field introduce interactions between the bosons at leading order $1/N$. A systematic expansion is possible to higher orders of $1/N$ with diagrams that describe interactions between the scalars and the auxiliary field. In this expansion, higher order contributions to the mass-gap and correlation functions can also be derived [9].

Chapter 3

The Classically Perfect Action for $O(3)$ Spins

3.1 Seeking Improvement

The classical $O(N)$ ferromagnet with nearest-neighbor coupling is not the only lattice regularized action for the continuum non-linear $O(N)$ model. In fact, there is an infinite number of lattice actions that can be constructed by adding spin-spin interactions at distances longer than a lattice spacing or with more complicated terms including more than two-spin interactions. As long as these terms obey the $O(N)$ symmetry of the model and basic requirements like 2-d lattice rotational and translational invariance, positivity under reflections, hermiticity and locality, they should all represent the same universal continuum physics. Locality in that context means that the spin interaction strength should decrease with the distance at least exponentially. The naive continuum limit $a \rightarrow 0$ should be the same for all these actions but their behavior at finite a is definitely not universal. Simulating any of these actions at a finite lattice spacing a is going to give results contaminated by the finite lattice cut-off. Therefore it is reasonable to ask if, among all the lattice actions that represent the same universal physics, there exist some for which the lattice artifacts for a fixed lattice spacing are smaller.

The idea of looking for these *improved actions* is not new. Symanzik originally

started a program [10] based on power counting, of adding new operators to the action with coefficients such as to cancel $\mathcal{O}(g^{2n}a^2)$ artifacts in the correlation functions. This program can be consistently implemented order by order in perturbation theory, but in a computationally difficult way. The program has also been extended to a non-perturbative numerical approach [11, 17] that can eliminate completely the $\mathcal{O}(a^2)$ artifacts from a bosonic action. (For fermionic actions the lattice artifacts appear at $\mathcal{O}(a)$ and therefore the application of the program in *QCD* leads to a non-perturbative $\mathcal{O}(a)$ improvement). Actions constructed perturbatively are expected to improve deep in the continuum limit, but the application on realistic lattices with moderate correlation lengths is not guaranteed to show any improvement.

Let us demonstrate a tree-level $\mathcal{O}(a^2)$ improvement for the $O(N)$ spins. Symanzik introduces a next-to-nearest neighbor spin-spin coupling

$$S_{Sym} = -\frac{1}{g} \sum_{x, \hat{\mu}=1,2} \left(\frac{4}{3} \vec{E}_x \cdot \vec{E}_{x+\hat{\mu}} - \frac{1}{12} \vec{E}_x \cdot \vec{E}_{x+2\hat{\mu}} \right). \quad (3.1)$$

In momentum space the action is

$$S_{Sym} = \frac{1}{2g} \int_B \frac{d^2k}{(2\pi)^2} \vec{E}(k) \cdot \Delta_{Sym}^{-1}(k) \vec{E}(-k) \quad (3.2)$$

with the inverse spin propagator

$$\begin{aligned} \Delta_{Sym}^{-1}(k) &= \sum_{\hat{\mu}=1,2} \frac{1}{a^2} \left[\frac{4}{3} 4 \sin^2 \left(\frac{k_\mu a}{2} \right) - \frac{1}{12} 4 \sin^2(k_\mu a) \right] \\ &= \sum_{\hat{\mu}=1,2} \frac{1}{a^2} \left\{ \frac{16}{3} \left[\left(\frac{k_\mu a}{2} \right)^2 - \frac{1}{3} \left(\frac{k_\mu a}{2} \right)^4 \right] - \frac{1}{3} \left[(k_\mu a)^2 - \frac{1}{3} (k_\mu a)^4 \right] \right\} + \mathcal{O}(k^6 a^4) \\ &= \sum_{\hat{\mu}=1,2} k_\mu^2 + \mathcal{O}(k^6 a^4). \end{aligned} \quad (3.3)$$

We therefore see how tuning the coefficients of the two operators in the action has led to the tree-level elimination of $\mathcal{O}(a^2)$ errors.

A different strategy for improving the lattice action is based on Wilson's renormalization group (RG) theory [12, 13]. In fact, Wilson's RG theory predicts that there exist so-called *perfect actions* which are free of any lattice artifact at any finite value

of the correlation length. A simulation on a coarse lattice with a perfect action would therefore produce the exact results of the continuum theory. Let us see how this is possible. Consider for example the space of lattice actions for the $O(N)$ model. This is an infinite-dimensional space consisting of the coupling constants $g, c_1, c_2, \dots, c_\infty$ which parameterize *all* the possible types of multi-spin interactions. Any point in this space should respect besides the $O(N)$ symmetry, 2-d lattice rotational and translational invariance, hermiticity and locality. In general the correlation length is finite in this space but there exists a hypersurface of couplings with the correlation length being infinite for any theory defined on it. This is called the *critical surface*. The fact that this is a hypersurface and not a set of isolated points can be understood since for any action with infinite correlation length marginal operators exist at least in the neighborhood of that point. An infinitesimal RG transformation step can be designed by adding these operators to the action with proper weights so that the correlation length remains infinite. Following Wilson, in this way we can construct hypersurfaces of fixed correlation length in this space for any value of the correlation length.

We can introduce a RG transformation step anywhere on the critical surface. Consider the blocking procedure of scale factor 2 which amounts to collecting the four spins that live at the centers of a 2×2 block of a lattice with spacing a and replacing them by the blocked spin. This process defines a new action on a lattice with spacing $2a$. Rescaling the spacing, we end up with a new action at spacing a and a correlation length $\xi' = \xi/2$. Applying the RG step n times decorrelates the system fast, leading to $\xi^{(n)} = \xi/2^n$. On the other hand, actions defined on the critical surface with $\xi = \infty$ will stay on the critical surface after the blocking step. The RG transformation defines therefore a RG flow on the critical surface. Repeated applications of the RG transformation step may lead to a *fixed point* (FP) action on the critical surface which generally depends on the RG transformation. Now, consider applying the RG step to an action in the neighborhood of the FP action, near the critical surface but not on it. Repeated blocking steps will induce a flow away from the critical surface to ever decreasing correlation length actions. Starting the blocking steps even closer to the critical surface, the flow will stay closer to the critical surface

and approach the FP more closely before turning away to small correlation lengths. Approaching the FP closer and closer, these flows are eventually going to define a unique line of actions coming out of the FP and extending to any finite value of the correlation length. This line of actions is the *renormalized trajectory* (RT). The actions defined on the RT are the perfect actions. The reason is that any action on the RT, even at very small correlation length, is connected to the infinitesimal neighborhood of the FP by infinitely many steps of the RG transformation. Small distances in the perfect action therefore correspond to very large distances near the FP before the transformation. The infinitesimal neighborhood of the FP is the continuum limit and actions there do not have cut-off effects. Since the partition function for the perfect action at small correlation length is equal to the partition function at the FP, measurements of the spectrum performed with the degrees of freedom of the perfect action will give the same result with the FP action measurements performed with the fields before the transformation. We therefore understand that we can use the perfect action at a small correlation length on a coarse lattice and still get results free of any lattice artifacts.

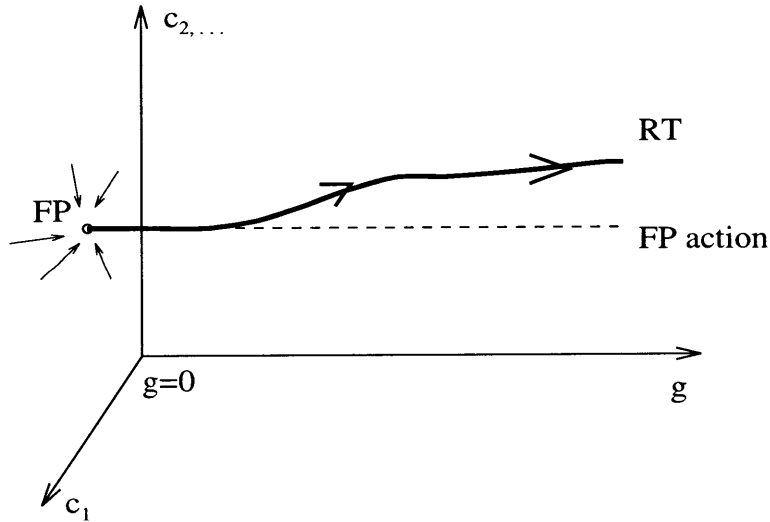


Figure 3-1: *RG flow of the couplings in the $O(N)$ non-linear σ -model. The FP action applied to finite correlation length runs close to the renormalized trajectory near the critical surface $g = 0$.*

We finally note that the RT depends on the RG transformation that is chosen.

There are therefore families of perfect actions at a given finite correlation length parameterized by the RG transformation parameters. This is an important observation when one actually looks for a perfect action since the proper RG transformation can make the action as short-ranged as possible.

3.2 The Classically Perfect Action

Wilson's ideas establish that perfect actions exist but they do not indicate how to locate one. In chapter 5 we are going to construct the perfect action for a free massive scalar and show how the same is possible for free fermions and gauge bosons. Hasenfratz and Niedermayer [14] developed a program for locating the FP action for asymptotically free theories and used it at finite correlation lengths as an approximation to the perfect action. As a prelude to *QCD* they performed the program for the non-linear σ -model and found that the FP action was free of lattice artifacts even at very small correlation lengths. The FP action for the $O(3)$ model is defined on the critical surface where $g = 0$. They considered the configuration of spins \vec{E}_x on a square lattice and defined the RG transformation $T(\vec{E}', \vec{E})$ which is a blocking transformation with scale factor 2. They divided the lattice in 2×2 blocks and associated a blocked spin with unit magnitude \vec{E}'_{x_B} which is a certain average of the original four spins with the center of the block x_B . The blocked action is therefore given by

$$\exp\left(-\frac{1}{g'} S'[\vec{E}']\right) = \prod_x \int d\vec{E}_x \delta(\vec{E}_x^2 - 1) \exp\left(-\frac{1}{g} \{S[\vec{E}] + T(\vec{E}', \vec{E})\}\right) \quad (3.4)$$

where both actions $S[\vec{E}]$ and $S'[\vec{E}']$ should have the naive continuum limit with the coupling scaled out. The RG transformation should leave the partition function unchanged

$$\prod_{x_B} \int d\vec{E}'_{x_B} \delta(\vec{E}'_{x_B}{}^2 - 1) \exp\left(-\frac{1}{g'} S'[\vec{E}']\right) = \prod_x \int d\vec{E}_x \delta(\vec{E}_x^2 - 1) \exp\left(-\frac{1}{g} S[\vec{E}]\right), \quad (3.5)$$

and this restricts the kernel $T(\vec{E}', \vec{E})$

$$\prod_{x_B} \int d\vec{E}'_{x_B} \delta(\vec{E}'_{x_B}{}^2 - 1) \prod_x \int d\vec{E}_x \delta(\vec{E}_x^2 - 1) \exp\left(-\frac{1}{g}T(\vec{E}', \vec{E})\right) = 1. \quad (3.6)$$

Hasenfratz and Niedermayer considered the kernel

$$\begin{aligned} \exp\left(-\frac{1}{g'}S'[\vec{E}']\right) &= \prod_x \int d\vec{E}_x \delta(\vec{E}_x^2 - 1) \exp\left\{-\frac{1}{g}S[\vec{E}] \right. \\ &\quad \left. + \sum_{x_B} \left[P \vec{E}'_{x_B} \cdot \sum_{x \in x_B} \vec{E}_x - \ln Y_N \left(P \left| \sum_{x \in x_B} \vec{E}_x \right| \right) \right] \right\}, \end{aligned} \quad (3.7)$$

where P is a parameter and Y_N a Bessel function chosen to satisfy (3.6) due to the property

$$\int d\vec{E} \delta(\vec{E}^2 - 1) \exp(\vec{E} \cdot \vec{E}') = \text{const} \cdot Y_N(|\vec{E}'|). \quad (3.8)$$

Specifically, it is easy to see that $Y_3(x) \sim \sinh(x)/x$. Taking $P \rightarrow \infty$ the transformation (3.7) goes to a δ -function blocking

$$\vec{E}'_{x_B} = \sum_{x \in x_B} \vec{E}_x / \left| \sum_{x \in x_B} \vec{E}_x \right|. \quad (3.9)$$

At large P we write $P = \frac{1}{g}[\kappa + \mathcal{O}(g)]$ with κ a free parameter and the transformation (3.7) becomes

$$\begin{aligned} \exp\left(-\frac{1}{g'}S'[\vec{E}']\right) &= \prod_x \int d\vec{E}_x \delta(\vec{E}_x^2 - 1) \exp\left(-\frac{1}{g}\left\{ S[\vec{E}] \right. \right. \\ &\quad \left. \left. - \kappa \sum_{x_B} \left[\vec{E}'_{x_B} \cdot \sum_{x \in x_B} \vec{E}_x - \left| \sum_{x \in x_B} \vec{E}_x \right| \right] \right\} \right). \end{aligned} \quad (3.10)$$

Near the FP, the coupling g goes to zero and therefore it scales asymptotically. Using the one-loop β -function for the RG transformation with scale factor 2 we get $\frac{1}{g'} \simeq$

$\frac{1}{g} - (1/2\pi) \ln 2$ and therefore for small g (3.10) becomes a saddle point problem

$$S'[\vec{E}'] = \min_{\{\vec{E}\}} \left\{ S[\vec{E}] - \kappa \sum_{x_B} \left[\vec{E}'_{x_B} \cdot \sum_{x \in x_B} \vec{E}_x - \left| \sum_{x \in x_B} \vec{E}_x \right| \right] \right\}. \quad (3.11)$$

The FP of the transformation can now be determined from the equation

$$S_{FP}[\vec{E}'] = \min_{\{\vec{E}\}} \left\{ S_{FP}[\vec{E}] - \kappa \sum_{x_B} \left[\vec{E}'_{x_B} \cdot \sum_{x \in x_B} \vec{E}_x - \left| \sum_{x \in x_B} \vec{E}_x \right| \right] \right\}. \quad (3.12)$$

This is a non-trivial problem which requires the numerical determination of the configuration on the fine lattice $[\vec{E}]$ which minimizes the functional in (3.12) for any configuration $[\vec{E}']$ on the coarse lattice. It is therefore an *inverse blocking* problem.

The action S_{FP}/g is perfect only at the fixed point $g = 0$. Due to asymptotic freedom, the line of actions S_{FP}/g is running close to the RT for small g but, in general, will diverge from the RT at moderate correlation lengths. It is shown in [14] that the action S_{FP} defines a perfect classical theory on the lattice. The statement is that if a configuration $[\vec{E}']$ satisfies the FP classical equations of motion, then the configuration $[\vec{E}]$ on the fine lattice determined by inverse blocking satisfies the FP classical equations. Furthermore, both configurations have the same value of the action. This immediately implies that in the $O(3)$ model, which has instantons, the FP action can describe arbitrarily large instantons perfectly, i.e. without any cut-off effects. The instantons are configurations that satisfy the classical equations of motion. They have an action proportional to their topological charge and a radius that can take any value for a given topological charge. An instanton on the lattice with radius ρ and topological charge 1 (which means action value 4π) can be inversely blocked to a finer lattice where it appears as an instanton of size 2ρ with the same action and therefore topological charge. Iterating this step we understand now that the FP action allows the existence of $O(3)$ instantons at any scale.

In order to solve the equation (3.12) one has to decide on a reasonable parameterization of the FP action such that a solution to the problem (3.12) is practically feasible. Hasenfratz and Niedermayer truncated the parameterization to two-spin, three-spin and four-spin terms

$$\begin{aligned}
S_{FP}[\vec{E}] &= -\frac{1}{2} \sum_{\mathbf{x}, \mathbf{r}} \rho(\mathbf{r}) \left(1 - \vec{E}_{\mathbf{x}} \cdot \vec{E}_{\mathbf{x}+\mathbf{r}}\right) \\
&+ \sum_{\mathbf{x}_1, \mathbf{x}_2, \mathbf{x}_3, \mathbf{x}_4} c(\mathbf{x}_1, \mathbf{x}_2, \mathbf{x}_3, \mathbf{x}_4) \left(1 - \vec{E}_{\mathbf{x}_1} \cdot \vec{E}_{\mathbf{x}_2}\right) \left(1 - \vec{E}_{\mathbf{x}_3} \cdot \vec{E}_{\mathbf{x}_4}\right) + \dots
\end{aligned} \tag{3.13}$$

where \mathbf{r} is a lattice vector and $c(\mathbf{x}_1, \mathbf{x}_2, \mathbf{x}_3, \mathbf{x}_4)$ determines the strength of the three-spin and four-spin interactions. A three-spin interaction term has $\mathbf{x}_1 = \mathbf{x}_3$ while a four-spin term has $\mathbf{x}_1, \mathbf{x}_2, \mathbf{x}_3, \mathbf{x}_4$ all different. An approximate determination of the couplings in (3.13) is possible if we assume a configuration $\{\vec{E}'\}$ on the coarse lattice which does not fluctuate much around the N -th axis. Then the configuration $\{\vec{E}\}$ on the fine lattice which solves (3.12) also fluctuates weakly around the N -th axis. Keeping quadratic and quartic order terms of the fluctuating fields in (3.12) leads to equations which determine $\rho(\mathbf{r})$ and $c(\mathbf{x}_1, \mathbf{x}_2, \mathbf{x}_3, \mathbf{x}_4)$. It is interesting that these equations are independent of N for $N \geq 3$ and their solutions determine a FP action valid in this limit for any non-Abelian $O(N)$ spin-model. The Abelian case $N = 2$ leads to different equations which therefore provide a FP action for weakly fluctuating XY model fields. It is not surprising also that in this limit the two-spin interaction $\rho(\mathbf{r})$ for the $N - 1$ fluctuation fields coincides with the FP interaction for free massless scalars derived in [4] and which in momentum space is

$$\tilde{\rho}^{-1}(q) = \sum_{l \in \mathbb{Z}^2} \frac{1}{(q + 2\pi l)^2} \prod_{\mu=1}^2 \frac{\sin^2(q_\mu/2)}{(q_\mu/2 + \pi l_\mu)^2} + \frac{1}{3\kappa}. \tag{3.14}$$

The configuration space couplings are determined from

$$\rho(\mathbf{r}) = \int_B \frac{d^2 q}{(2\pi)^2} \tilde{\rho}(q) \exp(iq\mathbf{r}) \tag{3.15}$$

and it turns out that they decrease exponentially fast with the distance \mathbf{r} for any choice

r	$\rho(r)$	r	$\rho(r)$
(1,0)	-0.61802	(4,1)	$7.064 \cdot 10^{-7}$
(1,1)	-0.19033	(4,2)	$1.327 \cdot 10^{-6}$
(2,0)	$-1.998 \cdot 10^{-3}$	(4,3)	$-7.953 \cdot 10^{-7}$
(2,1)	$-6.793 \cdot 10^{-4}$	(4,4)	$6.895 \cdot 10^{-8}$
(2,2)	$1.625 \cdot 10^{-3}$	(5,0)	$-8.831 \cdot 10^{-8}$
(3,0)	$-1.173 \cdot 10^{-4}$	(5,1)	$3.457 \cdot 10^{-8}$
(3,1)	$1.942 \cdot 10^{-5}$	(5,2)	$3.491 \cdot 10^{-8}$
(3,2)	$5.232 \cdot 10^{-5}$	(5,3)	$-3.349 \cdot 10^{-8}$
(3,3)	$-1.226 \cdot 10^{-5}$	(5,4)	$8.408 \cdot 10^{-9}$
(4,0)	$-2.632 \cdot 10^{-6}$	(5,5)	$-1.657 \cdot 10^{-10}$

Table 3.1: *The couplings of the spin-spin interaction terms at distance $r = (r_1, r_2)$ for the optimal choice of the RG transformation with $\kappa = 2$. In this convention, for the standard action the only non-vanishing entry in this list would be $\rho_{ST}(1, 0) = -1$.*

of the RG parameter κ . We call actions with this property *local*. It turns out that the choice $\kappa = 2$ makes the action (3.14) as short-ranged as possible, with a decay rate $\rho(r) \sim \exp(-3.44|r|)$. The inverse spin propagator should have the property $\tilde{\rho}(q) \rightarrow q^2$ for small q . This requires that in configuration space $\sum_r \rho(r)r^2 = -4$. The symmetries of the model require that $\rho(r_1, r_2) = \rho(r_2, r_1) = \rho(-r_1, r_2) = \rho(r_1, -r_2)$.

Using these couplings as a first approximation, the equation (3.12) was solved in [14] for $O(3)$ spins using a numerical multigrid procedure. Repetitive inverse blocking steps on smooth and rough configurations led to an accurate determination of the FP action parameterized with a set of 24 two-spin, three-spin and four-spin couplings (figure 3-2). It was noticed that although small, the three-spin and four-spin couplings are important for rough configurations.

3.3 A Scaling Test

Extrapolating quantities computed on a lattice with finite spacing to the continuum is a fundamental problem in lattice simulations. The results are always contaminated by lattice artifacts and it is desirable to have a well-defined method to estimate the dependence of physical quantities on the lattice spacing. Lüscher, Weisz and Wolff [15]


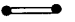















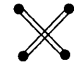
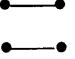
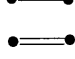
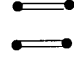
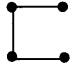
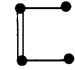
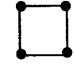
Type	Coupling	Type	Coupling	Type	Coupling
	0.61884		-0.04957		-0.01163
	0.19058		-0.02212		-0.00463
	0.01881		-0.00139		0.00497
	0.02155		0.00717		-0.00055
	0.01078		0.00765		-0.00557
	0.01209		-0.00114		0.00548
	-0.00258		0.00387		-0.00100
	-0.01817		-0.00772		0.04970

Figure 3-2: *Parameterization and couplings of the numerically determined FP action for the $O(3)$ non-linear σ -model. The form of the action is in [14], eq.(12').*

developed a method to compute the running coupling in asymptotically free theories through a finite-size scaling analysis that can be applied to moderate size lattices. In asymptotically free theories like Yang-Mills and the non-linear σ -model the continuum limit is reached when the dimensionless coupling g approaches zero. This is a high energy region and the running of the coupling (and other physical quantities) can be computed reliably from one or two-loop perturbation theory. The question that arises is how the perturbative regime results are connected to the low energy regime that is usually studied in the numerical simulations on finite lattices. The authors of [15] studied the 2-d $O(3)$ non-linear σ -model as a prototype. They consider the system on a lattice with finite spatial extent L and infinite Euclidean time extent T . In practice they used $T \approx 2L$ and applied open boundary conditions to the time direction in order to make it effectively infinite. Periodic boundary conditions are applied to the

finite spatial direction. They defined the dimensionless running coupling

$$\bar{g}(L) = m(L)L \tag{3.16}$$

where $m(L)$ is the mass-gap of the system and which is easily extracted from the spin-spin correlation function. It was shown in [16] that the one-loop β -function for this coupling coincides with the one-loop β -function for the coupling in the MS scheme and therefore the coupling (6.8) is running to asymptotic freedom. The perturbatively known β -function determines the running of $\bar{g}(L)$ with infinitesimal changes of L for small values of L where perturbation theory is a good approximation. Therefore connection with the values of the coupling at large volumes is not possible. In order to overcome this problem, the authors of [15] considered the *step scaling function* $\sigma(s, u)$ which describes what happens to the coupling when L is scaled by a factor s such as $s = 2$ for example. Thus they defined

$$\bar{g}(sL) = \sigma(s, \bar{g}(L)) . \tag{3.17}$$

The idea is that if the scaling function $\sigma(s, u)$ is known for a certain s and a range of coupling values u , the running of the coupling can be constructed from the sequence

$$u_n = \bar{g}(s^n L) = \sigma(s, u_{n-1}) . \tag{3.18}$$

Starting from a small volume, and iterating n times we can compute the coupling at a large volume $s^n L$ where the finite-volume effects on the mass-gap are negligible. The important thing to realize is that this extrapolation over orders of magnitude of L from the perturbative to the non-perturbative regime can be achieved with values of the scaling function $\sigma(s, u)$ computed on small or moderate size lattices. This program was applied in [15] for $s = 2$. The authors considered pairs of lattices from $(5 \times \infty, 10 \times \infty)$ up to $(16 \times \infty, 32 \times \infty)$. They fixed the bare coupling $1/g$ such that a desired value for $\bar{g}(L)$ was obtained. Then they doubled the spatial extent L keeping $1/g$ fixed and measured the new coupling $\bar{g}(2L)$. In this way they collected points of

the scaling function $\sigma(2, u)$ for various finite-spacing lattices and extrapolated reliably to the continuum value of $\sigma(2, u)$. These data constitute therefore a measure of the finite lattice spacing artifacts for the mass-gap of the theory.

Having the step-scaling function values, the iterative procedure (3.18) can be carried through. With the values $\sigma(2, u)$ at hand, g is tuned so that $\bar{g}(L) = u$ is obtained. Then we learn that at this g , $\bar{g}(2L) = u' = \sigma(2, u)$. If the continuum limit of $\sigma(2, u')$ is also known, the value $\bar{g}(4L) = \sigma(2, u')$ now becomes available. In this way, a reliable extrapolation to the infinite volume limit of the mass-gap was obtained in [15]. The finite spacing errors are shown to be small and under control. This method of *non-perturbative renormalization* of physical scales has been applied to QCD during the last years [17, 18, 19, 20] especially studying the running of the strong coupling and the running quark masses.

The study of the $O(3)$ running coupling in [15] was performed using the standard nearest-neighbor action and the lattice artifacts on the mass-gap are shown in figure 3 for the particular selection $\bar{g}(L) = 1.0595$. This scaling test is a classic test that any candidate improved action should undergo.

Hasenfratz and Niedermayer applied this scaling test to the FP action which was numerically determined from the multigrid procedure for the $O(3)$ spins. They put the system on a periodic square lattice of finite spatial extent L . They chose a time extent at least six times larger than the correlation length $\xi(L) = 1/m(L)$ so that it can be effectively considered infinite. They simulated the action at $L = 5a$ and tuned g so that $\bar{g}(L) = 1.0595$. Then they measured $\bar{g}(2L)$ and amazingly found no lattice artifacts for the mass-gap. They report that even on smaller lattices no lattice artifacts appear. These are lattices with $g \approx 1$ and very moderate correlation lengths. It appears therefore that the line of classically perfect actions S_{FP}/g runs very closely to the full RT even down to small correlation lengths. In principle this is an unexpected result that lacks explanation. Further tests that were performed using the FP action verified the perfection in all aspects studied. In particular, they showed that the rotational symmetry of the two-point function was perfectly restored [14]. They also observed perfect topology, i.e. the existence of $O(3)$ instantons at all

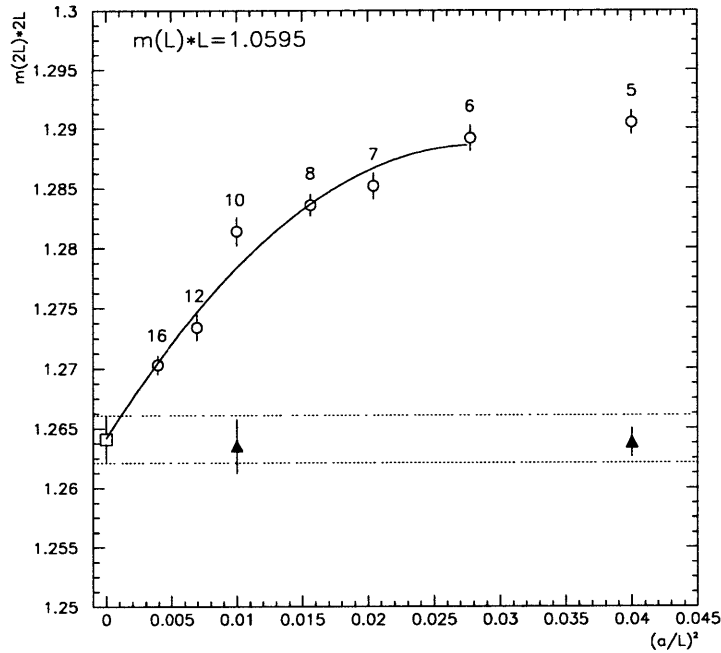


Figure 3-3: *Cut-off dependence of $m(2L)2L$ for fixed value of $m(L)L=1.0595$ for the standard action (circles) and the FP action (triangles). The values of L/a are indicated in the plot. The square is the extrapolated continuum value of a fit with a second order polynomial in $(a/L)^2$. No cut-off artifacts are seen with the FP action.*

scales [21, 22]. We finally note that despite the multispin couplings, the Wolff cluster algorithm [23] can be generalized [24] to include these couplings in a way shown in chapter 5 and therefore the FP action is simulated very efficiently.

Chapter 4

The Large N Quantum Perfect Action for $O(N)$ Spins

The complete elimination of cut-off effects with the FP action even at very small values of the correlation length is in principle unexpected and needs to be understood. It is not obvious why an action which is expected to be perfect only in the classical limit works so well for the full quantum theory of the $O(3)$ spins. In contrast to the classically perfect action, in this chapter we will attempt to locate a *quantum perfect action* which is an action on the RT. One approach will be to study the problem at large N . At large N the model simplifies substantially becoming basically a saddle point problem, while maintaining at the same time its central non-perturbative features. As we demonstrated in chapter 2, at large N the model becomes a free theory of N bosons with a non-perturbatively generated mass, determined from the mass-gap equation. The interaction appears only as an $1/N$ correction in the model.

The large N limit seems like a good starting point for capturing the $O(3)$ physics. Since there is no interaction at large N , we expect that a computation of the RT might be possible. Our strategy [25] will therefore be to try to construct the RT at large N and check if the quantum perfect action located on the RT at large N provides an improved behavior for the $O(3)$ system at small correlation lengths.

4.1 Quantum Perfect Action for a Free Massive Scalar

The FP action for the Gaussian model — which is a set of massless free fields — has been derived in [4] by iterating a blocking RG transformation step. Here we are going to show that the perfect action for the free massive scalar can also be constructed. Since the mass of the particle is the inverse correlation length of the theory, this action is a quantum perfect action for the massive scalar at any value of the correlation length.

Here also, instead of the blocking RG transformation step that takes a field configuration from a fine lattice to a coarse lattice, we are going to use a RG step that blocks the lattice fields directly out of the continuum. This method of “integrating out of the continuum” has been shown [26] to lead directly to the FP of repetitive iterations of the blocking step. Consider the continuum Euclidean action

$$s[\varphi] = \frac{1}{2} \int d^2x [\partial_\mu \varphi(x) \partial_\mu \varphi(x) + m^2 \varphi^2(x)] \quad (4.1)$$

and the RG transformation that integrates the continuum fields on a square block c_x with size a and centered at x , $c_x = [x_1 - a/2, x_1 + a/2] \times [x_2 - a/2, x_2 + a/2]$. The lattice field is

$$\Phi_x = \int_{c_x} d^2y \varphi(y) \quad (4.2)$$

and the corresponding blocking in momentum space can be found for the lattice fields in the first Brillouin zone $B =]-\pi, \pi]^2$ (we set $a = 1$ for convenience)

$$\begin{aligned} \Phi(p) &= \sum_x \int_{c_x} d^2y \varphi(y) e^{ipx} = \sum_x \int_{c_x} d^2y \int \frac{d^2q}{(2\pi)^2} \varphi(q) e^{iqy} e^{ipx} \\ &= \sum_x \int \frac{d^2q}{(2\pi)^2} \varphi(q) \prod_{\hat{\mu}=1,2} \frac{e^{iq_\mu(x_\mu+1/2)} - e^{iq_\mu(x_\mu-1/2)}}{iq_\mu} e^{ipx} \\ &= \sum_x \int \frac{d^2q}{(2\pi)^2} \varphi(q) \prod_{\hat{\mu}=1,2} \frac{2 \sin(q_\mu/2)}{q_\mu} e^{i(q+p)x}. \end{aligned} \quad (4.3)$$

The momentum integration is replaced by an integration over infinitely many copies

of the first Brillouin zone

$$\begin{aligned}
\Phi(p) &= \sum_{\mathbf{x}} \sum_{l \in \mathbb{Z}^2} \int_B \frac{d^2 q}{(2\pi)^2} \varphi(q + 2\pi l) \Pi(q + 2\pi l) e^{i(q+p)\mathbf{x}} \\
&= \sum_{l \in \mathbb{Z}^2} \int_B \frac{d^2 q}{(2\pi)^2} \varphi(q + 2\pi l) \Pi(q + 2\pi l) (2\pi)^2 \delta_P(q + p) \\
&= \sum_{l \in \mathbb{Z}^2} \varphi(p + 2\pi l) \Pi(p + 2\pi l) \quad ; \quad \Pi(p) = \prod_{\mu=1,2} \frac{2 \sin(p_\mu/2)}{p_\mu}.
\end{aligned} \tag{4.4}$$

Consider the RG transformation which smears the δ -function blocking to a Gaussian distribution of width α . The perfect action is

$$\exp(-S[\Phi]) = \int \mathcal{D}\varphi \prod_{\mathbf{x}} \exp \left[-\frac{1}{2\alpha} \left(\Phi_{\mathbf{x}} - \int_{c_{\mathbf{x}}} d^2 y \varphi(y) \right)^2 \right] \exp(-s[\varphi]), \tag{4.5}$$

and the RG transformation leaves the blocked partition function invariant as it should. The Gaussian blocking kernel is replaced by an integration over the auxiliary lattice field $\eta_{\mathbf{x}}$

$$\exp(-S[\Phi]) = \int \mathcal{D}\varphi \prod_{\mathbf{x}} \int d\eta_{\mathbf{x}} \exp \left[-\frac{\alpha}{2} \eta_{\mathbf{x}}^2 + i\eta_{\mathbf{x}} \left(\Phi_{\mathbf{x}} - \int_{c_{\mathbf{x}}} d^2 y \varphi(y) \right) \right] \exp(-s[\varphi]). \tag{4.6}$$

In momentum space we get

$$\begin{aligned}
\exp(-S[\Phi]) &= \int \mathcal{D}\varphi \mathcal{D}\eta \exp \left\{ -\frac{\alpha}{2} \int_B \frac{d^2 p}{(2\pi)^2} \eta(p) \eta(-p) \right. \\
&\quad + i \int_B \frac{d^2 p}{(2\pi)^2} \left(\Phi(p) - \sum_{l \in \mathbb{Z}^2} \varphi(p + 2\pi l) \Pi(p + 2\pi l) \right) \eta(-p) \\
&\quad \left. - \frac{1}{2} \int \frac{d^2 p}{(2\pi)^2} \varphi(p) (p^2 + m^2) \varphi(-p) \right\}
\end{aligned} \tag{4.7}$$

and the Gaussian integration over the continuum field φ can be solved as an exact saddle point. The classical continuum field which minimizes (4.7) is

$$\varphi_c(p) = -\frac{i\Pi(p)}{p^2 + m^2} \eta(p) \quad ; \quad p \in (-\infty, \infty)^2 \tag{4.8}$$

and by replacement in (4.7) we get

$$\exp(-S[\Phi]) = \int \mathcal{D}\eta \exp \left\{ -\frac{1}{2} \int_B \frac{d^2 p}{(2\pi)^2} \eta(p) \left[\alpha + \sum_{l \in \mathbb{Z}^2} \frac{\Pi^2(p + 2\pi l)}{(p + 2\pi l)^2 + m^2} \right] \eta(-p) \right. \\ \left. + i \int_B \frac{d^2 p}{(2\pi)^2} \Phi(p) \eta(-p) \right\}. \quad (4.9)$$

The remaining integration is also Gaussian and therefore the saddle point auxiliary field replacement gives the exact answer for the perfect action

$$S[\Phi] = \frac{1}{2} \int_B \frac{d^2 p}{(2\pi)^2} \Phi(p) \Delta^{-1}(p; m) \Phi(-p) \quad (4.10)$$

where the blocked propagator $\Delta(p; m)$ is given by

$$\Delta(p; m) = \sum_{l \in \mathbb{Z}^2} \frac{\Pi^2(p + 2\pi l)}{(p + 2\pi l)^2 + m^2} + \alpha. \quad (4.11)$$

The configuration space couplings are determined by the Fourier transform of the inverse propagator

$$\rho(r; m) = \int_B \frac{d^2 p}{(2\pi)^2} \Delta^{-1}(p; m) \exp(ipr) \quad (4.12)$$

and the perfect action in configuration space is

$$S[\Phi] = \frac{1}{2} \sum_{x, r} \Phi_x \rho(r; m) \Phi_{x+r}. \quad (4.13)$$

The RG parameter α can be tuned such that the action is maximally local. We should note also that the result is trivially extended to any dimension. It turns out that the summations in (4.11) cannot be performed analytically in more than one dimension. This is not a problem because a numerical optimization is possible to high accuracy. In any case, the couplings decay exponentially fast with the distance. In 1-d, the sum can also be done analytically (appendix A) using the complex residue theorem. The

value

$$\alpha = \frac{\sinh m}{m^3} - \frac{1}{m^2} \quad (4.14)$$

ultralocalizes the action to the standard nearest-neighbor coupling. We call ultralocal the actions that extend over a finite number of couplings. It is important to realize that the action (4.13) is a perfect action at any value of the correlation length $\xi = 1/m$. Therefore, the couplings from (4.11) parameterize the full RT and provide the quantum perfect action for any massive free scalar theory.

Let us demonstrate the perfectness of the theory by computing the spectrum from the two-point function at large time separation. Consider the field operator that creates a particle with spatial momentum p_1 at a (Euclidean) time x_2 . (Direction 1 is space and direction 2 is time)

$$\Phi(p_1)_{x_2} = \int_{-\pi}^{\pi} \frac{dp_2}{2\pi} \Phi(p_1, p_2) \exp(ip_2 x_2). \quad (4.15)$$

The two-point function $\langle \Phi(-p_1)_\tau \Phi(p_1)_0 \rangle$ describes the creation of a particle with spatial momentum p_1 at time 0, its Hamiltonian evolution in time and its annihilation at time τ . Inserting a complete set of energy eigenstates $|n\rangle$ we get

$$\langle \Phi(-p_1)_\tau \Phi(p_1)_0 \rangle = \langle p_1 | \exp(-\tau H) | p_1 \rangle = \sum_n |\langle p_1 | n \rangle|^2 \exp(-\tau E_n) \quad (4.16)$$

which for large times is dominated by the ground state

$$\langle \Phi(-p_1)_\tau \Phi(p_1)_0 \rangle \approx C(p_1) \exp(-\tau E_0(p_1)). \quad (4.17)$$

We can therefore compute

$$\begin{aligned} \langle \Phi(-p_1)_\tau \Phi(p_1)_0 \rangle &= \int_{-\pi}^{\pi} \frac{dp_2}{2\pi} \int_{-\pi}^{\pi} \frac{dp'_2}{2\pi} \langle \Phi(-p_1, p'_2) \Phi(p_1, p_2) \rangle \exp(ip'_2 \tau) \quad (4.18) \\ &= \int_{-\pi}^{\pi} \frac{dp_2}{2\pi} \int_{-\pi}^{\pi} \frac{dp'_2}{2\pi} \Delta(p_1, p_2) 2\pi \delta_P(p_2 + p'_2) \exp(ip'_2 \tau) \\ &= \int_{-\pi}^{\pi} \frac{dp_2}{2\pi} \Delta(p_1, p_2) \exp(-ip_2 \tau) = \int_{-\pi}^{\pi} \frac{dp_2}{2\pi} \left[\sum_{l \in \mathbb{Z}^2} \frac{\Pi^2(p + 2\pi l)}{(p + 2\pi l)^2 + m^2} + \alpha \right] \exp(-ip_2 \tau) \end{aligned}$$

$$= \sum_{l_1 \in \mathbb{Z}} \int_{-\infty}^{\infty} \frac{dp_2}{2\pi} \frac{\Pi^2(p_1 + 2\pi l_1, p_2)}{(p_1 + 2\pi l_1)^2 + p_2^2 + m^2} \exp(-ip_2\tau) + \alpha\delta_{\tau,0}$$

where in the last step we combined the sum over l_2 and the integration over the Brillouin zone to a full momentum integration. The integral is computed with the complex residue method and the summation over l_1 provides infinitely many poles that contribute

$$p_2 = -i\sqrt{(p_1 + 2\pi l_1)^2 + m^2}. \quad (4.19)$$

The correlation function is therefore decaying like

$$\langle \Phi(-p_1)_\tau \Phi(p_1)_0 \rangle = \sum_{l_1 \in \mathbb{Z}} C(p_1 + 2\pi l_1) \exp(-E(p_1 + 2\pi l_1)\tau) + \alpha\delta_{\tau,0} \quad (4.20)$$

and the energy eigenstates of the system agree exactly with the continuum dispersion relation for a relativistic particle with mass m

$$E(p_1 + 2\pi l_1) = \sqrt{(p_1 + 2\pi l_1)^2 + m^2}. \quad (4.21)$$

It becomes clear that the reason the spectrum is restored completely is due to the contribution of all the Brillouin zones to the perfect propagator (4.11). This is in contrast to the standard action where there is only one pole and the spectrum $\sinh(E(p_1)a/2) = \sin(p_1 a/2)$ has strong lattice artifacts. Any analytical or numerical computation on a lattice with finite spacing using the quantum perfect action (4.13) will be free of any lattice artifacts.

4.2 The Large N Quantum Perfect Action

With the perfect action for free massive scalars at hand we can now develop a program for the computation of the quantum perfect action for $O(N)$ spins at large N . We consider the $O(N)$ system on a lattice and use the quantum perfect action for free

massive scalars as the action for the kinetic part of the spins

$$Z = \prod_{\mathbf{x}} \int d\vec{E}_{\mathbf{x}} \delta(\vec{E}_{\mathbf{x}}^2 - 1) \exp \left[-\frac{1}{2g} \sum_{\mathbf{x}, \mathbf{r}} \vec{E}_{\mathbf{x}} \cdot \rho(\mathbf{r}; m) \vec{E}_{\mathbf{x}+\mathbf{r}} \right]. \quad (4.22)$$

We express the constraint as an integration over the Lagrange multiplier field $\lambda_{\mathbf{x}}$ which enforces the constraint locally

$$Z = \prod_{\mathbf{x}} \int d\vec{E}_{\mathbf{x}} d\lambda_{\mathbf{x}} \exp \left[-\frac{1}{2g} \sum_{\mathbf{x}, \mathbf{r}} \vec{E}_{\mathbf{x}} \cdot \rho(\mathbf{r}; m) \vec{E}_{\mathbf{x}+\mathbf{r}} - \frac{1}{2g} \sum_{\mathbf{x}} \lambda_{\mathbf{x}} (\vec{E}_{\mathbf{x}}^2 - 1) \right]. \quad (4.23)$$

Based on chapter 2, we introduced $\lambda_{\mathbf{x}}$ with the right sign so that $\lambda_0 > 0$. As we already demonstrated in chapter 2, the large N limit of the theory is the saddle point taken with gN fixed and finite. Only the zero mode λ_0 is important in that limit, or equivalently the local constraint field is replaced by a soft global constraint. The N fields are free with the zero mode λ_0 contributing to the square of the mass. The effective potential for λ_0 is

$$\exp(-V_{\text{eff}}(\lambda_0)V) = \exp \left\{ -\frac{N}{2} V \int_B \frac{d^2 p}{(2\pi)^2} \ln [\Delta^{-1}(p; m) + \lambda_0] + \frac{1}{2g} \lambda_0 V \right\} \quad (4.24)$$

and its minimization determines the saddle point value of the auxiliary field

$$\int_B \frac{d^2 p}{(2\pi)^2} \frac{1}{\Delta^{-1}(p; m) + \lambda_0} = \frac{1}{gN}. \quad (4.25)$$

The action will be a perfect action for the $O(N)$ model at $N \rightarrow \infty$ if the parameter m coincides with the non-perturbative mass-gap of the model. The action will become perfect therefore if the dynamics at large N set $\lambda_0 = 0$. The full RT is given by the mass-gap equation

$$\int_B \frac{d^2 p}{(2\pi)^2} \frac{1}{\Delta^{-1}(p; m(g))} = \frac{1}{gN} \quad (4.26)$$

which determines the quantum perfect action couplings $\rho(\mathbf{r}; m(g))$ for any value of the correlation length $\xi = 1/m(g)$.

4.3 Scaling in the $O(3)$ Non-Linear σ -Model

We applied the large N quantum perfect action to the $O(3)$ model and checked its scaling behavior [25]. We performed the Lüscher-Weisz-Wolff scaling test [15] and measured the lattice artifacts of the renormalized coupling $\bar{g}(L) = m(L)L$ where $m(L)$ is the mass-gap of the system at finite spatial extent L . Periodic boundary conditions are applied to both directions. The time extent of the lattice is taken at least six times larger than the measured correlation length so that it appears effectively infinite. We implemented the program following the steps

- For a lattice of spatial size L , we aim at a mass gap fixed by $m(L)L = 1.0595$. This is chosen so that we can compare with the results in [15, 14].
- We tune the coupling g so that the action is perfect at large N . This requires the use of the free perfect action $\rho(r; m(g))$ with the parameter $m(g)$ tuned such that it coincides with the measured mass-gap $m(L)$ of the system. This procedure converges to a unique point in the parameter space $(g, m(g))$. The mass-gap is extracted from an exponential fit of the zero-spatial momentum two-point function at large time separation. The parameter α is fixed to the 1-d ultralocalization value $\alpha = \sinh m/m^3 - 1/m^2$ which is checked numerically to be near the ultralocal point in 2-d also. The Fourier transform of $\Delta^{-1}(p; m)$ is computed numerically on a mesh with high accuracy.
- Keeping the coupling g fixed, we double the lattice spatial size. We simulate the system and tune the parameter m so that the action now becomes perfect on the $2L$ lattice. This requires $m = m(2L)$. The value of the running coupling $\bar{g}(2L) = m(2L)2L$ determines to what extent lattice artifacts contaminate the results.

The large N action contains only two-spin couplings. The action is truncated to a set of nearest-, diagonal- and next-to-nearest neighbor couplings. It was checked that further couplings are insignificant. The truncation respects $\sum_r \rho(r)r^2 = 4$ which follows from $\rho(p) \rightarrow p^2$ for small momenta.

r	$\rho(r; m)$
(1,0)	0.61880
(1,1)	0.19033
(2,0)	$1.9930 \cdot 10^{-3}$
(2,1)	$6.7863 \cdot 10^{-4}$
(2,2)	$-1.6177 \cdot 10^{-3}$
(3,0)	$2.3413 \cdot 10^{-4}$

Table 4.1: *Truncated large N perfect couplings for $L = 6$, $m(L)L = 1.0595$. The symmetries of the model require that $\rho(r_1, r_2) = \rho(r_2, r_1) = \rho(-r_1, r_2) = \rho(r_1, -r_2)$.*

We tested the scaling at two lattices $L = 6, 8$ where the correlation length is small and the lattice artifacts stronger. We simulated the system using the Wolff cluster algorithm (chapter 5). The scaling properties as shown in figure 1 are not improved, in fact they turn out to be even worse than the standard action.

4.4 Final Comments

The classically perfect action presented in chapter 3 is a truncation to 24 terms that include two-, three- and four-spin couplings. It is surprising that this action scales so well even for small correlation lengths. As demonstrated in chapter 4, the full RT can be computed for the $O(N)$ non-linear σ -model in the large N limit. Although this action knows about the dynamical mass generation and in fact provides a way to compute non-perturbatively the mass gap, it fails to show improved scaling when applied to the $O(3)$ model. Clearly, large N dynamics does not explain why the classically perfect action for $O(3)$ stays close to the RT.

We noticed that the large N truncated couplings are very close to the two-spin couplings of the classically perfect action. But the three- and four-spin couplings in the classically perfect action seem to be important in capturing the physics of rough configurations. In particular they have been shown to be important for topological effects [22]. In the large N scheme, three- and four-spin couplings occur in the $1/N$ expansion, indicating a possible direction for improving the scaling of the large N action when applied to $N = 3$.

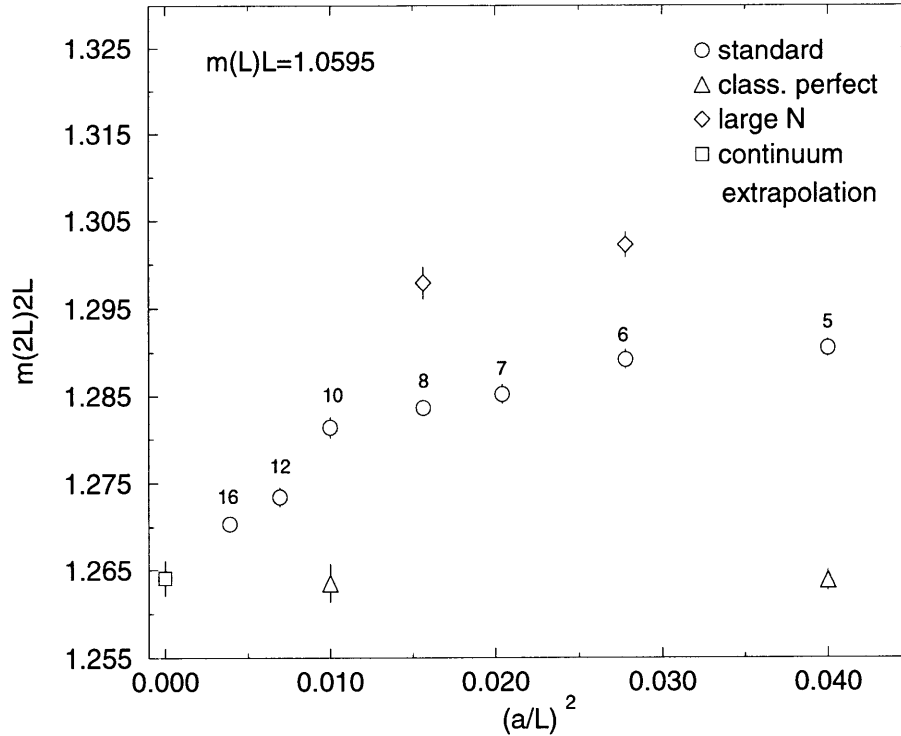


Figure 4-1: *Cut-off dependence of $m(2L)2L$ for fixed value of $m(L)L=1.0595$ for the standard action, the FP action and the large N quantum perfect action. The values of L/a are indicated in the plot. The square is the extrapolated continuum value of a fit with a second order polynomial in $(a/L)^2$.*

Other strategies have also been employed in an attempt to understand the scaling properties of the classically perfect action. The authors of [27] combined Monte Carlo and RG methods with a truncated action containing up to 13 different patterns of two-, three- and four-spin couplings. No considerable improvement with respect to the standard action was recovered either. The authors of [28] considered a large N Symanzik improved action applied to $N = 3$. Their action contains only two-spin couplings. They report some improvement compared to the standard action but their action scales far worse than the classically perfect action.

It seems that one needs quite a large set of couplings (including three- and four-spin ones) in order to catch the physics of rough configurations and to improve scaling. There has been no analytical understanding yet of the mechanism responsible for these couplings which make a classically perfect action scale so amazingly at small correlation lengths.

The quest for improved actions for QCD has been very intense during the last years ([29, 30] and references therein). One approach is to look for the classically perfect action for QCD which requires an extensive parameterization and determination of the couplings through the multigrid minimization. It turns out that the problem is far more complicated than the $O(N)$ model. It is an on-going project to determine the perfect action that will systematically eliminate the lattice artifacts from every measurable quantity. Another approach developed from the MIT group [26] is looking for the perfect action starting from the perfect action for free fields. As we saw in section 4.2, the perfect action can be found by integrating the scalar fields out of the continuum. We should not be surprised that the same is possible for free fermions and gauge bosons since the Gaussian action and Gaussian RG kernel path integrals can be performed exactly. The perfect action for Wilson fermions was found in [31] and for gauge bosons in [26]. The structure of the perfect propagators is similar consisting of infinite poles from a summation over all the Brillouin zones. The propagators also contain extra functions that ensure the right polarization states. In all cases the RG parameter α can be tuned so that the action is maximally local. These actions are the starting point for a perturbative construction to $\mathcal{O}(g)$ of lattice chiral fermions [32] and the $\mathcal{O}(g)$ quark-gluon and three-gluon perfect vertices [26]. The method can be combined with multigrid minimization techniques for the determination of the non-perturbative perfect action for QCD [33].

Chapter 5

The Cluster Algorithm for Classical $O(N)$ Spins

5.1 The Monte Carlo Method

Given a partition function of a system like the $O(N)$ model on a lattice the question raised is how to make a practically feasible study of it. The number of configurations that are summed over is tremendous —just consider that for an Ising model on a 10^2 lattice we get $2^{100} \approx 10^{30}$ configurations. Let us denote a general configuration of the fields by C . The action of the configuration is $S[C]$ and the partition function is

$$Z = \sum_C \exp(-S[C]) \quad (5.1)$$

where the summation includes in general integrations with a suitable measure for fields with continuous internal spaces, for example integrations over the S^{N-1} spheres for the $O(N)$ model. The idea that allows a numerical simulation is *importance sampling*. If the action is bounded from below, a shift can in general make it positive for any configuration. The sum (5.1) will be dominated from the configurations that maximize $\exp(-S[C])$. The expectation value of an observable

$$\langle \mathcal{O} \rangle = \frac{1}{Z} \sum_C \mathcal{O}[C] \exp(-S[C]) \quad (5.2)$$

is dominated therefore by those configurations that have the maximal Boltzmann weight $\exp(-S[C])/Z$. The idea of importance sampling is to generate an *equilibrium ensemble* of configurations where each configuration has a probability density

$$W[C] = \frac{1}{Z} \exp(-S[C]) \quad (5.3)$$

with respect to the *same* measure used in (5.1). The probability density should satisfy the axioms of a probability, i.e. $0 < W[C] < 1$ for any C and $\sum_C W[C] = 1$. In the equilibrium ensemble the configurations which are most important to the path integral will occur more frequently than the ones with small Boltzmann weight. The expectation value of an observable can then be measured directly as the statistical average

$$\langle \mathcal{O} \rangle \approx \frac{1}{N} \sum_{i=1}^N \mathcal{O}[C_i]. \quad (5.4)$$

In principle, an infinite number of configurations is required to ensure (5.3) but we expect that with a finite number N the error in $\langle \mathcal{O} \rangle$ will be typical of a canonical ensemble, i.e. $\sim 1/\sqrt{N}$. Therefore making the ensemble larger guarantees that the statistical error will always decrease to the desired accuracy. Generating the configurations that constitute the equilibrium ensemble is a stochastic process. This means that given a configuration C already in the ensemble, there is a given transition probability $\mathcal{P}(C \rightarrow C')$ which depends on C to generate a new configuration C' of the ensemble. The transition probability should satisfy

$$\sum_{C'} \mathcal{P}(C \rightarrow C') = 1 \quad (5.5)$$

for every configuration C of the system. In a general ensemble, the sequence of configurations generated with $\mathcal{P}(C \rightarrow C')$ will alter their probability density. After a configuration is generated, the probability density $W[C]$ will change to

$$W'[C'] = \sum_C W[C] \mathcal{P}(C \rightarrow C'). \quad (5.6)$$

We see that in general the transition probability $\mathcal{P}(C \rightarrow C')$ defines a motion of the probability density. We would like this motion to converge to the Boltzmann distribution (5.3). Configurations generated after that will constitute the equilibrium ensemble. For this reason we require that a fixed point is reached

$$\sum_C W[C] \mathcal{P}(C \rightarrow C') = W[C'] = \frac{1}{Z} \exp(-S[C']). \quad (5.7)$$

We should be careful that whatever choice of $\mathcal{P}(C \rightarrow C')$ is made, the fixed point of the weight density should be unique otherwise the results of the simulation will be ambiguous. We require also that the transition probability obeys the *ergodicity* condition. This is the requirement that starting from any configuration, we can reach any other configuration in a finite number of transitions.

The equilibrium ensemble which is generated with the ergodic transition probability $\mathcal{P}(C \rightarrow C')$ is called a *Markov chain* and the process of generating the sequence a *Markov process*.

One way to generate a Markov chain is to select the transition probability so that it obeys the so-called *detailed balance* equation

$$\exp(-S[C]) \mathcal{P}(C \rightarrow C') = \exp(-S[C']) \mathcal{P}(C' \rightarrow C) \quad (5.8)$$

for every pair of configurations C, C' . A summation over C or C' is easily seen to verify (5.7). We note that this is only a sufficient condition for (5.7). By construction, a Markov chain is guaranteed to move through the phase space of the system ensuring that configurations which contribute more to the path integral occur with correspondingly larger probability.

5.2 The Metropolis Algorithm

Having understood the importance sampling and the requirements for the generation of a Markov chain, we proceed to specific algorithms which generate the sequence and which essentially are a choice of a transition probability. The first algorithm

proposed historically is the Metropolis algorithm [34]. In this algorithm the transition probability is determined from two steps. The first step is a probabilistic suggestion for a new configuration and the second step is a probabilistic acceptance or rejection of the transition. The combined process defines the transition probability which should respect the detailed balance and ergodicity conditions. Given a configuration C , the algorithm first makes a suggestion for a possible transition with the probability $\mathcal{P}_S(C \rightarrow C')$. The suggestion probability is required to be symmetric, i.e

$$\mathcal{P}_S(C \rightarrow C') = \mathcal{P}_S(C' \rightarrow C) . \quad (5.9)$$

After that, the algorithm examines the action of the new configuration and decides if it will accept the transition. In particular, if the action is lowered, i.e. $S[C'] < S[C]$ the algorithm always accepts the change. If the action is raised, the algorithm accepts the transition with the probability

$$\mathcal{P}_A(C \rightarrow C') = \exp \left(- \left(S[C'] - S[C] \right) \right) . \quad (5.10)$$

It is important that there is always the possibility to have a transition to higher action because in this way the algorithm cannot get trapped for ever in local minima of the action. The acceptance probability depends on the change of the action $\Delta S[C] \equiv S[C'] - S[C]$ and in any case is given by

$$\mathcal{P}_A(C \rightarrow C') = \min \left\{ 1, \exp(-\Delta S[C]) \right\} . \quad (5.11)$$

The suggestion probability should be chosen such that the algorithm is ergodic. The detailed balance is seen easily to be obeyed. Indeed, if $S[C'] < S[C]$ then

$$\mathcal{P}_A(C \rightarrow C') = 1 \quad \text{and} \quad \mathcal{P}_A(C' \rightarrow C) = \exp \left(- \left(S[C] - S[C'] \right) \right) \quad (5.12)$$

and therefore using also (5.9) we verify

$$\exp(-S[C])\mathcal{P}_S(C \rightarrow C')\mathcal{P}_A(C \rightarrow C') = \exp(-S[C'])\mathcal{P}_S(C' \rightarrow C)\mathcal{P}_A(C' \rightarrow C). \quad (5.13)$$

Otherwise, if $S[C'] > S[C]$ we have

$$\mathcal{P}_A(C \rightarrow C') = \exp\left(-\left(S[C'] - S[C]\right)\right) \quad \text{and} \quad \mathcal{P}_A(C' \rightarrow C) = 1 \quad (5.14)$$

and again detailed balance is satisfied. In practice we cannot suggest configurations that differ much because the change in action is large and they will almost always be rejected. Instead we have to perform local changes to the configuration. In particular, we apply the algorithm to the $O(N)$ model by visiting all the sites of the lattice one after the other. On each site x we make the suggestion to reverse the direction of the spin component which is parallel to a randomly chosen direction \vec{R} with probability 1. More precisely, we consider the random direction \vec{R} and decompose the vector \vec{E}_x into components parallel and perpendicular to \vec{R}

$$\vec{E}_x^{\parallel} = (\vec{E}_x \cdot \vec{R})\vec{R} \quad , \quad \vec{E}_x^{\perp} = \vec{E}_x - (\vec{E}_x \cdot \vec{R})\vec{R}. \quad (5.15)$$

The suggested reflection — which is called a Wolff flip — results in the spin

$$\vec{E}'_x = -\vec{E}_x^{\parallel} + \vec{E}_x^{\perp} = \vec{E}_x - 2(\vec{E}_x \cdot \vec{R})\vec{R}. \quad (5.16)$$

This process does not alter the unit-length property of the vector since

$$\vec{E}'_x \cdot \vec{E}'_x = (-\vec{E}_x^{\parallel} + \vec{E}_x^{\perp})^2 = \vec{E}_x^{\parallel} \cdot \vec{E}_x^{\parallel} + \vec{E}_x^{\perp} \cdot \vec{E}_x^{\perp} = 1. \quad (5.17)$$

We then compute the change in the action which is due only to the four nearest neighbors

$$\Delta S = \frac{2}{g}(\vec{E}_x \cdot \vec{R}) \left[\sum_{\hat{\mu}=1,2} (\vec{E}_{x+\hat{\mu}} + \vec{E}_{x-\hat{\mu}}) \cdot \vec{R} \right] \quad (5.18)$$

and decide on the acceptance from (5.11). The ergodicity of the algorithm is ensured from the random choice of \vec{R} and the fact that any two $O(N)$ vectors can be connected with a suitable Wolff flip.

Local changes like the ones proposed by the Metropolis algorithm result in slow motion through the phase space of the model. The situation becomes even worse as we approach the continuum limit where the correlation length ξ grows large. The system is organized at large scales and the site-by-site changes that we make are very slow in creating a statistically independent configuration. More precisely, we define the *autocorrelation time* τ which measures how many Markov steps are needed in order to produce a statistically independent configuration. The autocorrelation time depends on the observable examined, for example the energy density of the system. The statistical error of the observable becomes roughly $\sqrt{\tau}$ larger than the naive one if it has an autocorrelation time τ . The observable which has the largest autocorrelation time is the actual measure of autocorrelations in the Markov chain. As the correlation length grows, the autocorrelation time will generally grow as

$$\tau \propto \xi^z, \tag{5.19}$$

where z is called the *dynamical critical exponent* and is the true measure of the efficiency of the algorithm. If $z > 0$, near the continuum limit the algorithm will become extremely slow in producing a statistically independent configuration —this is called the *critical slowing down* problem. Local changes are updating the system in a random walk manner and therefore demand about ξ^2 steps in order to find an independent configuration in the phase space. The Metropolis algorithm consequently has $z \approx 2$. Notice that we have scaled out the volume dependence of the autocorrelations from τ which is slowing down the update of the d -dimensional system by an extra factor of ξ^d .

Various improvements of the basic Metropolis algorithm logic have been proposed in order to reduce the dynamical critical exponent. At present the most efficient local algorithm for Wilson's gauge theory is the overrelaxation algorithm which has $z \approx 1$.

5.3 The Cluster Algorithm for Classical Spins

A radical solution to the critical slowing down for various spin models has been discovered over the last decade. This is a non-local algorithm called the cluster algorithm which in some cases has dynamical critical exponent $z \approx 0$ and consequently eliminates critical slowing down completely. We note here that the computing effort still increases as ξ^d for a d -dimensional system but this is an unavoidable problem connected with how closely we want to approach the continuum limit on a given volume. Swendsen and Wang [35] discovered the cluster algorithm for Ising-like spin models. They first noticed that Fortuin and Kasteleyn [36] had mapped the partition function of the Potts model to the so-called random bond model. The random bond model is formulated in terms of 0 or 1 valued variables that live on the links connecting two neighboring sites. Links with value 1 necessarily occur between sites with the same spin and have a weight p in the partition function with $0 < p < 1$. Links with value 0 are indifferent to the spin states and have weight $1 - p$ in the partition function.

Swendsen and Wang realized that each link which has value 1 can be thought of as a *bond* created with probability p , connecting the two same-state adjacent spins. They turned this picture into a Markov step for the Potts model in the following way. Starting from a spin, bonds are placed connecting it with its same-state adjacent spins with probability p . When the growth of the cluster of connected spins has stopped, a new spin is chosen and a new cluster is grown. In this way, the lattice is decomposed into same-state clusters of spins. The update consists of a random selection of a new Potts state for the spins in a cluster and was shown to be ergodic and obeying detailed balance. Since clusters of spins are updated simultaneously, the algorithm results in a very effective motion through the phase space even near the critical point. For example, the dynamical critical exponent for the 2-d Ising model was found to be $z \approx 0.35$.

The idea of a cluster algorithm was soon extended successfully to the $O(N)$ non-linear σ -model by Wolff [23, 37]. The Wolff cluster algorithm for $O(N)$ spins was

shown to eliminate critical slowing down completely and to improve tremendously the accuracy on the measured quantities. Wolff's idea was to embed an Ising spin in the $O(N)$ sphere and apply the Swendsen-Wang percolation ideas to the partition function. More precisely, Wolff selects randomly a unit vector \vec{R} in the $O(N)$ space — called the Wolff direction — and decomposes the vector \vec{E}_x into components parallel and perpendicular to the Wolff direction

$$\vec{E}_x^{\parallel} = (\vec{E}_x \cdot \vec{R})\vec{R} \quad , \quad \vec{E}_x^{\perp} = \vec{E}_x - (\vec{E}_x \cdot \vec{R})\vec{R} . \quad (5.20)$$

The direction of \vec{E}_x^{\parallel} defines the Ising variable $s_x = \text{sign}(\vec{E}_x \cdot \vec{R})$. The update of this variable is the Wolff flip, $\vec{E}_x^{\parallel} \rightarrow -\vec{E}_x^{\parallel}$. The growth of the cluster starts with the random selection of a site x . Next the algorithm examines every nearest-neighbor y and decides if it is going to put a bond between x and y . If a bond is put, y becomes also a member of the cluster and the Ising spin on y will be flipped along with the rest of the cluster. If s_y is flipped, the contribution of the $\langle xy \rangle$ pair to the action will not change since

$$-\frac{1}{g}\vec{E}'_x \cdot \vec{E}'_y = -\frac{1}{g}(\vec{E}_x - 2(\vec{E}_x \cdot \vec{R})\vec{R}) \cdot (\vec{E}_y - 2(\vec{E}_y \cdot \vec{R})\vec{R}) = -\frac{1}{g}\vec{E}_x \cdot \vec{E}_y \equiv S_{xy} . \quad (5.21)$$

If s_y is not flipped, the action will change

$$-\frac{1}{g}\vec{E}'_x \cdot \vec{E}_y = -\frac{1}{g}(\vec{E}_x - 2(\vec{E}_x \cdot \vec{R})\vec{R}) \cdot \vec{E}_y = -\frac{1}{g}\vec{E}_x \cdot \vec{E}_y + \frac{2}{g}(\vec{E}_x \cdot \vec{R})(\vec{E}_y \cdot \vec{R}) \equiv S'_{xy} . \quad (5.22)$$

If flipping both spins is more favorable for the action, i.e. if $S_{xy} < S'_{xy}$, the algorithm puts a bond on $\langle xy \rangle$ with probability

$$P_{xy} = 1 - \exp\left(- (S'_{xy} - S_{xy})\right) . \quad (5.23)$$

If $S_{xy} > S'_{xy}$, it is more favorable to leave the spins independent and the algorithm

puts no bond on $\langle xy \rangle$. In any case, the probability for a bond is given by

$$P_{xy} = 1 - \exp\left(\min\{0, S_{xy} - S'_{xy}\}\right) = 1 - \exp\left(\min\left\{0, -\frac{2}{g}(\vec{E}_x \cdot \vec{R})(\vec{E}_y \cdot \vec{R})\right\}\right). \quad (5.24)$$

When the iterative process of including neighbors in the cluster is completed, all the Ising spins in the cluster are flipped. This results in a very efficient motion through phase space. Let us demonstrate the detailed balance of this algorithm. Consider a configuration C and a new configuration C' which is the result of flipping a cluster c of spins in C . Consider the pair $\langle xy \rangle$ with action S_{xy} given by (5.21). If one spin is flipped, the action becomes S'_{xy} given from (5.22). The probability that in the C' configuration one of the two spins is flipped is equal to the probability that no bond is put on the link which is $1 - P_{xy} = \exp\left(\min\{0, S_{xy} - S'_{xy}\}\right)$. Starting now from the pair in configuration C' , the probability for independent flips which results in C is $1 - P'_{xy} = \exp\left(\min\{0, S'_{xy} - S_{xy}\}\right)$. The detailed balance is then verified for the pair $\langle xy \rangle$ since in any case one of the probabilities will be 1

$$\exp(-S_{xy}) \exp\left(\min\{0, S_{xy} - S'_{xy}\}\right) = \exp(-S'_{xy}) \exp\left(\min\{0, S'_{xy} - S_{xy}\}\right). \quad (5.25)$$

On the other hand, for a pair of sites $\langle xy \rangle$ in which both spins are flipped, the probability for the flip is the probability to activate the bond P_{xy} given by (5.24). Since the action does not change in this case, the return probability is also P_{xy} . Detailed balance therefore holds also for these pairs. The new configuration C' differs from C with regards to pairs with both spins in the cluster and pairs on the boundary of the cluster where only one spin is updated. Since detailed balance holds for each pair, it holds also for the update of the whole lattice. The ergodicity of the algorithm is easy to verify since there is always a finite probability to have a cluster with just one spin. There is also always a Wolff direction \vec{R} that takes a vector \vec{E}_x to any other vector after the Wolff flip. Combinations of these moves can connect any two configurations of the system.

Wolff's original algorithm is constructing one cluster which is flipped with probability 1. The algorithm can be generalized to a multi-cluster algorithm. After the

first cluster is grown, we select a new site outside the cluster and grow a new cluster. We continue this process until the whole lattice is decomposed into clusters. The system is then updated by flipping independently the clusters with probability 1/2.

Besides solving the critical slowing down problem, cluster algorithms offer *improved estimators* for various physical quantities. The improved estimators measure the physical quantity only from information on the cluster and therefore reduce significantly the computing cost. It is shown in [37] that the spin-spin correlation function $\langle \vec{E}_x \cdot \vec{E}_y \rangle$ can be measured only from the Ising spins on x, y that both belong to the cluster

$$\langle \vec{E}_x \cdot \vec{E}_y \rangle = N \left\langle \frac{V}{|c|} (\vec{E}_x \cdot \vec{R})(\vec{E}_y \cdot \vec{R}) \right\rangle \quad (5.26)$$

where V is the volume of the system and $|c|$ the size of the cluster. Notice that this quantity is taking contributions only from parallel Ising spins and therefore there are no sign cancelations in it. As expected, this improved estimator leads to strong reduction of the statistical error in the correlation function besides the already reduced cost for measuring it. The magnetic susceptibility of the model χ also has an improved estimator [37] in terms of the Ising spins that belong to the cluster

$$\chi = \frac{1}{V} \left\langle \left(\sum_x \vec{E}_x \right)^2 \right\rangle = N \left\langle \frac{1}{|c|} \left(\sum_{x \in c} \vec{E}_x \cdot \vec{R} \right)^2 \right\rangle \sim \langle |c| \rangle. \quad (5.27)$$

The last step is very important since it shows that the size of the cluster is proportional a physical quantity, the magnetic susceptibility, and therefore it cannot grow large outside the critical region. This property guarantees the efficiency of the algorithm since the size of the updated cluster of spins and therefore the propagation of information is connected to the correlation length. If such a connection does not exist, there is always the danger that the clusters may grow too large rendering the algorithm inefficient.

Finally, we mention that the Wolff cluster algorithm is applicable to the $O(N)$ spin model with multi-spin couplings in the action as, for example, the classically perfect action of chapter 3. Niedermayer has developed a general strategy for doing that [24]. For example, consider a three-spin coupling involving spins on the sites x, y, z where

one spin already belongs to the cluster. The algorithm then examines all possibilities, i.e. including none, one, or both of the other spins in the cluster. Then it finds the maximum value S_{xyz}^{max} for the action of all the possibilities and decides if it will include *all* the rest of the spins in the cluster with the probability

$$\mathcal{P}_{xyz} = 1 - \exp\left(\min\{0, S_{xyz} - S_{xyz}^{max}\}\right). \quad (5.28)$$

It can be seen [24] that besides ergodicity this choice satisfies detailed balance.

Despite the effort, efficient cluster algorithms have not been found for the Wilson formulation of lattice gauge theory. The ideas in the following chapters will allow us to construct a cluster algorithm for the quantum link formulation of the $U(1)$ gauge theory and indicate how the same may be possible for non-Abelian gauge theories also.

Chapter 6

Classical $O(3)$ Spins and Quantum Antiferromagnets

6.1 Introduction

The starting point of part II of this work is the classical $O(3)$ spin model in two dimensions which was the object of study in part I. But the motivation now is completely different. What we aim at is to demonstrate that the physics of the classical $O(3)$ spins can be described in a different framework which uses only *discrete* variables. Nevertheless, the continuous symmetry is still represented exactly in the discrete theory by properly identifying the finite Hilbert space of the states and the action of the symmetry generators on it. We are going to demonstrate how the discrete variables can build collective excitations in the discrete theory which, when the correlations grow large, can be identified with the classical $O(3)$ spins. The mass-gap of the $O(3)$ spin model will be in fact connected to the correlations of the collective excitations in the discrete theory. Therefore, we will argue that the discrete theory constitutes a new non-perturbative formulation of the classical spin theory and is based on the promotion of the classical spins to quantum spin operators. This will be the first example of what turns out to be a very general framework for the non-perturbative study of field theories with global or gauge symmetries and is referred to as D -theory.

In order to motivate this approach, we are going to present in the following a study

of the 2-d Heisenberg Antiferromagnet. Although this model has its own merit, we are going to show that the nature of its excitations makes it a natural D -theory formulation of the physics of 2-d $O(3)$ spins.

6.2 The 2-d Heisenberg Antiferromagnet

Since the discovery of high-temperature superconductivity, the $2-d$ Heisenberg quantum antiferromagnet has been the subject of many theoretical investigations. It has been found experimentally that the precursor insulators like La_2CuO_4 or $\text{Sr}_2\text{CuO}_2\text{Cl}_2$, which under doping can turn into superconductors, have crystal structure where the dominant interaction is between neighboring atoms fixed on the sites of square lattice planes. Neutron scattering has experimentally verified long range order in these materials [38]. This is the Néel ordered state in which spins are arranged with alternating orientations on alternating lattice sites, therefore with a spontaneously generated staggered magnetization. Correlation lengths are observed to grow exponentially large with the inverse temperature as the temperature is lowered towards zero.

From the field-theoretic point of view, the ordered state of these materials signals the existence of infinite correlations and therefore massless excitations in the dynamics of the system. These characteristics are described by the $2-d$ Heisenberg Hamiltonian

$$H = J \sum_{\mathbf{x}, \hat{\mu}=1,2} [S_{\mathbf{x}}^1 S_{\mathbf{x}+\hat{\mu}}^1 + S_{\mathbf{x}}^2 S_{\mathbf{x}+\hat{\mu}}^2 + S_{\mathbf{x}}^3 S_{\mathbf{x}+\hat{\mu}}^3] \quad (6.1)$$

with the antiferromagnetic coupling $J > 0$. A spin operator $\vec{S}_{\mathbf{x}} = (S_{\mathbf{x}}^1, S_{\mathbf{x}}^2, S_{\mathbf{x}}^3)$ is defined on every site \mathbf{x} of the square lattice satisfying the local $SU(2)$ algebra

$$[S_{\mathbf{x}}^a, S_{\mathbf{y}}^b] = i\delta_{\mathbf{x}\mathbf{y}}\epsilon^{abc}S_{\mathbf{x}}^c. \quad (6.2)$$

The Hamiltonian is invariant under global $SO(3)$ rotations of the spin operators. These rotations are generated by the total spin operator $\sum_{\mathbf{x}} \vec{S}_{\mathbf{x}}$ which is therefore

conserved

$$[H, \sum_{\mathbf{x}} \vec{S}_{\mathbf{x}}] = 0. \quad (6.3)$$

Numerical simulations [39, 40, 41] study the quantum partition function of the model at temperature $T = 1/\beta$,

$$Z = \text{Tr} \exp(-\beta H), \quad (6.4)$$

which is also pictured as describing the evolution of the system for a Euclidean time interval β . They have shown that the staggered magnetization,

$$\vec{M} = \sum_{\mathbf{x}=(\mathbf{x}_1, \mathbf{x}_2)} (-1)^{\mathbf{x}_1 + \mathbf{x}_2} \vec{S}_{\mathbf{x}}, \quad (6.5)$$

which is not conserved, gets a non-zero expectation value as $\beta \rightarrow \infty$, signaling therefore a phase transition at zero temperature. The simulations show that indeed the correlation length grows exponentially with β as $\beta \rightarrow \infty$ and therefore verify the long range order.

The physics of this growth can be understood. When the staggered magnetization becomes non-zero, a direction is preferred in the internal spin space and therefore the $SO(3)$ rotational symmetry of the spins breaks spontaneously to the $SO(2)$ rotations around the preferred direction. According to the classic analysis by Goldstone on the spontaneous breaking of global symmetries, a number of massless particles — Goldstone bosons — will appear. Their number equals the number of broken symmetry generators which in this system is the number of $SO(3)$ generators minus the number of $SO(2)$ generators, i.e. $3 - 1 = 2$. These fields belong to the coset space $SO(3)/SO(2) \simeq S^2$. Therefore, the two Goldstone bosons can be described by the classical $O(3)$ spin vectors \vec{e} with $\vec{e} \cdot \vec{e} = 1$. For the 2-d Heisenberg antiferromagnet these fields describe the antiferromagnetic magnons.

The partition function (6.4) describes a classical theory in a (2+1)-d slab with time extent β . For large β , the physics is dominated by the Goldstone fields and is to a large extent determined by the $O(3)$ symmetry. The system is in the universality class of the 3-d $O(3)$ non-linear σ -model. Therefore, at low energy we can write an effective

$O(3)$ action based on the simplest interaction between the magnons. Following the principles of chiral perturbation theory, this action has been written [42] as

$$S[\vec{e}] = \int_0^\beta dt \int d^2x \frac{\rho_s}{2} [\partial_\mu \vec{e} \cdot \partial_\mu \vec{e} + \frac{1}{c^2} \partial_t \vec{e} \cdot \partial_t \vec{e}], \quad (6.6)$$

with the spin stiffness ρ_s and the spin-wave velocity c . In this framework of *chiral perturbation theory*, higher derivative terms would be needed to capture the behavior of the magnons at higher energies. For β strictly infinite, the theory is effectively the 3-d $O(3)$ non-linear σ -model. In the ground state, the spin vectors are spontaneously oriented along a direction and the symmetry is broken to the $O(2)$ rotations around the direction of the staggered magnetization. Therefore we understand the infinite correlations as due to the existence of Goldstone bosons in the $3 - d$ volume.

Now consider the slab with large but still finite β . The correlation length of the magnons — as will be shown later — is much larger than β . The Euclidean time extent is negligible compared to this scale of the theory and therefore can be safely ignored. The system appears *dimensionally reduced* to a 2-d theory of interacting magnons. For the action (6.6) dimensional reduction amounts to ignoring the time dependence of \vec{e} , i.e. setting $\partial_t \vec{e} = 0$. The time integration is then performed trivially. The magnons appear as the interacting fields of the 2-d $O(3)$ non-linear σ -model,

$$S[\vec{e}] = \frac{1}{2g} \int d^2x \partial_\mu \vec{e} \cdot \partial_\mu \vec{e}, \quad (6.7)$$

with the coupling

$$g = \frac{1}{\beta \rho_s}. \quad (6.8)$$

The Coleman-Mermin-Wagner theorem [3] forbids the spontaneous breaking of a continuous global symmetry in two-dimensional field theories. Although the $O(3)$ action (6.7) has no scale classically, a scale is generated non-perturbatively from the quantum fluctuations. The magnons acquire a non-perturbative mass which has been

computed [7] in the \overline{MS} scheme

$$m = \frac{8}{e} \Lambda_{\overline{MS}} \quad (6.9)$$

and therefore the correlation length is kept finite due to non-perturbative effects.

A more elaborate picture to understand the non-perturbative mass of the magnons at low temperatures has been suggested by Hasenfratz and Niedermayer [43]. A block-spin renormalization group transformation can be performed on the (2+1)-d slab by averaging the fields in a cube and defining the average field at the center of the cube. The length of the cube in the time direction is β since the theory is strongly correlated along this direction. Due to the spin-wave velocity c , the scale of correlations along the spatial directions is βc and therefore the spatial side of the averaging cube is taken to be βc . The result of this RG transformation is the mapping of the theory in the slab to a 2-d lattice theory defined on a coarse lattice with spacing $a' = \beta c$, different from the original quantum spin lattice spacing a . Furthermore, since the nature of this RG transformation is to integrate out the fields of the continuum, the resulting action is the fixed point action for the $O(3)$ non-linear σ -model on a coarse lattice. As argued in part I, this action is free of any lattice artifacts and therefore, after dimensional reduction, any lattice artifacts will be entirely due to the spacing of the microscopic quantum spin lattice.

We can finally derive the exponential growth of the magnon correlation length with the inverse temperature. At large β , we see from (6.8) that we are in the weak coupling region of the 2-d effective $O(3)$ model. In this phase we can trust the perturbative beta-function of the model to predict the scaling of the coupling. The beta-function $\beta(g)$ describes the change of the coupling with the momentum cutoff $\Lambda = 1/a'$ given the reference scale m and in one-loop perturbation theory is given by

$$\frac{d}{d \ln \frac{\Lambda}{m}} g(\Lambda) \equiv \beta(g) = -\frac{1}{2\pi} g^2. \quad (6.10)$$

Integrating this relation at large Λ we get

$$\frac{\Lambda}{m} \sim \exp\left(\frac{2\pi}{g}\right) \quad (6.11)$$

and using (6.8) we confirm the exponential growth of the correlation length at low temperatures

$$\xi = m^{-1} \propto \exp(2\pi\beta\rho_s) . \quad (6.12)$$

Dimensional reduction therefore occurs as β approaches infinity, which from (6.8) gives the continuum limit $g \rightarrow 0$ of the classical $O(3)$ spin model.

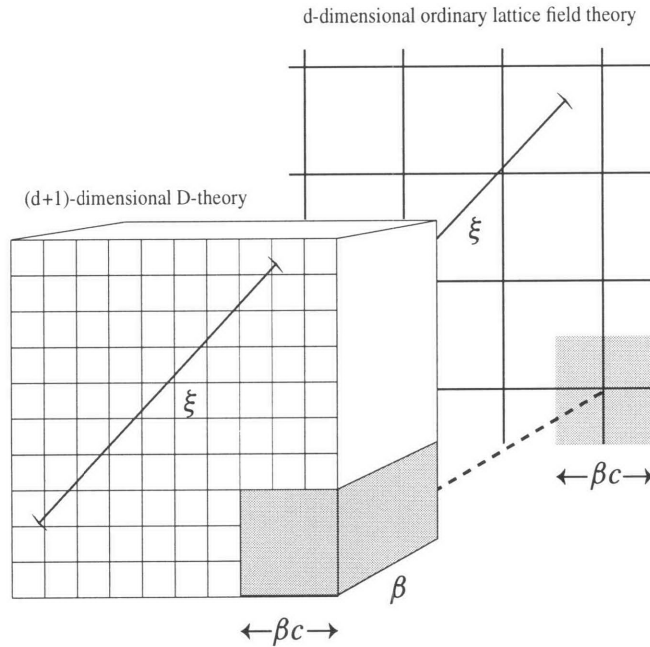


Figure 6-1: *Dimensional reduction of a D-theory: Averaging the $(d + 1)$ -dimensional effective field of the D-theory over blocks of size β in the extra dimension and βc in the physical directions results in an effective d -dimensional Wilsonian lattice field theory with lattice spacing βc .*

The experimental neutron scattering data [38, 44] do not agree with the higher loop analysis [45, 43] of the correlation length growth. The available numerical data around $\xi \approx 10^2 a$ — where a is the actual lattice spacing of the undoped antiferromagnetic planes — agree with the scaling predicted by the four-loop beta function. The numerical simulation of the 2-d Heisenberg antiferromagnet with the loop-cluster algorithm in continuous time [41, 46], as described in chapters 11 and 12, combined

with the precisely-known finite size scaling behavior of the $O(3)$ model [47, 48] has provided accurate data for correlation lengths up to $\xi \approx 10^5 a$ where the three-loop asymptotic scaling sets in. The fact that asymptotic scaling sets in at correlation lengths $10^5 a$ and not $10^5 a'$ as one would naively expect for the $O(3)$ model [47], confirms that the dimensional reduction leads to a perfect $O(3)$ action on the coarse lattice of lattice spacing a' with lattice artifacts entirely due to the microscopic lattice spacing a .

Besides the extremely interesting applications of quantum antiferromagnets in condensed matter physics, its presentation here has a different motivation. What we actually want to emphasize is the field-theoretic approach to the study of the $O(3)$ non-linear σ -model. For that reason, we quantized the spin variables and constructed the antiferromagnetic Hamiltonian which leads to a spontaneously ordered ground state at zero temperature. Due to this order, the Goldstone bosons are collective excitations of the *discrete* spin states which provide infinite correlations in the (2+1)-d theory. Dimensional reduction of these fields results in the 2-d theory of classical spin fields. The dynamically generated mass-gap of the $O(3)$ model has been connected with the low temperature mass of the magnons. Therefore, a new non-perturbative treatment of the $O(3)$ theory has been obtained, formulated entirely in terms of discrete variables. This formulation will be our *paradigm* for the D -theory description of gauge theories which will be presented in the next chapter.

Chapter 7

Non-Abelian Gauge Theories on a Lattice: Classical and Quantum Links

7.1 Introduction

Gauge symmetry stands at the heart of our understanding of the fundamental interactions in Nature. The theory which describes the interaction of light with charged matter is Quantum Electrodynamics (QED). QED is a quantum field theory which exhibits the phenomenon of invariance under local Abelian transformations of the photon and the charged fermion fields. In QED the photon is described by a spin-1 field A_μ while the electron is described by a Dirac spinor field Ψ . The Euclidean Lagrangian of the theory is

$$\mathcal{L}_{QED} = \frac{1}{4} F_{\mu\nu} F_{\mu\nu} + \bar{\Psi}(\gamma_\mu \partial_\mu + m)\Psi + e\bar{\Psi}\gamma_\mu A_\mu \Psi \quad (7.1)$$

where $F_{\mu\nu} = \partial_\mu A_\nu - \partial_\nu A_\mu$ is the field strength, e is the electron charge and γ_μ the Euclidean Dirac matrices which satisfy $\{\gamma_\mu, \gamma_\nu\} = 2\delta_{\mu\nu}$.

This Lagrangian is invariant under Abelian gauge transformations of the fields

$$A'_\mu(x) = A_\mu(x) + \frac{1}{e} \partial_\mu \alpha(x), \quad \Psi'(x) = \exp(i\alpha(x))\Psi(x), \quad \bar{\Psi}'(x) = \bar{\Psi}(x) \exp(-i\alpha(x)) \quad (7.2)$$

Quantization of this action with the usual commutation and anticommutation relations for the bosonic and fermionic fields along with a perturbative expansion in terms of the coupling constant e results in excellent understanding of all the electromagnetic phenomena in Nature. The key of this success is the fact that the expansion is carried out in terms of the fine structure constant $\alpha = e^2/4\pi \simeq 1/137$ and therefore a few Feynman diagrams are enough to give excellent agreement with experimental data. Renormalization theory predicts that the interaction gets stronger and α gets larger as the energy is increased, but the rate of increase is slow and the perturbative analysis is very reliable at all energy scales reached by experiment.

Yang and Mills generalized QED to a theory exhibiting invariance under non-Abelian local transformations of the fields. The photon field is promoted to a Lie Algebra valued vector field, $A_\mu = A_\mu^a T^a$, which describes a set of *gauge bosons* A_μ^a . The T^a s are the Hermitian generators of a Lie Algebra in the fundamental representation with commutation relations and normalization

$$[T^a, T^b] = i f^{abc} T^c, \quad \text{Tr}(T^a T^b) = \frac{1}{2} \delta^{ab}. \quad (7.3)$$

The Yang-Mills Lagrangian is formulated in terms of the non-Abelian field strength

$$F_{\mu\nu} = F_{\mu\nu}^a T^a$$

$$\mathcal{L}_{YM} = \frac{1}{2} \text{Tr} F_{\mu\nu} F_{\mu\nu}, \quad F_{\mu\nu} = \partial_\mu A_\nu - \partial_\nu A_\mu - ig[A_\mu, A_\nu], \quad (7.4)$$

with a dimensionless coupling constant g in four dimensions.

A local transformation $U(x) = \exp(i\alpha^a T^a)$ transforms the gauge field inhomogeneously

$$A'_\mu(x) = U(x)A_\mu(x)U^\dagger(x) - \frac{i}{g}U(x)\partial_\mu U^\dagger(x), \quad (7.5)$$

it transforms the field strength and the covariant derivative $D_\mu = \partial_\mu + igA_\mu$ homogeneously

$$F'_{\mu\nu}(x) = U(x)F_{\mu\nu}(x)U^+(x), \quad D'_\mu(x) = U(x)D_\mu(x)U^+(x) \quad (7.6)$$

and leaves the Yang-Mills Lagrangian invariant.

Charged fields under the gauge group can be easily introduced as covariantly coupled to the gauge field. These theories are central in the Standard Model describing both the weak and strong interactions of Nature. Quantum Chromodynamics (QCD) describes the strong interaction sector of the Standard Model. It assumes that an $SU(3)$ gauge theory describes the strong interaction between quarks and gluons. The strong interactions are mediated by 8 gauge bosons — the gluons — and each quark takes one of three color values, i.e. transforms in the fundamental representation of $SU(3)$. The gluons are also charged and therefore self-interacting. They transform under the adjoint representation of $SU(3)$. The Euclidean QCD Lagrangian has the form

$$\mathcal{L}_{QCD} = \frac{1}{2} \text{Tr} F_{\mu\nu} F_{\mu\nu} + \sum_{f=1}^{N_f} \left(\bar{\Psi}_f \gamma_\mu (\partial_\mu + m_f) \Psi_f + g \bar{\Psi}_f \gamma_\mu A_\mu \Psi_f \right) \quad (7.7)$$

for a number of flavored quarks of mass m_f . Ψ_f denotes an $SU(3)$ triplet of colored quarks with $\bar{\Psi}_f$ the corresponding anti-triplet of antiquarks.

Despite the simplicity of the appearance, QCD incorporates extremely diverse and complicated phenomena. A perturbative analysis indicates that the coupling constant gets smaller, i.e. the interaction gets *weaker*, as the energy scale is increased. This is the effect of *asymptotic freedom*; the expectation that quarks and gluons become free at very high energies. At energy scales of a few GeV, the coupling is small enough that the perturbative description through Feynman diagrams becomes reliable. Cross sections involving quarks and gluons carrying high energy can be estimated and compare favorably with experimental data building a strong confidence that we have the correct theory of strong interactions.

On the other end, we do not observe quarks and gluons as free particles. Instead we see the colorless bound states we call hadrons: the fermionic baryons — among

them the proton and the neutron — and the lighter unstable bosons we call mesons. This is the effect of *confinement*; the colored constituents are permanently confined in the hadrons.

QCD develops a scale quantum mechanically through the regularization of Feynman diagrams in perturbation theory. This scale in the \overline{MS} scheme is roughly estimated to be $\Lambda_{\overline{MS}} \approx 150$ MeV. The hadronic states appear with quantum numbers consistent with the fact that the constituent particles are the $SU(3)$ -colored, spin-1/2, fractionally charged quarks. Only the three lighter quarks, up, down and strange are relevant to low-energy QCD. Considering that the up and down quarks have masses of 5-10 MeV but the pions appear with a mass around 150 MeV and the nucleons with a mass around 1 GeV, we see that the binding effects are very strong. The mass of the hadrons is a non-perturbative quantity and therefore a connection to the scale $\Lambda_{\overline{MS}}$ cannot be derived in the diagrammatic expansion of QCD. The phenomenological approach to low energy QCD is based on the fact that the light quarks appear almost massless compared to the scales of the pions and the nucleons. The approximate chiral symmetry gets spontaneously broken at low energies and the pseudoscalar mesons are naturally identified as Goldstone bosons. An analytical understanding of the chiral symmetry breaking mechanism in QCD is also not available at present time.

Despite the lack of an analytical understanding of the confinement in QCD, a mechanism which asserts confinement does exist. Confinement of the quarks means that the chromoelectric field between two colored charges does not spread out in space as the electric field between two electric charges does. Instead, it is confined in a narrow *flux tube* between the quarks. Based on that, 't Hooft and Mandelstam have proposed [49, 50] that the ground state of QCD should behave like a type II superconductor. In a type II superconductor the so-called Meissner effect takes place. Electrons couple into Cooper pairs and condense in the superconducting ground state. The ground state becomes perfectly diamagnetic which means that the magnetic field gets expelled from the superconducting region. If two magnetically charged objects are kept in the region, then the magnetic flux forms a narrow tube — named Abrikosov line — which connects the magnetic charges and has an energy proportional to its

length.

A favorite picture for QCD confinement is that a dual Meissner effect appears. Non-Abelian magnetic monopoles condense in the vacuum and restrict the chromo-electric fields into bound states. The flux tube has an energy proportional to its length, therefore a linear potential connecting the quark pair would naturally arise. The *string tension* which is the energy per length of the tube is a very important phenomenological parameter that needs to be computed in some frame. If the quarks are dynamical, then it is understood that, as we invest energy trying to separate them into asymptotic states, a quark-antiquark pair will be created from the vacuum and break the tube into two new hadronic states enforcing the permanent confinement of color.

The belief in this picture has been enforced by non-perturbative results that became available during the last years in supersymmetric formulations of QCD(SQCD). The ground state of $\mathcal{N} = 2$ SQCD has been found analytically [51] and presents confinement due to the dual Meissner effect, i.e. condensation of magnetic monopoles. The assumption that the same is true for Nature's QCD is being examined in the non-perturbative lattice formulation for QCD that we are going to discuss next.

7.2 Wilson Formulation of Non-Abelian Gauge Theories

A very important framework for the non-perturbative understanding of gauge theories was presented by Wilson in 1974 [52]. Wilson regularized the infinities that plague continuum field theory by replacing space-time with a four-dimensional hypercubic lattice of spacing a . He introduced as fundamental gauge degrees of freedom the parallel transporters $u_{x,\mu}$ which are the Wilson lines of the continuum gauge theory between two neighboring sites

$$u_{x,\mu} = \mathcal{P} \exp\left(i \int_x^{x+\hat{\mu}} dy A_\mu(y)\right). \quad (7.8)$$

Here we consider a general $SU(N)$ gauge theory. Therefore the parallel transporters are members of an $SU(N)$ group living on the *links* connecting the lattice sites. Under gauge transformations the parallel transporter transforms as a Wilson line usually does, i.e. by group elements at both ends of the oriented path

$$u'_{x,\mu} = \exp(i\alpha_x^a T^a) u_{x,\mu} \exp(-i\alpha_{x+\hat{\mu}}^a T^a). \quad (7.9)$$

For the $SU(N)$ group, a runs over the $N^2 - 1$ generators T^a . Let us consider the *plaquette variable* $U_{x,\mu\nu}$ as the discretized version of a Wilson loop around an elementary plaquette of sites

$$U_{x,\mu\nu} = \text{Tr}[u_{x,\mu} u_{x+\hat{\mu},\nu} u_{x+\hat{\nu},\mu}^\dagger u_{x,\nu}^\dagger]. \quad (7.10)$$

By construction, the plaquette variable is gauge invariant and the Wilson action for the $SU(N)$ gauge theory takes the form

$$S_{gauge}[u] = \frac{2N}{g^2} \sum_{x,\mu < \nu} \left(1 - \frac{1}{2N} [U_{x,\mu\nu} + U_{x,\mu\nu}^\dagger] \right). \quad (7.11)$$

This action has the correct continuum limit as the lattice spacing a tends to zero. This can be seen easily if we consider a gluon field A_μ^a on each link and replace the parallel transporters $u_{x,\mu} \rightarrow \exp(iaA_{x,\mu}^a T^a)$.

The plaquette variables then can be approximated as

$$U_{x,\mu\nu} = \text{Tr}[\exp(iaA_{x,\mu}) \exp(iaA_{x+\hat{\mu},\nu}) \exp(-iaA_{x+\hat{\nu},\mu}) \exp(-iaA_{x,\nu})]. \quad (7.12)$$

Carrying out the Taylor expansion $A_{x+\hat{\mu},\nu} \simeq A_{x,\nu} + a\partial_\mu A_{x,\nu} + \dots$ and using the Baker-Hausdorff lemma $e^X e^Y = e^{X+Y+\frac{1}{2}[X,Y]+\dots}$ we get for the plaquette, keeping the lowest orders in a ,

$$U_{x,\mu\nu} \simeq \text{Tr} \left[\exp(iaA_{x,\mu}) \exp \left(ia(A_{x,\nu} + a\partial_\mu A_{x,\nu} + \dots) \right) \right. \\ \left. \exp \left(-ia(A_{x,\mu} + a\partial_\nu A_{x,\mu} + \dots) \right) \exp(-iaA_{x,\nu}) \right] \quad (7.13)$$

$$\begin{aligned}
&\simeq \text{Tr} \left[\exp \left(ia(A_{x,\mu} + A_{x,\nu} + a\partial_\mu A_{x,\nu} + \frac{1}{2}ia[A_{x,\mu}, A_{x,\nu}] + \dots) \right) \right. \\
&\quad \left. \exp \left(-ia(A_{x,\mu} + A_{x,\nu} + a\partial_\nu A_{x,\mu} - \frac{1}{2}ia[A_{x,\mu}, A_{x,\nu}] + \dots) \right) \right] \\
&\simeq \text{Tr} \left[\exp \left(ia^2(\partial_\mu A_{x,\nu} - \partial_\nu A_{x,\mu} + i[A_{x,\mu}, A_{x,\nu}]) + \mathcal{O}(a^3) \right) \right] \\
&= \text{Tr} \exp \left(ia^2 F_{x,\mu\nu} + \mathcal{O}(a^3) \right) \simeq \text{Tr} \left[1 + ia^2 F_{x,\mu\nu} - \frac{a^4}{2} F_{x,\mu\nu} F_{x,\mu\nu} + \mathcal{O}(a^5) \right] \\
&\simeq N - \frac{a^4}{2} \text{Tr} F_{x,\mu\nu} F_{x,\mu\nu} + \mathcal{O}(a^5).
\end{aligned}$$

Notice that the $\mathcal{O}(a^3)$ correction in the plaquette is a commutator and therefore its trace vanishes. Therefore, for small spacing a the Wilson action approaches

$$\begin{aligned}
S_{gauge}[u] &= \frac{2N}{g^2} \sum_{x,\mu<\nu} \left(1 - \frac{1}{2N} [U_{x,\mu\nu} + U_{x,\mu\nu}^\dagger] \right) \quad (7.14) \\
&\simeq \frac{2N}{g^2} \sum_{x,\mu<\nu} \left(1 - \frac{1}{2N} (2N - a^4 \text{Tr} F_{x,\mu\nu} F_{x,\mu\nu}) \right) = \frac{1}{2g^2} \sum_{x,\mu\neq\nu} a^4 \text{Tr} F_{x,\mu\nu} F_{x,\mu\nu} \\
&\longrightarrow \frac{1}{2g^2} \int d^4x \text{Tr} F_{\mu\nu} F_{\mu\nu},
\end{aligned}$$

which is the correct Euclidean action for a four-dimensional non-Abelian gauge theory.

The Wilson action is not the only lattice action that has the correct continuum limit as a becomes small. Gauge invariant terms with higher order dependence on a are certainly allowed since they become irrelevant for small a . In fact, as discussed in part I of this thesis, such terms can be used in order to construct an action with improved scaling properties. As we have seen explicitly in the $O(N)$ classical spin model, the renormalization group flow indicates that a perfect action exists which is free of any lattice artifacts. Although finding the perfect action for QCD seems very difficult, *improved actions* which add higher order terms in a and suitably eliminate lattice errors to $O(a)$ or $O(a^2)$ have been constructed and used with encouraging results.

Fermions can be easily included in this formalism with a suitable discretization of the Dirac action. The fermions are defined on the sites of the lattice and are minimally coupled to the link elements. Wilson proposed the complete lattice QCD

action with naive discretization

$$\begin{aligned}
S_{QCD}[u, \Psi, \bar{\Psi}] &= S_{gauge}[u] + (m_q + 4r) \sum_x \bar{\Psi}_x \Psi_x \\
&- \frac{1}{2} \sum_{x, \mu} [\bar{\Psi}_{x+\hat{\mu}}(r + \gamma_\mu) u_{x, \mu}^\dagger \Psi_x + \bar{\Psi}_x (r - \gamma_\mu) u_{x, \mu} \Psi_{x+\hat{\mu}}].
\end{aligned}
\tag{7.15}$$

Due to the first order derivative structure of the Dirac operator extra unphysical states appear for the fermions. This *fermion doubling problem* was eliminated by Wilson with the introduction of the r dependent terms. Unfortunately, these terms now violate explicitly the chiral symmetries of the quarks even when their bare mass m_q is zero. In order to study the chiral symmetry breaking on the lattice we have to fine-tune m_q such that the pion on the lattice appears massless. Ways out of this problem have been proposed in the last years. The *domain wall fermions* [53, 54, 55] make use of a fifth unphysical dimension where two domain walls transverse to the 4-d physical universe are defined. Fermion modes with properly selected boundary conditions on the walls result in massless fermions without fine tuning in the 4-d bulk. Another way is to use the *Wilson-Ginsparg* fermions, defined through a local discrete Dirac operator which involves the fields at any distance with exponentially small couplings. This operator satisfies a certain defining relation which turns out to maintain the chiral properties of the quarks without fine-tuning.

The study of QCD can now be rephrased as a study of a statistical mechanics system. We have to simulate the partition function

$$Z = \int \mathcal{D}u \mathcal{D}\Psi \mathcal{D}\bar{\Psi} \exp(-S_{QCD}[u, \Psi, \bar{\Psi}])
\tag{7.16}$$

by properly generating a Markov chain of configurations of the fields on the lattice. Correlation functions of various fields can easily be studied by constructing the wave functions with proper quantum numbers and averaging the values of these fields. In order to extract physical results we need to approach the continuum limit. The continuum limit is approached as the lattice spacing is driven to zero while keeping the physical mass scales fixed, i.e. under the limit $ma \rightarrow 0$. Inversely, in a given

simulation with finite lattice spacing, we must have large correlations in order to measure successfully the physical particle masses. In that sense, the continuum limit is approached in the critical region of the theory which is at bare coupling $g \rightarrow 0$.

The difficulty of the problem lies precisely in the fact that we cannot update efficiently lattice QCD at criticality. Only local algorithms are available so far for QCD. The Metropolis algorithm has a dynamical exponent $z \approx 2$ while the state of the art overrelaxation algorithm which is presently used has dynamical exponent $z \approx 1$. Therefore the critical slowing down problem is still present and makes simulations at criticality difficult. Despite many attempts, efficient cluster algorithms have not been found for QCD or even the simpler $U(1)$ lattice gauge theory. The major amount of work goes into approaching the continuum limit from rather small lattices and time consuming calculations.

7.3 Phases and Order Parameters for Gauge Theories

There are three phases that can appear in a gauge theory and they are identified from the behavior of the Wilson loop order parameter which will be introduced shortly.

i. The Coulomb phase is a phase with massless particles. This is an *ordered phase*, i.e. a phase with infinite correlation lengths, in the corresponding statistical physics system. Charges in the Coulomb phase interact weakly through a Coulomb law, therefore there is no confinement. The Wilson loop in this phase presents a perimeter law behavior.

ii. The confinement phase is a phase with massive particles which are neutral under the gauge group. The correlation length remains finite in physical units. Static charged particles are confined with a linear potential. This fact leads to an area law for the Wilson loop expectation value. If the charges are dynamical then the Wilson loop presents a perimeter law.

iii. The Higgs phase is a phase in which part of or all the gauge symmetry is broken through the Higgs mechanism. Short correlation lengths corresponding to

the massive gauge bosons are naturally introduced in this phase due to the vacuum value of the Higgs field. The electrically charged particles interact weakly and the Wilson loop follows again a perimeter law. In order to distinguish the Higgs phase from the confinement phase one can also construct another order parameter. In order to do that one investigates the behavior of magnetically charged particles in the theory. A dual or magnetic gauge potential responsible for the chromomagnetic fields can under certain assumptions be defined — unambiguously at least for the Abelian gauge theory. The corresponding Wilson loop for the dual potential is called the 't Hooft loop and similarly reflects the interaction between magnetic monopoles. In the Higgs phase the 't Hooft loop shows an area law while in the Coulomb or the confinement phase it has a perimeter law.

The most important order parameter for the study of a gauge theory is the expectation value of the Wilson loop. In the continuum, the Wilson loop is a gauge invariant non-local quantity defined along an oriented space-time path \mathcal{C}

$$W_{\mathcal{C}} = \text{Tr} \mathcal{P} \exp(i \oint_{\mathcal{C}} dx^{\mu} A_{\mu}(x)) , \quad (7.17)$$

while the corresponding lattice theory expression uses the ordered product of parallel transporters on the links along the discretized path

$$W_{\mathcal{C}} = \text{Tr} \prod_{l \in \mathcal{C}} u_l . \quad (7.18)$$

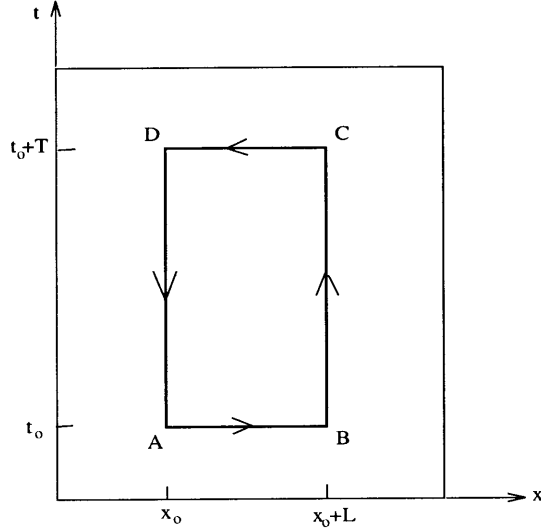
The order parameter studied in the lattice formulation is the expectation value

$$\langle W_{\mathcal{C}} \rangle = \frac{\int \mathcal{D}u \exp(-S_{gauge}[u]) \text{Tr} \prod_{l \in \mathcal{C}} u_l}{\int \mathcal{D}u \exp(-S_{gauge}[u])} . \quad (7.19)$$

The static quark-antiquark potential can be extracted from the rectangular space-time Wilson loop shown below.

Let us consider the Wilson line W_{AB} . Under a gauge transformation it transforms as

$$W_{AB} \longrightarrow g_A W_{AB} g_B^{\dagger} \quad (7.20)$$



The quark-antiquark operator $\Psi_A \bar{\Psi}_B$ creates a quark at B and an antiquark at A and transforms the same way

$$\Psi_A \bar{\Psi}_B \longrightarrow g_A \Psi_A \bar{\Psi}_B g_B^\dagger \quad (7.21)$$

therefore the line W_{AB} creates the external quark-antiquark source at time $t = t_0$. In the Hamiltonian picture, the lines W_{BC} and W_{DA} describe the evolution of the static sources forward and backward in time for the quark and antiquark respectively. Finally, the line W_{CD} which corresponds to the fermionic operator $\Psi_C \bar{\Psi}_D$ destroys the quark at C and the antiquark at D at time $t = t_0 + T$. Therefore, the path integral value for $\langle W_C \rangle$ describes the gluonic system in the presence of a static quark-antiquark pair which lived for a time period T . The Hamiltonian evolution between t_0 and $t_0 + T$ filters out the lowest energy gluonic state in the presence of the two static charges and therefore for very large T the path integral value will be dominated by this state

$$\langle W(L, T) \rangle \sim \exp(-T E_0(L)) . \quad (7.22)$$

The lowest energy $E_0(L)$ is the static quark-antiquark potential which in the confinement phase increases linearly with the distance $E_0(L) = \sigma L$. In the confinement

phase therefore, the order parameter shows the *area law* dependence of the loop

$$\langle W(L, T) \rangle \sim \exp(-\sigma LT) \quad (7.23)$$

from which the string tension can be extracted for large T .

More precisely, we should also take into account the self-energy of the quark sources along the loop which contributes a term proportional to the loop perimeter plus possible constant terms to the energy. Therefore, at large T the confining ground state energy should be parameterized as

$$-\ln \langle W(L, T) \rangle = C_0 + C_1(L + T) + \sigma LT . \quad (7.24)$$

In order to get precise measurements of the string tension in the simulations, the *Creutz ratio* can be defined and it is easy to show that it equals the string tension

$$\chi(L, T) \equiv -\ln \left(\frac{W(L, T) W(L-1, T-1)}{W(L, T-1) W(L-1, T)} \right) = \sigma . \quad (7.25)$$

In the absence of confinement, the ground state energy is dominated by the quark self-energies. Therefore, a *perimeter law* dependence of $\langle W(L, T) \rangle$ for an unbroken gauge theory signals a Coulomb phase.

An important observable for the finite temperature behavior of a gauge theory is the Polyakov line. It requires a finite extent β in the time direction and is simply the Wilson line along a fixed space, time ordered path from 0 to β . In the path integral picture it describes the worldline of a static quark in a field theory with temperature β^{-1} . Therefore, the Polyakov line expectation value is related to the free energy F_q of a static quark in the gluonic system

$$\langle P \rangle = \frac{\int \mathcal{D}u \exp(-S_{gauge}[u]) \text{Tr} \prod_{t=0}^{\beta} u_{\vec{x}t,4}}{\int \mathcal{D}u \exp(-S_{gauge}[u])} \propto \exp(-\beta F_q) . \quad (7.26)$$

Its significance to the finite temperature deconfinement phase transition becomes now evident. In the low temperature phase with confinement, a single quark has infinite

free energy in the gluonic system and therefore $\langle P \rangle = 0$. On the other hand, if at some finite temperature the system becomes deconfined, a single quark only costs a finite amount of free energy and $\langle P \rangle \neq 0$.

It is very interesting to notice that there is a symmetry connected with this order parameter, just like the magnetization of a spin system is connected with the breaking of a global symmetry. For the $SU(N)$ Wilson theory, this is the symmetry of the action under the multiplication of all the links in the time direction in a certain timeslice (e.g. the last) by an element of the center group Z_N of $SU(N)$

$$u_{\vec{x}\beta,4} \longrightarrow u_{\vec{x}\beta,4} \mathcal{Z} \quad , \quad \mathcal{Z} = \exp\left(\frac{2\pi i}{N}n\right) \mathbb{1}_N \quad , \quad n = 0, 1, \dots, N-1 \quad (7.27)$$

where $\mathbb{1}_N$ is the unit $N \times N$ matrix. Since \mathcal{Z} commutes with all the $SU(N)$ group elements, the spacetime plaquettes on the last timeslice which get a factor \mathcal{Z} and a factor \mathcal{Z}^\dagger from their time directed links, remain invariant. On the other hand, the Polyakov line has one time link affected and therefore the order parameter transforms as $P \rightarrow \mathcal{Z}P$.

In the confining phase where $\langle P \rangle = 0$, the order parameter is invariant under the Z_N transformation. If a deconfinement phase exists at high temperature then the order parameter will break the Z_N symmetry. Numerical simulations for the $SU(2)$ and $SU(3)$ Wilson theory confirm that the center symmetry is broken at finite temperature and therefore a deconfining phase exists. Near the phase transition, the standard Landau-Ginzburg action can be constructed based on the long wavelength degrees of freedom. Universality suggests that the order of the phase transition should be the same as that of a three-dimensional Potts-like Z_N spin model. The prediction is a second order phase transition for the $SU(2)$ theory and first order transition for the $SU(3)$ theory, in agreement with the results from Monte Carlo simulations.

If dynamical fermions are added to the gauge theory, the Polyakov line is not an order parameter for deconfinement anymore. In fact, due to screening effects between quarks and gluons a deconfinement order parameter cannot be defined at all. On the other hand, for (almost) massless quarks a chiral phase transition now appears

at finite temperature with $\langle \bar{\Psi}\Psi \rangle$ as an order parameter signaling the existence of a quark-gluon plasma phase.

We have argued so far that the Wilson theory is a well defined gauge theory on a discretized space-time. But it is not *a priori* obvious that the continuum limit will indeed correspond to Nature's QCD. Renormalization arguments of the Wilson theory show that the continuum limit is approached as the coupling g tends to zero. Wilson computed the Wilson loop of the lattice gauge theory at large g and showed an area law, therefore confinement of the charges. There is strong belief based on the numerical simulations that the 4-d non-Abelian lattice gauge theory does not have a phase transition at arbitrarily small values of the coupling. The consensus is that the continuum limit of lattice gauge theory will indeed be Nature's QCD. On the other hand, it has been established numerically that in 5-d the non-Abelian gauge theory has a transition to a deconfined phase at non-zero temperature. This very fact will prove crucial in the development of a model with discrete variables for QCD as will be shown in the next section.

7.4 Quantum Link Formulation of Non-Abelian Gauge Theory

We will now show that quantum versions of $SU(N)$ lattice gauge theory can be constructed [56, 57] in the same sense that quantum spin models were constructed as quantized versions of the classical spin systems in the previous chapter. A special construction of the $SU(2)$ theory was already found in [58]. Since the fundamental variables are based on the links of a lattice, the name “Quantum Link Models” seems natural.

Consider the classical links $u_{x,\mu}$ which are $SU(N)$ matrices in the fundamental representation, therefore $N \times N$ matrices whose elements are complex numbers. We are going to promote them to quantum link operators $U_{x,\mu}$ by quantizing those N^2 complex numbers and keeping the $SU(N)$ matrix structure. Therefore each quantum link is a $N \times N$ matrix of operators.

The models are constructed by simply promoting the Wilson action to a Hamilton operator H by replacing the classical links $u_{x,\mu}$ with the quantum link operators

$$H = -J \sum_{x,\mu < \nu} \text{Tr}[U_{x,\mu} U_{x+\hat{\mu},\nu} U_{x+\hat{\nu},\mu}^\dagger U_{x,\nu}^\dagger + U_{x,\nu} U_{x+\hat{\nu},\mu} U_{x+\hat{\mu},\nu}^\dagger U_{x,\mu}^\dagger]. \quad (7.28)$$

The multiplication between the link operators is the $N \times N$ matrix multiplication and the trace is taken only in the $N \times N$ matrix space. In order to ensure the Hermiticity of H , $U_{x,\mu}^\dagger$ denotes the Hermitian conjugate of $U_{x,\mu}$ in both the operator and the $SU(N)$ matrix space. This $SU(N)$ matrix space is generated from $N^2 - 1$ generators. In this section we work with the Hermitian generators $\lambda^a = 2T^a$ which have commutation relations and normalization

$$[\lambda^a, \lambda^b] = 2if^{abc}\lambda^c \quad , \quad \text{Tr}(\lambda^a \lambda^b) = 2\delta^{ab}. \quad (7.29)$$

For the model to possess the non-Abelian gauge invariance, we require that local gauge

generators G_x^a satisfying the $SU(N)$ algebra exist and commute with the Hamiltonian

$$[H, G_x^a] = 0 \quad , \quad [G_x^a, G_y^b] = 2i\delta_{xy}f^{abc}G_x^c \quad (7.30)$$

The G_x^a are the generators of infinitesimal gauge transformations at the site x and a general unitary operator representing gauge transformations can be constructed

$$\mathcal{G} = \prod_x \exp(-i\alpha_x^a G_x^a) . \quad (7.31)$$

In order to ensure that H is invariant under the action of \mathcal{G} , we require that the link operators transform as

$$U'_{x,\mu} = \mathcal{G} U_{x,\mu} \mathcal{G}^\dagger = \exp(i\alpha_x^a \lambda^a) U_{x,\mu} \exp(-i\alpha_{x+\hat{\mu}}^a \lambda^a) . \quad (7.32)$$

If we consider an infinitesimal gauge transformation at the edges of a link, the LHS of eq.(7.32) becomes

$$\begin{aligned} \exp(-i\alpha_x^a G_x^a) \exp(-i\alpha_{x+\hat{\mu}}^a G_{x+\hat{\mu}}^a) U_{x,\mu} \exp(i\alpha_x^a G_x^a) \exp(i\alpha_{x+\hat{\mu}}^a G_{x+\hat{\mu}}^a) &\simeq \quad (7.33) \\ (1 - i\alpha_x^a G_x^a)(1 - i\alpha_{x+\hat{\mu}}^a G_{x+\hat{\mu}}^a) U_{x,\mu} (1 + i\alpha_x^a G_x^a)(1 + i\alpha_{x+\hat{\mu}}^a G_{x+\hat{\mu}}^a) &\simeq \\ U_{x,\mu} - i\alpha_x^a [G_x^a, U_{x,\mu}] - i\alpha_{x+\hat{\mu}}^a [G_{x+\hat{\mu}}^a, U_{x,\mu}] \end{aligned}$$

while the RHS becomes

$$\begin{aligned} \exp(i\alpha_x^a \lambda^a) U_{x,\mu} \exp(-i\alpha_{x+\hat{\mu}}^a \lambda^a) &\simeq (1 + i\alpha_x^a \lambda^a) U_{x,\mu} (1 - i\alpha_{x+\hat{\mu}}^a \lambda^a) \simeq \quad (7.34) \\ U_{x,\mu} + i\alpha_x^a \lambda^a U_{x,\mu} - iU_{x,\mu} \alpha_{x+\hat{\mu}}^a \lambda^a \end{aligned}$$

and we arrive at the fundamental commutation relations of the links with the generators

$$[G_y^a, U_{x,\mu}] = \delta_{y,x+\hat{\mu}} U_{x,\mu} \lambda^a - \delta_{y,x} \lambda^a U_{x,\mu} . \quad (7.35)$$

These relations can be satisfied if we introduce the generators of the left and right

gauge transformations $L_{x,\mu}^a$ and $R_{x,\mu}^a$ which are naturally defined on the links

$$G_x^a = \sum_{\mu} (R_{x-\hat{\mu},\mu}^a + L_{x,\mu}^a), \quad (7.36)$$

and satisfy independent $SU(N)$ algebras on every link

$$[L_{x,\mu}^a, L_{y,\nu}^b] = 2i\delta_{xy}\delta_{\mu\nu}f^{abc}L_{x,\mu}^c, \quad [R_{x,\mu}^a, R_{y,\nu}^b] = 2i\delta_{xy}\delta_{\mu\nu}f^{abc}R_{x,\mu}^c, \quad [L_{x,\mu}^a, R_{y,\nu}^b] = 0. \quad (7.37)$$

Using eq.(7.36) in eq.(7.35) we find the local commutation relations

$$[L_{x,\mu}^a, U_{y,\nu}] = -\delta_{xy}\delta_{\mu\nu}\lambda^a U_{x,\mu}, \quad [R_{x,\mu}^a, U_{y,\nu}] = \delta_{xy}\delta_{\mu\nu}U_{x,\mu}\lambda^a. \quad (7.38)$$

These relations should not surprise us. In fact the same relations appear in the Hamiltonian formulation of Wilson's theory (see in [59] for a thorough discussion). The difference here is that the U 's are operators which do not commute with the U^\dagger 's and will in general act on a *finite* dimensional Hilbert space per link. In the Wilson theory, the link variable is a group element commuting with its conjugate and lives in the infinite dimensional space of functions on the $SU(N)$ group space.

Let us examine the algebra of operators living on a link. Each link operator consists of N^2 operators or $2N^2$ Hermitian operators $\text{Re}U_{ij}$ and $\text{Im}U_{ij}$ defined from (dropping the link indices)

$$U_{ij} = \text{Re}U_{ij} + i\text{Im}U_{ij}, \quad (U^\dagger)_{ij} = \text{Re}U_{ji} - i\text{Im}U_{ji}. \quad (7.39)$$

We also have the $2(N^2 - 1)$ generators of the $SU(N)_L \otimes SU(N)_R$ transformations and it is possible to embed all these operators in an $SU(2N)$ algebra. Let us define a set of N^2 matrices $M^{(ij)}$ such that $M_{kl}^{(ij)} = \delta_{il}\delta_{jk}$. Then, in the fundamental representation of $SU(2N)$ we can write

$$R^a = \begin{pmatrix} \lambda^a & 0 \\ 0 & 0 \end{pmatrix}, \quad L^a = \begin{pmatrix} 0 & 0 \\ 0 & \lambda^a \end{pmatrix},$$

$$\text{Re}U_{ij} = \begin{pmatrix} 0 & M^{(ij)} \\ M^{(ji)} & 0 \end{pmatrix}, \quad \text{Im}U_{ij} = \begin{pmatrix} 0 & -iM^{(ij)} \\ iM^{(ji)} & 0 \end{pmatrix}. \quad (7.40)$$

It can be checked that these operators have $SU(2N)$ commutation relations

$$\begin{aligned} [\text{Re}U_{ij}, \text{Re}U_{kl}] &= [\text{Im}U_{ij}, \text{Im}U_{kl}] = -i(\delta_{ik} \text{Im}\lambda_{jl}^a R^a + \delta_{jl} \text{Im}\lambda_{ik}^a L^a), \\ [\text{Re}U_{ij}, \text{Im}U_{kl}] &= i(\delta_{ik} \text{Re}\lambda_{jl}^a R^a - \delta_{jl} \text{Re}\lambda_{ik}^a L^a + \frac{2}{N}\delta_{ik}\delta_{jl}T). \end{aligned} \quad (7.41)$$

from which we also learn that

$$[U_{ij}, U_{kl}] = [(U^\dagger)_{ij}, (U^\dagger)_{kl}] = 0, \quad [U_{ij}, (U^\dagger)_{kl}] = 2 \left(\delta_{il}\lambda_{kj}^a R^a - \delta_{kj}\lambda_{il}^a L^a + \frac{2}{N}\delta_{il}\delta_{kj}T \right) \quad (7.42)$$

A new operator T has appeared

$$T = \begin{pmatrix} \mathbb{1} & 0 \\ 0 & -\mathbb{1} \end{pmatrix}, \quad (7.43)$$

which together with the $2N^2$ operators of U and the $2(N^2-1)$ L^a 's and R^a 's complete the $4N^2 - 1$ generators of $SU(2N)$. The significance of T will be appreciated if we notice its commutation relations

$$[T, L^a] = [T, R^a] = 0, \quad [T, U] = 2U, \quad [T, U^\dagger] = -2U^\dagger, \quad (7.44)$$

from which we realize that T is responsible for an extra $U(1)$ gauge symmetry. Indeed, the generator

$$G_x = \frac{1}{2} \sum_{\mu} (T_{x,\mu} - T_{x-\hat{\mu},\mu}) \quad (7.45)$$

will transform the links under an extra local Abelian group

$$U'_{x,\mu} = \prod_y \exp(i\alpha_y G_y) U_{x,\mu} \prod_z \exp(-i\alpha_z G_z) = \exp(i\alpha_x) U_{x,\mu} \exp(-i\alpha_{x+\hat{\mu}}). \quad (7.46)$$

The Hamiltonian presented in eq.(7.28) turns out to describe a $U(N)$ lattice gauge

theory. It is not difficult to turn this into an $SU(N)$ gauge theory. What we have to do is to add a term which breaks the extra $U(1)$ symmetry while respecting the $SU(N)$ invariance. A natural term to select is $\det U_{x,\mu} + \det U_{x,\mu}^\dagger$. This has all the right properties since under $SU(N)$ transforms with the unimodulus elements g_x and $g_{x+\hat{\mu}}$

$$\det U'_{x,\mu} = \det \left(g_x U_{x,\mu} g_{x+\hat{\mu}}^\dagger \right) = \det g_x \det U_{x,\mu} \det g_{x+\hat{\mu}}^\dagger = \det U_{x,\mu}, \quad (7.47)$$

while under the Abelian group

$$\det U'_{x,\mu} = \det \left(\exp(i\alpha_x) U_{x,\mu} \exp(-i\alpha_{x+\hat{\mu}}) \right) = \exp(i\alpha_x) \det U_{x,\mu} \exp(-i\alpha_{x+\hat{\mu}}). \quad (7.48)$$

A quantum link formulation of $SU(N)$ gauge theory is therefore given by

$$H = -J \sum_{x,\mu \neq \nu} \text{Tr} [U_{x,\mu} U_{x+\hat{\mu},\nu} U_{x+\hat{\nu},\mu}^\dagger U_{x,\nu}^\dagger] + J' \sum_{x,\mu} [\det U_{x,\mu} + \det U_{x,\mu}^\dagger]. \quad (7.49)$$

Notice that since $[U_{ij}, U_{kl}] = 0$, there are no operator ordering ambiguities in the definition of $\det U_{x,\mu}$. On the other hand, in the fundamental representation relations (7.40) $\det U_{x,\mu}$ vanishes identically. Therefore, in order to break the extra $U(1)$ successfully we need to choose a representation for the operators where $\det U_{x,\mu}$ will be non-trivial. It will become clear from the rishon representation to be presented later that the lowest representation of $SU(2N)$ with non-trivial $\det U_{x,\mu}$ is the $(2N)!/(N!)^2$ -dimensional one. This means that for the $SU(2)$ and $SU(3)$ quantum link theories we require a 6-dimensional and a 20-dimensional Hilbert space per link respectively, as opposed to the compact group manifolds required per link for the Wilson formulation. Despite this drastic reduction, the gauge symmetry remains intact.

Contrasting the Hamiltonian (7.49) with the Wilson theory Hamiltonian formulation, which can be found in [59], we realize that we can add to the Hamiltonian the electric term constructed from the left and right $SU(N)$ Casimir operators

$$H_{electric} = J_E \sum_{x,\mu} [L_{x,\mu}^a L_{x,\mu}^a + R_{x,\mu}^a R_{x,\mu}^a]. \quad (7.50)$$

Due to the finiteness of the representation and therefore the non-commutativity of U and U^\dagger , the QLM Hamiltonian (7.49) is already a non-trivial dynamical problem in (4+1)-d. As the dimension of the representation becomes very large, the link operators tend to the classical link group elements and (7.49) to the diagonal magnetic energy term of the (4+1)-d gauge theory.

7.5 Dimensional reduction and the Gauss Law

So far we have presented the construction of a Hamiltonian in 4-d which has a local $SU(N)$ symmetry. We are now going to discuss how this theory becomes relevant to the Wilson theory and eventually Nature's theory of strong interactions by following precisely the steps presented for the quantum spins. The quantum link Hamiltonian defines evolution in a fifth Euclidean time coordinate not to be confused with the physical time coordinate which is part of the 4-d lattice. Therefore the quantum partition function appears also as the partition function of a 5-d gauge theory with finite extent β of the fifth direction

$$Z = \text{Tr} \exp(-\beta H). \quad (7.51)$$

The key feature is that the 5-d non-Abelian gauge theory has massless gluonic excitations and therefore infinite correlation lengths. Early numerical evidence of this property was presented by Creutz [60] and a recent study can be found in [61]. Therefore, for finite β the infinite correlation length makes the theory appear dimensionally reduced to the 4-d gauge theory. Notice that we wrote the partition function (7.51) *without* a projection to gauge invariant states in contrast to what is done in ordinary Hamiltonian formulations of gauge theory. As is well known, the Gauss law constraint appears in the path integral formulation as a non-trivial Polyakov line of the 5-d theory with the A_5 component of the gauge potential appearing as the Lagrange multiplier field enforcing the constraint.

It is precisely the non-trivial Polyakov line in the fifth direction that we want to

avoid. The reason is that after dimensional reduction, the fifth direction is lost and the Polyakov line appears as a scalar in 4-d transforming in the adjoint representation of the group. In order to avoid the presence of these scalars we select the temporal gauge $A_5(x) = 0$. Note that for infinite β such a selection is legal as any other gauge selection and the theory would possess a full 5-d gauge invariance. For finite β though, only the 4-d gauge invariance is present. This should not worry us because this is the physical symmetry we want to obtain. We should not worry also if this gauge in finite β spoils the Coulomb phase of the 5-d theory. This is easy to understand if we think that a Coulomb phase implies that massless modes can be excited in the world-volume. If we do not enforce Gauss's law, we simply allow more states to propagate in the world-volume and as long as the ground state remains gauge invariant the massless modes would still be present.

Based on the $SU(N)$ symmetry, we can write a low energy effective action describing the massless gluonic excitations of the 5-d quantum link model with finite β in the $A_5 = 0$ gauge

$$S[A_\mu] = \int_0^\beta dx_5 \int d^4x \frac{1}{2e^2} [\text{Tr} F_{\mu\nu} F_{\mu\nu} + \frac{1}{c^2} \text{Tr} \partial_5 A_\mu \partial_5 A_\mu]. \quad (7.52)$$

The indices μ, ν run over 1 – 4 only. We have defined the 5-d dimensional gauge coupling e and the 5-d velocity of light c (the 4-d velocity of light is set to 1). Given the infinite correlations in this theory, dimensional reduction will take place and we can ignore the x_5 -dependence of A_μ . The x_5 integration is then trivially performed and the reduced theory is non other than

$$S[A_\mu] = \int d^4x \frac{1}{2g^2} \text{Tr} F_{\mu\nu} F_{\mu\nu} \quad (7.53)$$

with effective coupling

$$\frac{1}{g^2} = \frac{\beta}{e^2}. \quad (7.54)$$

We can also imagine the reduced theory as a lattice theory if we repeat the renormalization arguments given by Hasenfratz and Niedermayer [43] for the 2-d Heisenberg

antiferromagnets. We can perform a blocking renormalization step by averaging the field A_μ in the action (7.52) over a cube of size β in the fifth direction. Since β is a time extent and c the velocity of light in 5-d, the blocking cube size in the four physical directions should be βc . The result of such a blocking will be a lattice version of the gauge theory in (7.53) with spacing $a' = \beta c$, different from the quantum link model spacing which is a . Furthermore, we should notice that as with the quantum spins, the blocked action is the fixed point action for the 4-d Wilsonian gauge theory and therefore any finite spacing artifacts are entirely due to the microscopic quantum link lattice.

The 4-d lattice gauge theory approaches its continuum limit as $g \rightarrow 0$. This is due to the asymptotic freedom property of these theories. The beta-function $\beta(g)$ describes the change of the coupling with the momentum cutoff $\Lambda = 1/a'$ given a reference scale m and in one-loop perturbation theory is given by

$$\frac{d}{d \ln \frac{\Lambda}{m}} g(\Lambda) \equiv \beta(g) = -\frac{11N}{48\pi^2} g^3 . \quad (7.55)$$

Integrating this relation at large Λ we get

$$\frac{\Lambda}{m} \sim \exp\left(\frac{24\pi^2}{11Ng^2}\right) \quad (7.56)$$

A mass scale is expected to be generated non-perturbatively in the 4-d gauge theory. The mechanism responsible for that is the confinement of color and creation of glueballs. From the relation (7.54) we see that the continuum limit $g \rightarrow 0$ is reached in the 5-d formulation when $\beta \rightarrow \infty$. Therefore, the dimensional reduction will actually happen for *large* fifth time extent. Using the confinement assumption, it is possible then to predict the scaling of the glueball correlation lengths ξ with β

$$\xi = m^{-1} \propto \exp\left(\frac{24\pi^2\beta}{11Ne^2}\right) . \quad (7.57)$$

We have established now that indeed the 4-d non-Abelian gauge theory has been formulated as a Hamiltonian model with discrete variables. We required an extra

coordinate where the discrete variables can build modes with infinite length correlations and therefore dimensionally reduce to 4-d physics with the usual classical fields. Information about the physical $SU(N)$ spectrum can be found in the correlations of these fields in the physical 4-d volume after the dimensional reduction at large β . Although a fifth dimension is required, the advantage of the formulation is clear. Only a discrete state is required per link, e.g. a 20-state link for the $SU(3)$ theory. It is plausible that powerful cluster algorithms can now be constructed for these models, as has been done for the spin models. In that case, more efficient sampling of the QCD phase space is to be expected with more accurate physical predictions than the ones available today.

The analogy of this construction with the 2-d quantum antiferromagnet physics is complete. The quantum antiferromagnet used the 3-d $O(3)$ broken phase with Goldstone bosons while the quantum links used the 5-d Coulomb phase with massless gluons. Both models exhibit dimensional reduction at large β . A non-perturbative mass gap is generated for the reduced theories, due to the Coleman-Mermin-Wagner theorem for the 2-d spin theory and due to color confinement for the 4-d gauge theory. Finally, the scaling of the mass gap with β and the dimensionless couplings g is the same, dictated by the asymptotic freedom of both theories.

7.6 Rishon formulation of Quantum Link Models

We are now going to present an elegant representation of the algebra of quantum link operators and gauge transformation generators [57, 61]. Recall from section 4 that each link carries its own Hilbert space with $SU(2N)$ generators acting on it with commutation relations

$$\begin{aligned}
[L^a, L^b] &= 2if^{abc}L^c, & [R^a, R^b] &= 2if^{abc}R^c, & [L^a, R^b] &= 0, & (7.58) \\
[L^a, U_{ij}] &= -\lambda_{ik}^a U_{kj}, & [R^a, U_{ij}] &= U_{ik}\lambda_{kj}^a, \\
[T, U_{ij}] &= 2U_{ij}, & [T, R^a] &= [T, L^a] = 0, \\
[U_{ij}, U_{kl}] &= 0, & [U_{ij}, (U^\dagger)_{kl}] &= 2\left(\delta_{il}\lambda_{kj}^a R^a - \delta_{kj}\lambda_{il}^a L^a + \frac{2}{N}\delta_{il}\delta_{kj}T\right).
\end{aligned}$$

These operator relations can be satisfied if we define fundamental fermionic operators on each link. We need two N -plets of fermions associated with the left and right edges of a link. We define $c_{x,\mu}^i, c_{x,\mu}^{i\dagger}$ the fermionic operators at the left of the link $U_{x,\mu}$ i.e. the μ direction of site x , and $c_{x,-\mu}^i, c_{x,-\mu}^{i\dagger}$ the operators at the right of the link $U_{x-\hat{\mu},\mu}$ i.e. the $-\mu$ direction of site x . The index $i = 1, 2, \dots, N$ labels the $SU(N)$ color of the fermions, therefore they transform in the fundamental representation of the left or right gauge transformation groups on the links. We postulate the fundamental anticommutation relations

$$\{c_{x,\pm\mu}^i, c_{y,\pm\nu}^{j\dagger}\} = \delta_{xy}\delta_{\pm\mu,\pm\nu}\delta_{ij}, \quad \{c_{x,\pm\mu}^i, c_{y,\pm\nu}^j\} = \{c_{x,\pm\mu}^{i\dagger}, c_{y,\pm\nu}^{j\dagger}\} = 0. \quad (7.59)$$

These fundamental $2N$ colored fermions that live on each link shall be called *rishons*. We can construct all the $SU(2N)$ operators with them in a way that the relations (7.58) are satisfied

$$\begin{aligned} (U_{x,\mu})_{ij} &= c_{x,\mu}^i c_{x+\hat{\mu},-\mu}^{j\dagger}, & (U_{x,\mu}^\dagger)_{ij} &= c_{x+\hat{\mu},-\mu}^i c_{x,\mu}^{j\dagger} \\ L_{x,\mu}^a &= \sum_{i,j} c_{x,\mu}^{i\dagger} \lambda_{ij}^a c_{x,\mu}^j, & R_{x,\mu}^a &= \sum_{i,j} c_{x+\hat{\mu},-\mu}^{i\dagger} \lambda_{ij}^a c_{x+\hat{\mu},-\mu}^j \\ T_{x,\mu} &= \sum_i (c_{x+\hat{\mu},-\mu}^{i\dagger} c_{x+\hat{\mu},-\mu}^i - c_{x,\mu}^{i\dagger} c_{x,\mu}^i). \end{aligned} \quad (7.60)$$

We should notice that we can also quantize the rishons with bosonic commutation relations and the representation (7.60) would still hold. However, the determinant of the link operator vanishes and we get back the $U(N)$ gauge symmetry. It can be shown that the rishon number operator

$$\mathcal{N}_{x,\mu} = \sum_i (c_{x+\hat{\mu},-\mu}^{i\dagger} c_{x+\hat{\mu},-\mu}^i + c_{x,\mu}^{i\dagger} c_{x,\mu}^i) \quad (7.61)$$

commutes with all the $SU(2N)$ operators in (7.60) and therefore there is a superselection rule of fixed number of rishons per link. This rule, which fixes the dimensionality of the Hilbert space per link, is equivalent to a selection of a certain irreducible representation of $SU(2N)$ per link.

We can now express the $SU(N)$ gauge theory completely in terms of the rishons. Let us first evaluate the $U(1)$ breaking term

$$\begin{aligned}
\det U_{x,\mu} &= \frac{1}{N!} \epsilon_{i_1 i_2 \dots i_N} (U_{x,\mu})_{i_1 i'_1} (U_{x,\mu})_{i_2 i'_2} \dots (U_{x,\mu})_{i_N i'_N} \epsilon_{i'_1 i'_2 \dots i'_N} \quad (7.62) \\
&= \frac{1}{N!} \epsilon_{i_1 i_2 \dots i_N} c_{x,+ \mu}^{i_1} c_{x+\hat{\mu}, -\mu}^{i_1 \dagger} c_{x,+ \mu}^{i_2} c_{x+\hat{\mu}, -\mu}^{i_2 \dagger} \dots c_{x,+ \mu}^{i_N} c_{x+\hat{\mu}, -\mu}^{i_N \dagger} \epsilon_{i'_1 i'_2 \dots i'_N} \\
&= N! c_{x,+ \mu}^1 c_{x+\hat{\mu}, -\mu}^{1 \dagger} c_{x,+ \mu}^2 c_{x+\hat{\mu}, -\mu}^{2 \dagger} \dots c_{x,+ \mu}^N c_{x+\hat{\mu}, -\mu}^{N \dagger} .
\end{aligned}$$

Notice from the second line that $\det U_{x,\mu}$ is zero if the rishons are quantized as bosons due to the antisymmetry of the ϵ -tensor. In fact it will have a non-trivial action only on a unique state half-filled with N rishons. We conclude that in order to construct an $SU(N)$ quantum link model we must work with fixed $\mathcal{N} = N$ fermionic rishons on every link. The corresponding $SU(2N)$ representation has the dimensionality

$$\binom{2N}{N} = \frac{(2N)!}{(N!)^2} . \quad (7.63)$$

The $SU(N)$ rishon formulated quantum link Hamiltonian is

$$\begin{aligned}
H &= -J \sum_{x,\mu \neq \nu} \sum_{i,j,k,l} \left(c_{x,+ \mu}^i c_{x+\hat{\mu}, -\mu}^{j \dagger} c_{x+\hat{\mu}, +\nu}^k c_{x+\hat{\mu}+\hat{\nu}, -\nu}^{k \dagger} c_{x+\hat{\mu}+\hat{\nu}, -\mu}^l c_{x+\hat{\nu}, +\mu}^{l \dagger} c_{x+\hat{\nu}, -\nu}^m c_{x,+\nu}^{m \dagger} \right) \\
&+ J' \sum_{x,\mu} N! \left[c_{x,+ \mu}^1 c_{x+\hat{\mu}, -\mu}^{1 \dagger} \dots c_{x,+ \mu}^N c_{x+\hat{\mu}, -\mu}^{N \dagger} + c_{x+\hat{\mu}, -\mu}^1 c_{x,+ \mu}^{1 \dagger} \dots c_{x+\hat{\mu}, -\mu}^N c_{x,+ \mu}^{N \dagger} \right] \\
&= J \sum_{x,\mu \neq \nu} (\Phi_{x+\hat{\mu}, -\mu, +\nu} \Phi_{x+\hat{\mu}+\hat{\nu}, -\nu, -\mu} \Phi_{x+\hat{\nu}, +\mu, -\nu} \Phi_{x, +\nu, +\mu}) \\
&+ J' \sum_{x,\mu} N! \left[c_{x,+ \mu}^1 c_{x+\hat{\mu}, -\mu}^{1 \dagger} \dots c_{x,+ \mu}^N c_{x+\hat{\mu}, -\mu}^{N \dagger} + c_{x+\hat{\mu}, -\mu}^1 c_{x,+ \mu}^{1 \dagger} \dots c_{x+\hat{\mu}, -\mu}^N c_{x,+ \mu}^{N \dagger} \right] \quad (7.64)
\end{aligned}$$

where we have also reexpressed the $U(N)$ part in terms of the color singlet ‘‘glueball’’ operators

$$\Phi_{x,\pm\mu,\pm\nu} = \sum_i c_{x,\pm\mu}^{i \dagger} c_{x,\pm\nu}^i . \quad (7.65)$$

The picture that emerges for the $SU(N)$ gauge theory reminds us of an *abacus*. N colored objects live on every link. The plaquette term of the Hamiltonian shifts these objects around the corners of the plaquettes as prescribed from the glueball operators.

Besides, the determinant term acts on every link and shifts the N -plet of rishons from one end of the link to the other. The dynamical evolution of these discrete states in the fifth direction may lead to the excitation of five-dimensional massless gluonic states. For large extent β , the dimensional reduction of this picture is non-other than the 4-d gauge theory.

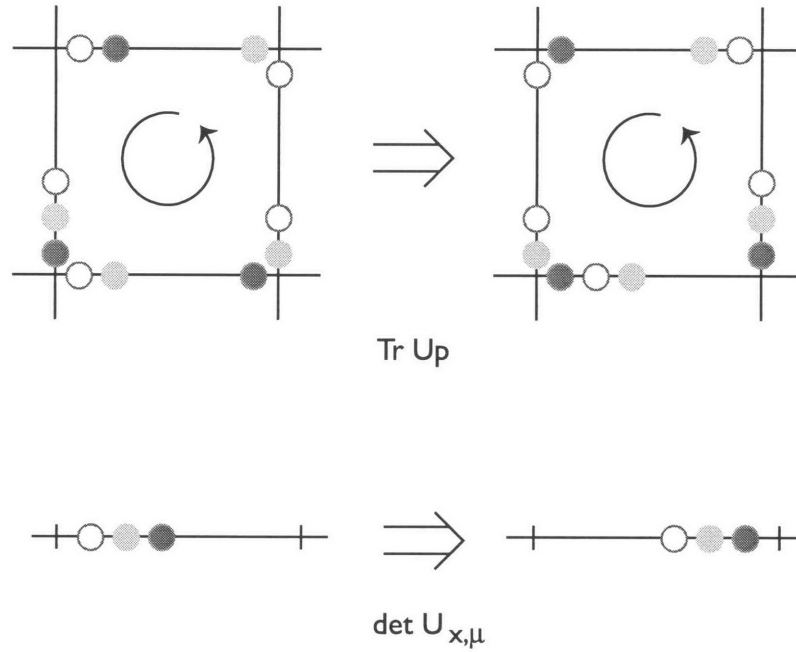


Figure 7-1: *QCD dynamics as a rishon abacus: The trace part of the Hamiltonian induces hopping of rishons of various colors around a plaquette. The determinant part shifts a color-neutral combination of N rishons from one end of a link to the other.*

Chapter 8

Classical and Quantum Spins with Global $U(1)$ Symmetry

8.1 The 2-d Classical XY Model

In this chapter we are going to apply the D -theory approach to the study of the two-dimensional spin model with continuous global Abelian symmetry. The model which goes under the name $O(2)$ Heisenberg magnet or $U(1)$ spin model or simply XY model is by itself interesting because it possesses an infinite order phase transition at finite temperature separating an ordered phase at low temperatures from a phase with short correlations. We will show how a natural quantization of this model in the framework of D -theory results in the 2-d quantum XY model and study the dimensional reduction from the ordered phase to the classical XY model. We will use this model as a playground for the D -theory formulation of the Abelian gauge theory since the 4-d Wilson Abelian gauge theory also has a phase transition at finite coupling separating the Coulomb phase from a disordered confined phase.

There are a couple of equivalent ways to define the spin model with the Abelian symmetry. Consider an $O(2)$ vector $\vec{e}_x = (e_x^1, e_x^2)$ at every site x with $\vec{e}_x^2 = 1$. The

action of the classical $O(2)$ Heisenberg magnet is given by

$$S[\vec{e}] = -\frac{1}{g} \sum_{\mathbf{x}} \sum_{\hat{\mu}=1,2} \vec{e}_{\mathbf{x}} \cdot \vec{e}_{\mathbf{x}+\hat{\mu}}. \quad (8.1)$$

We can solve the unimodulus condition for the $O(2)$ vector by introducing the angle $\varphi_{\mathbf{x}}$ on each site \mathbf{x} with $e_{\mathbf{x}}^1 = \cos \varphi_{\mathbf{x}}$, $e_{\mathbf{x}}^2 = \sin \varphi_{\mathbf{x}}$. Then we obtain the action in the form that we are going to use further

$$\begin{aligned} S[\varphi] &= -\frac{1}{2g} \sum_{\mathbf{x}} \sum_{\hat{\mu}=1,2} \left[\exp(i\varphi_{\mathbf{x}}) \exp(-i\varphi_{\mathbf{x}+\hat{\mu}}) + \exp(-i\varphi_{\mathbf{x}}) \exp(i\varphi_{\mathbf{x}+\hat{\mu}}) \right] \\ &= -\frac{1}{g} \sum_{\mathbf{x}} \sum_{\hat{\mu}=1,2} \cos(\varphi_{\mathbf{x}} - \varphi_{\mathbf{x}+\hat{\mu}}). \end{aligned} \quad (8.2)$$

In this form the invariance under a global $U(1)$ rotation

$$\exp(i\varphi_{\mathbf{x}}) \longrightarrow \exp(i\alpha) \exp(i\varphi_{\mathbf{x}}) \quad (8.3)$$

is transparent. The generator of this transformation is given by

$$G = -i \sum_{\mathbf{x}} \frac{d}{d\varphi_{\mathbf{x}}} \quad (8.4)$$

and satisfies the fundamental commutation relations with the $U(1)$ spins

$$\begin{aligned} [G, \exp(i\varphi_{\mathbf{x}})] &= \exp(i\varphi_{\mathbf{x}}) \quad , \quad [G, \exp(-i\varphi_{\mathbf{x}})] = -\exp(-i\varphi_{\mathbf{x}}) \\ [\exp(i\varphi_{\mathbf{x}}), \exp(-i\varphi_{\mathbf{x}})] &= 0. \end{aligned} \quad (8.5)$$

The last relation although trivial is the statement that the model is formulated with classical fields since a complex number commutes with its conjugate. The quantum spin model as will be shown in the next section is formulated with spin operators which do not commute with their Hermitian conjugates.

The path integral formulation of the model

$$Z = \prod_{\mathbf{x}} \int_{S^1} d\varphi_{\mathbf{x}} \exp(-\beta S[\varphi]) \quad (8.6)$$

has been studied with both analytical and Monte Carlo methods. The numerical simulations of the model have shown that there is a phase transition at some finite critical coupling g_c . The correlation function decays at large distances $|\mathbf{x} - \mathbf{y}|$ as

$$\text{Re}\langle \exp(i\varphi_{\mathbf{x}}) \exp(-i\varphi_{\mathbf{y}}) \rangle \sim \exp(-|\mathbf{x} - \mathbf{y}|/\xi) \quad (8.7)$$

where ξ is the coupling dependent correlation length. It has been found that the correlation length is short for $g > g_c$ and diverges as it approaches the critical coupling. The correlation length stays infinite in the weak coupling region $g < g_c$. We can take the continuum limit of the lattice action (8.1) everywhere in the ordered phase by driving the lattice spacing a to zero

$$\begin{aligned} S[\vec{e}] &= -\frac{1}{g} \sum_{\mathbf{x}} \sum_{\hat{\mu}=1,2} \vec{e}_{\mathbf{x}} \cdot \vec{e}_{\mathbf{x}+\hat{\mu}} = \frac{1}{g} \sum_{\mathbf{x}} a^2 \sum_{\hat{\mu}=1,2} \frac{(\vec{e}_{\mathbf{x}+\hat{\mu}} - \vec{e}_{\mathbf{x}})^2}{2a^2} + \text{constant} \\ &\longrightarrow \frac{1}{2g} \int d^2\mathbf{x} \partial_{\mu} \vec{e}(\mathbf{x}) \cdot \partial_{\mu} \vec{e}(\mathbf{x}), \end{aligned} \quad (8.8)$$

or in terms of the angular variable

$$S[\varphi] \longrightarrow \frac{1}{2g} \int d^2\mathbf{x} (\partial_{\mu} \varphi(\mathbf{x}))^2, \quad (8.9)$$

and recover that the ordered phase is the theory of a massless non-interacting scalar in the 2-d continuum. This scalar is the Goldstone boson of the spontaneous breaking of the $O(2)$ symmetry in the ground state. The breaking occurs because the classical $O(2)$ action is minimized when all the spins pick a direction in the $O(2)$ plane and is allowed by the Coleman-Mermin-Wagner theorem since the Goldstone bosons are not interacting.

The phase transition separating this phase from the disordered phase has been established to be of infinite order and is called the Kosterlitz–Thouless (KT) phase

transition [62]. A phase transition can occur at the thermodynamical limit only, i.e. in the infinite volume limit of the system. An n -th order transition is identified if the quantity

$$\left\langle \frac{\partial^n \ln Z}{\partial \beta^n} \right\rangle \quad (8.10)$$

has a discontinuity at the critical coupling while it is smooth for all powers smaller than n . Since the free energy of the system is defined through $F = -\ln Z$, the n -th order transition signals an n -th order pole of the free energy at the critical value of the (complexified) inverse temperature. The KT phase transition is therefore connected with the existence of an essential singularity at g_c of the free energy of the 2-d classical XY model. Instead of the usual power law divergence of the correlation length $\xi \sim (g/g_c - 1)^{-\nu}$ typical for a second order phase transition, the KT phase transition is characterized by an exponential growth of the correlation length.

Analytical manipulations of the partition function have shown that it can be reexpressed as a gas of vortices with a long-range interaction. These vortices are configurations carrying an integer topological charge. At strong coupling the vortices form a gas which disorders the vacuum and keeps the correlation length short. The topological charge is indefinite in this phase and therefore it is understood that the strong coupling phase of the XY model is a *vortex condensate*. When the coupling is lowered, vortices with charge $+q$ bind with antivortices carrying charge $-q$ into neutral states. The neutral bound states can no longer disorder the vacuum and we expect the transition to a phase with infinite correlation length.

8.2 The 2-d Quantum XY Model

In this section we are going to construct the 2-d quantum XY model as a D -theory approach to the classical $O(2)$ Heisenberg magnet in two dimensions. Although the model is long known to the physics community, we are going to reconstruct it based on the D -theory methodology as a warm-up for the Abelian gauge theory. Recalling the form of the action (8.2) we are going to promote the $U(1)$ spins to non-Hermitian operators defined on the sites. The complex conjugation of the classical spins maps

to the Hermitian conjugation

$$\exp(i\varphi_x) \longrightarrow S_x^+ \quad , \quad \exp(-i\varphi_x) \longrightarrow S_x^- \quad , \quad (8.11)$$

and the quantum XY model will be defined by the Hamiltonian

$$H = -\frac{J}{2} \sum_x \sum_{\hat{\mu}=1,2} [S_x^+ S_{x+\hat{\mu}}^- + S_x^- S_{x+\hat{\mu}}^+] . \quad (8.12)$$

The global $U(1)$ invariance generated by G acts on the spins as

$$\exp(i\alpha G) S_x^+ \exp(-i\alpha G) = \exp(i\alpha) S_x^+ \quad , \quad \exp(i\alpha G) S_x^- \exp(-i\alpha G) = \exp(-i\alpha) S_x^- \quad , \quad (8.13)$$

from which the commutation relations are immediately derived for small α

$$[G, S_x^+] = S_x^+ \quad , \quad [G, S_x^-] = -S_x^- . \quad (8.14)$$

At this point we can decompose $G = \sum_x S_x^3$ and recover the commutation relations of a local $SU(2)$ algebra on every site x

$$[S_x^3, S_x^+] = S_x^+ \quad , \quad [S_x^3, S_x^-] = -S_x^- . \quad (8.15)$$

A *quantum spin* $\vec{S}_x = (S_x^1, S_x^2, S_x^3)$ lives on every site x satisfying the fundamental $SU(2)$ algebra

$$[S_x^a, S_y^b] = i\delta_{xy} \epsilon^{abc} S_x^c \quad , \quad (8.16)$$

while $S_x^\pm = S_x^1 \pm iS_x^2$ are identified with the raising and lowering operators of the quantum spin states. The $U(1)$ invariance is guaranteed by the commutation relations (8.14) which are the same as the classical relations (8.5). What distinguishes the quantum XY model is that it is defined with a finite $SU(2)$ representation where $[S_x^+, S_x^-] = 2S_x^3$ instead of zero.

8.3 Dimensional Reduction to the Classical XY Model

Having defined the quantum spin model with Abelian invariance, we will study as usual its dynamics through the quantum partition function at temperature $T = 1/\beta$

$$Z = \text{Tr} \exp(-\beta H) . \quad (8.17)$$

Once more, this partition function will be interpreted as the partition function of a classical theory defined in the (2+1)-d slab under the evolution of the Hamiltonian in the finite extent β Euclidean time. The theory in the (2+1)-d slab is invariant under $O(2)$ transformations and therefore is in the universality class of the 3-d classical $O(2)$ Heisenberg magnet. It is known that this theory is ordered at low temperatures and describes a massless non-interacting spin-wave. There is a phase transition which separates the spin-wave phase from a disordered phase. We will therefore expect that above a *finite* critical extent β_c we can describe the low energy excitations of the quantum XY model with the action for a massless 3-d spin-wave $\varphi(\mathbf{x}, t)$ at finite temperature

$$S[\varphi] = \int_0^\beta dt \int d^2 \mathbf{x} \frac{\rho_s}{2} [(\partial_\mu \varphi)^2 + \frac{1}{c^2}(\partial_t \varphi)^2] . \quad (8.18)$$

The correlation length is infinite everywhere in the spin-wave phase and therefore the Euclidean time extent β will be negligible compared to the scales over which the theory is correlated. The model will therefore undergo dimensional reduction. This is expressed in the action (8.18) by ignoring the time-dependence of the spin-wave, i.e. by setting $\partial_t \varphi(\mathbf{x}, t) = 0$ and performing the trivial integration in time

$$S[\varphi] \longrightarrow \frac{\beta \rho_s}{2} \int d^2 \mathbf{x} (\partial_\mu \varphi(\mathbf{x}))^2 . \quad (8.19)$$

As promised, we recover the classical XY model action with an induced dimensionless coupling $g = 1/\beta \rho_s$. Since the model is non-interacting, the beta-function is zero and g does not run.

We can again apply the blocking renormalization group transformation to the 3-d spin-wave theory by averaging over the cube with extent β in Euclidean time and βc in the spatial directions. This results in the fixed-point action of the XY model on a square lattice with effective spacing $a' = \beta c$. We have therefore established that the physics of the 2-d quantum XY model in the spin-wave phase is described, after dimensional reduction, by the spin-wave of the classical XY model. As the critical temperature is approached from above, the correlation length of the quantum XY model diverges. Due to dimensional reduction, the correlation length will grow large with an exponential law as predicted by the classical XY model and therefore the phase transition at β_c is expected to be the infinite order Kosterlitz-Thouless transition. The model can be simulated very efficiently with the loop-cluster algorithm as will be described in detail in chapter 11. Simulations of the model in the spin-1/2 representation and a scaling analysis at the critical point indicate [63, 64] that the system undergoes the KT phase transition at finite temperature.

Chapter 9

Abelian Gauge Theory in the Wilson and Quantum Link Formulation

9.1 The Wilson Formulation

The D -theory formulation of the $U(1)$ gauge theory will be presented in this chapter. The theory in the continuum is the non-interacting theory of photons. Wilson formulated gauge theories on a space-time lattice which regularizes the infinities of the continuum. It turns out that the Abelian Wilson theory is a non-trivial theory with interesting phases and the nature of its phase transition is still under investigation and debate. The current numerical investigations of the theory are performed with local algorithms on medium size lattices and are not conclusive. Therefore proposing an alternative non-perturbative formulation of the Abelian lattice gauge theory which further leads to a natural cluster algorithm for numerical simulations seems a well-motivated task.

The Wilson theory is formulated with the parallel transporters

$$u_{x,\mu} = \exp(i \int_x^{x+\hat{\mu}} dy A_\mu(y)) \quad (9.1)$$

as the fundamental fields living on the links connecting two neighboring sites \mathbf{x} and $\mathbf{x} + \hat{\mu}$ of a four-dimensional hypercubic lattice. These fields are simply phases and therefore belong in the infinite dimensional representation of the $U(1)$ group. The Wilson action is

$$S[u] = -\frac{1}{2g^2} \sum_{\mathbf{x}, \mu < \nu} [u_{\mathbf{x}, \mu} u_{\mathbf{x} + \hat{\mu}, \nu} u_{\mathbf{x} + \hat{\nu}, \mu}^\dagger u_{\mathbf{x}, \nu}^\dagger + u_{\mathbf{x}, \nu} u_{\mathbf{x} + \hat{\nu}, \mu} u_{\mathbf{x} + \hat{\mu}, \nu}^\dagger u_{\mathbf{x}, \mu}^\dagger] \quad (9.2)$$

or in term of the $U(1)$ angles $u_{\mathbf{x}, \mu} = \exp(i\varphi_{\mathbf{x}, \mu})$

$$S[\varphi] = \frac{1}{g^2} \sum_{\mathbf{x}, \mu < \nu} [1 - \cos \vartheta_{\mathbf{x}, \mu\nu}] \quad ; \quad \vartheta_{\mathbf{x}, \mu\nu} = \varphi_{\mathbf{x}, \mu} + \varphi_{\mathbf{x} + \hat{\mu}, \nu} - \varphi_{\mathbf{x} + \hat{\nu}, \mu} - \varphi_{\mathbf{x}, \nu} . \quad (9.3)$$

The continuum limit $a \rightarrow 0$ is easy to show if we replace $\varphi_{\mathbf{x}, \mu} \approx aA_\mu(\mathbf{x})$ and Taylor expand

$$\begin{aligned} \vartheta_{\mathbf{x}, \mu\nu} &\approx aA_\mu(\mathbf{x}) + a(A_\nu(\mathbf{x}) + a\partial_\mu A_\nu(\mathbf{x}) + \dots) - \\ &a(A_\mu(\mathbf{x}) + a\partial_\nu A_\mu(\mathbf{x}) + \dots) - aA_\nu(\mathbf{x}) \approx a^2 F_{\mu\nu}(\mathbf{x}) + \mathcal{O}(a^3) \end{aligned} \quad (9.4)$$

from which we get

$$S[\varphi] \approx \frac{1}{g^2} \sum_{\mathbf{x}, \mu < \nu} \left[\frac{\vartheta_{\mathbf{x}, \mu\nu}^2}{2} + \dots \right] \longrightarrow \frac{1}{4g^2} \int d^4\mathbf{x} F_{\mu\nu} F_{\mu\nu}(\mathbf{x}) . \quad (9.5)$$

The Hamiltonian of the theory is defined on a fixed time-slice. The spatial links defined on the 3-d spatial lattice with sites \vec{x} are denoted $u_{\vec{x}, i}$ with $i = 1, 2, 3$. The theory is invariant under the local $U(1)$ transformations defined on the sites \vec{x} of the spatial lattice which transform the links as

$$u_{\vec{x}, i} \longrightarrow \exp(i\alpha_{\vec{x}}) u_{\vec{x}, i} \exp(-i\alpha_{\vec{x} + \hat{i}}) . \quad (9.6)$$

The gauge transformations are generated from the local operators $G_{\vec{x}}$ which act on

the links as

$$\begin{aligned} \exp(i\alpha_{\vec{x}}G_{\vec{x}}) \exp(i\varphi_{\vec{x},i}) \exp(-i\alpha_{\vec{x}}G_{\vec{x}}) &= \exp(i\alpha_{\vec{x}}) \exp(i\varphi_{\vec{x},i}) , \\ \exp(i\alpha_{\vec{x}+\hat{i}}G_{\vec{x}+\hat{i}}) \exp(i\varphi_{\vec{x},i}) \exp(-i\alpha_{\vec{x}+\hat{i}}G_{\vec{x}+\hat{i}}) &= \exp(-i\alpha_{\vec{x}+\hat{i}}) \exp(i\varphi_{\vec{x},i}) . \end{aligned} \quad (9.7)$$

These relations expanded for small $\alpha_{\vec{x}}$ lead to the commutation relations

$$[G_{\vec{x}}, \exp(i\varphi_{\vec{x},i})] = \exp(i\varphi_{\vec{x},i}) , \quad [G_{\vec{x}+\hat{i}}, \exp(i\varphi_{\vec{x},i})] = -\exp(i\varphi_{\vec{x},i}) \quad (9.8)$$

from which the generator $G_{\vec{x}}$ is determined

$$G_{\vec{x}} = \sum_i (G_{\vec{x},i} - G_{\vec{x}-\hat{i},i}) , \quad G_{\vec{x},i} = -i \frac{\partial}{\partial \varphi_{\vec{x},i}} . \quad (9.9)$$

These relations with the following commutation relations define that we work with the classical $U(1)$ links

$$[G_{\vec{x},i}, u_{\vec{x},i}] = u_{\vec{x},i} , \quad [G_{\vec{x},i}, u_{\vec{x},i}^\dagger] = -u_{\vec{x},i}^\dagger , \quad [u_{\vec{x},i}, u_{\vec{x},i}^\dagger] = 0 . \quad (9.10)$$

The quantization of the theory in the Hamiltonian formulation proceeds by first imposing the temporal gauge $u_{\vec{x},0} = 1$ and working on a fixed time-slice. The canonical momentum conjugate to the gauge potential $A_i(\vec{x}) = a^{-1}\varphi_{\vec{x},i}$ is the electric field $E_i(\vec{x})$ satisfying

$$[A_i(\vec{x}), E_j(\vec{y})] = \frac{\delta_{ij}\delta_{\vec{x}\vec{y}}}{a^3} \quad (9.11)$$

from which we get the electric field defined on the space-like links of the Wilson theory

$$E_i(\vec{x}) = -\frac{i}{\alpha^2} \frac{\partial}{\partial \varphi_{\vec{x},i}} . \quad (9.12)$$

The lattice Hamiltonian is

$$H = -\frac{g^2}{2a} \sum_{\vec{x},i} \frac{\partial^2}{\partial \varphi_{\vec{x},i}^2} + \frac{1}{g^2 a} \sum_{\vec{x},i<j} [1 - \cos \vartheta_{\vec{x},ij}] \quad (9.13)$$

and has the correct continuum limit

$$H \approx \frac{g^2}{2} \sum_{\vec{x}, i} a^3 E_i E_i(\vec{x}) + \frac{1}{2g^2} \sum_{\vec{x}, i < j} a^3 F_{ij} F_{ij}(\vec{x}) \longrightarrow \int d^3 \vec{x} \left[\frac{g^2}{2} \vec{E}^2 + \frac{1}{2g^2} \vec{B}^2 \right]. \quad (9.14)$$

The Gauss' law $\vec{\nabla} \cdot \vec{E} = 0$ is the constraint equation which in the quantum theory has to be imposed on the states of the Hilbert space in order to enforce gauge invariance. The corresponding lattice generator is given by the lattice divergence of the electric field

$$G_{\vec{x}} = \sum_i \left(E_{\vec{x}, i} - E_{\vec{x}-\hat{i}, i} \right) = -\frac{i}{a^2} \sum_i \left(\frac{\partial}{\partial \varphi_{\vec{x}, i}} - \frac{\partial}{\partial \varphi_{\vec{x}-\hat{i}, i}} \right). \quad (9.15)$$

This generator which is locally conserved has to annihilate the physical, i.e. gauge invariant, states of the lattice Hilbert space

$$[H, G_{\vec{x}}] = 0, \quad G_{\vec{x}} |\Psi\rangle_{phys} = 0. \quad (9.16)$$

The physical states are those which have zero total electric flux flowing in and out of every lattice site. The theory can be studied in the Hamiltonian formalism through the quantum partition function

$$Z = \text{Tr}[P_G \exp(-\beta H)] = \sum_{|\Psi_{phys}\rangle} \langle \Psi_{phys} | \exp(-\beta H) | \Psi_{phys} \rangle, \quad (9.17)$$

where the projector P_G makes sure that only the physical states contribute.

Some intuition about the structure of the theory can be gained also in the conjugate electric representation where the states are diagonal to the electric field on the links. Since the link variable is a $U(1)$ angle, the momentum state is characterized by the integer $m_{\vec{x}, i}$ with matrix element $\langle \varphi_{\vec{x}, i} | m_{\vec{x}, i} \rangle = \exp(i m_{\vec{x}, i} \varphi_{\vec{x}, i})$. In the momentum representation therefore, the Hilbert space states are characterized by their integer electric flux on the links. The magnetic field term now induces an interaction on the plaquette due to the matrix elements

$$\langle m' | \exp(\pm i \varphi) | m \rangle = \int \int \frac{d\varphi}{2\pi} \frac{d\varphi'}{2\pi} \langle m' | \varphi' \rangle \langle \varphi' | \exp(\pm i \varphi) | \varphi \rangle \langle \varphi | m \rangle = \quad (9.18)$$

$$\int \int \frac{d\varphi}{2\pi} \frac{d\varphi'}{2\pi} \exp(-im'\varphi') 2\pi\delta(\varphi' - \varphi) \exp(\pm i\varphi) \exp(im\varphi) = \delta_{m',m\pm 1} ,$$

and the Hamiltonian matrix elements are

$$\langle [m'] | H | [m] \rangle = \frac{g^2}{2\alpha} \sum_{\vec{x},i} m_{\vec{x},i}^2 \prod_l \delta_{m'_l, m_l} - \frac{1}{2g^2\alpha} \sum_{P=(l_1 l_2 l_3 l_4)} \prod_{l \notin P} \delta_{m'_l, m_l} \quad (9.19)$$

$$\left[\delta_{m'_1, m_{l_1}+1} \delta_{m'_2, m_{l_2}+1} \delta_{m'_3, m_{l_3}-1} \delta_{m'_4, m_{l_4}-1} + \delta_{m'_1, m_{l_1}-1} \delta_{m'_2, m_{l_2}-1} \delta_{m'_3, m_{l_3}+1} \delta_{m'_4, m_{l_4}+1} \right]$$

where l labels the links and P the plaquettes of the lattice. We therefore see that the role of the interaction induced by the magnetic field is to shift one unit of electric flux clockwise and counterclockwise around each plaquette P of the lattice.

9.2 Phases of the Wilson Theory

The Wilson theory defined with the Euclidean action (9.3) can be studied through the path integral

$$Z = \prod_{x,\mu} \int d\varphi_{x,\mu} \exp(-S[\varphi]) . \quad (9.20)$$

The Wilson loop is the order parameter of the theory which can distinguish between the Coulomb and the confining phase. Wilson estimated the expectation value of the loops in the strong coupling limit of the theory, i.e. when g is very large. He demonstrated that the Wilson loop expectation value shows an area law which means that the theory is in the confining phase and therefore two static electric charges in this region would attract each other with a linearly rising potential. This is in fact a general result which holds independent of the dimensionality of the system. In order for the Wilson theory to be relevant to the 4-d physics of photons we see in reality, the Wilson theory should show a phase transition at some finite value of the coupling g_c to a phase with infinite correlation length and the Coulomb law interaction between static charges. Guth presented a rigorous proof in 1980 [65] that this anticipation is indeed true. He showed that at sufficiently small values of the coupling g , the Wilson loop expectation value is bounded by a perimeter law and the electrostatic potential

is bounded by the Coulomb law behavior. Therefore, a phase transition occurs at some finite coupling to a phase with the correct physical properties.

Numerical simulations of the partition function (9.20) with local algorithms have verified this picture. Wilson loop fits in the weak coupling phase show that the electrostatic potential indeed follows the Coulomb law and therefore the continuum limit of the theory can be taken in this phase resulting in Nature's electromagnetism. On the other hand, there is still dispute over the phase transition being first or second order. It is not clear if the metastability observed in the simulations is a finite size effect and if the correlation length at criticality scales according to the first order prediction or scales with a second order exponent. Simulations on larger lattices with better statistics are needed in order to conclusively settle this matter.

Banks, Kogut and Myerson [66] have reexpressed the partition function of the model as a gas of monopole loops. The loops are the worldlines of monopoles in 4-d interacting through a long-range potential. Their magnetic charge is inversely proportional to g and therefore this is a strong-weak coupling dual formulation of the $U(1)$ theory. In this picture, we can understand qualitatively the phases of the theory. The strong coupling phase of the system is a dense gas of weakly interacting monopoles and antimonopoles. The monopole loops therefore become large and extend through the system disordering it at large distances. The magnetic charge is indefinite in this phase and therefore the strong coupling phase is a monopole condensate. The existence of the condensate pushes the electric flux lines of a pair of electric sources into a tube connecting the charges. Therefore the origin of confinement in this phase is the dual Meissner effect. In the weak coupling phase the magnetic charge strengthens and the monopole interaction becomes stronger. Monopoles tend to bind with antimonopoles and the monopole loops become rare and small in size. The vacuum in this phase becomes ordered and the electric field lines can now spread out and induce the Coulomb law electrostatic potential. The monopole condensate and the monopole mass have also been studied in the numerical simulations of the theory.

In fact, the form of the action most suitable for the analytical manipulations

mentioned above is not the Wilson action but instead the Villain form

$$Z = \prod_{\mathbf{x}, \mu} \int d\varphi_{\mathbf{x}, \mu} \prod_P \sum_{n_P} \exp \left(-\frac{1}{g^2} (\vartheta_P + 2\pi n_P)^2 \right), \quad (9.21)$$

which approaches the Wilson action for small and large g and provides an equal footing regularization of the theory. We note that the partition function of the $U(1)$ theory can be rewritten on the dual lattice as a \mathbf{Z} gauge theory, i.e. a gauge theory with integer valued links. This action is the most suitable for the Monte Carlo study of the monopole condensate and monopole mass [67]. Finally we note that this theory can be expressed as the infinite-coupling limit of the non-compact Abelian Higgs model.

The three-dimensional lattice $U(1)$ theory in the Wilson or Villain form has also attracted many studies. It has been established analytically [68, 69] that the theory does not have a phase transition and remains confining for arbitrarily small coupling. The theory has been reexpressed as a gas of interacting monopoles [68] which stay in a condensate phase for all couplings. Therefore we cannot take the continuum limit to the 3-d theory of free photons anywhere in this theory.

9.3 The $U(1)$ Quantum Link Model

We proceed now to the D -theory formulation of the Abelian gauge theory. The model was presented in [70] before its reinvention in [56]. We will consider a 4-d hypercubic lattice with spacing a and postulate the existence of a Hilbert space on each link. We are going to promote the classical fields $u_{\mathbf{x}, \mu}$ and $u_{\mathbf{x}, \mu}^\dagger$ to the operators $U_{\mathbf{x}, \mu}$ and $U_{\mathbf{x}, \mu}^\dagger$ acting on the Hilbert space of the link. The classical Wilson action will be promoted to the Hamiltonian of the $U(1)$ quantum link model

$$H = -J \sum_{\mathbf{x}, \mu < \nu} [U_{\mathbf{x}, \mu} U_{\mathbf{x}+\hat{\mu}, \nu} U_{\mathbf{x}+\hat{\nu}, \mu}^\dagger U_{\mathbf{x}, \nu}^\dagger + U_{\mathbf{x}, \nu} U_{\mathbf{x}+\hat{\nu}, \mu} U_{\mathbf{x}+\hat{\mu}, \nu}^\dagger U_{\mathbf{x}, \mu}^\dagger]. \quad (9.22)$$

The theory possesses a $U(1)$ gauge invariance if there is a local generator $G_{\mathbf{x}}$ of the symmetry on the sites of the lattice which transforms the quantum link operators

under gauge transformations from the left and right

$$\begin{aligned} \exp(i\alpha_x G_x) U_{x,\mu} \exp(-i\alpha_x G_x) &= \exp(i\alpha_x) U_{x,\mu} \quad , \quad (9.23) \\ \exp(i\alpha_{x+\hat{\mu}} G_{x+\hat{\mu}}) U_{x,\mu} \exp(-i\alpha_{x+\hat{\mu}} G_{x+\hat{\mu}}) &= U_{x,\mu} \exp(-i\alpha_{x+\hat{\mu}}) . \end{aligned}$$

A general gauge transformation $\mathcal{G} = \prod_y \exp(i\alpha_y G_y)$ transforms the links as

$$U'_{x,\mu} = \mathcal{G} U_{x,\mu} \mathcal{G}^\dagger = \exp(i\alpha_x) U_{x,\mu} \exp(-i\alpha_{x+\hat{\mu}}) , \quad (9.24)$$

and leaves the Hamiltonian (9.22) invariant. Expanding the transformation relations (9.23) for small α_x we get the commutation relations

$$[G_y, U_{x,\mu}] = (\delta_{y,x} - \delta_{y,x+\hat{\mu}}) U_{x,\mu} , \quad [G_y, U_{x,\mu}^\dagger] = (\delta_{y,x+\hat{\mu}} - \delta_{y,x}) U_{x,\mu}^\dagger . \quad (9.25)$$

The generator G_x should be expressed as the lattice divergence of the link-based Hermitian electric field operator $G_{x,\mu}$

$$G_x = \sum_{\mu} (G_{x,\mu} - G_{x-\hat{\mu},\mu}) , \quad (9.26)$$

with the local commutation relations

$$[G_{x,\mu}, U_{x,\mu}] = U_{x,\mu} , \quad [G_{x,\mu}, U_{x,\mu}^\dagger] = -U_{x,\mu}^\dagger . \quad (9.27)$$

These relations are the same with the Wilson theory relations (9.10) with the added modification that the quantum link operators $U_{x,\mu}$ and $U_{x,\mu}^\dagger$ will no longer commute. These relations are interpreted as raising and lowering relations if we embed these operators in the link-based $SU(2)$ algebra

$$[S_{x,\mu}^a, S_{y,\nu}^b] = i\delta_{xy}\delta_{\mu\nu}\epsilon^{abc}S_{y,\nu}^c , \quad (9.28)$$

with the identification

$$U_{x,\mu} = S_{x,\mu}^1 + iS_{x,\mu}^2 = S_{x,\mu}^+ , \quad U_{x,\mu}^\dagger = S_{x,\mu}^1 - iS_{x,\mu}^2 = S_{x,\mu}^- , \quad G_{x,\mu} = S_{x,\mu}^3 . \quad (9.29)$$

The $U(1)$ quantum link model is therefore formulated with quantum spin operators on the lattice space-time links. The quantum spins can be chosen in any $SU(2)$ representation. The $SU(2)$ j -representations have dimensionality $2j + 1$ with $j = 1/2, 1, 3/2, \dots$ and therefore the Hilbert space of the links is discrete and finite. Nevertheless, the continuous $U(1)$ gauge symmetry is represented exactly in the model. The electric field operator is identified with the third component of the quantum spin and the link operators $U_{x,\mu}$ and $U_{x,\mu}^\dagger$ increase and decrease the electric flux by one unit. A natural basis is the electric basis where a state of the system is characterized by the electric flux units $-j, -j + 1, \dots, j - 1, j$ on the links. The dynamics of the Hamiltonian is to shift one unit of flux clockwise and counterclockwise around each plaquette of the lattice. Notice that this is precisely the behavior of the magnetic term in the Hamiltonian formulation of the Wilson theory (9.19). The difference is that the electric flux space of the Wilson theory contains all the integer states, while the quantum link electric flux is truncated between $-j$ and j .

Motivated from the Wilson theory Hamiltonian (9.19) we observe that we can add also an electric term to the model

$$H_E = J_E \sum_{x,\mu} S_{x,\mu}^3 S_{x,\mu}^3 \quad (9.30)$$

which is by construction gauge invariant. Of course in the quantum link model, the magnetic term is already non-trivial because of the non-commutativity of the link operators. The electric term will give a non-trivial contribution to the energy in any representation except the lowest $j = 1/2$ where it becomes a trivial constant.

We finally note that the model has the charge conjugation symmetry which in the classical theory takes each link to its conjugate $u_{x,\mu} \longrightarrow u_{x,\mu}^\dagger$ or equivalently flips the electric flux $E_{x,\mu} \longrightarrow -E_{x,\mu}$. In the $j = 1/2$ quantum link model the charge

conjugation operator is given from

$$C = \prod_{x,\mu} \sigma_{x,\mu}^1, \quad (9.31)$$

which transforms the operators as $CS_{x,\mu}^\pm C^\dagger = S_{x,\mu}^\mp$, $CS_{x,\mu}^3 C^\dagger = -S_{x,\mu}^3$ and is obviously a symmetry of the model.

9.4 Dimensional Reduction

Working with a finite representation of the quantum links, the 4-d Hamiltonian (9.22) induces a non-trivial dynamical evolution in a fifth unphysical Euclidean direction x_5 . The quantum partition function at temperature $T = 1/\beta$

$$Z = \text{Tr} \exp(-\beta H) \quad (9.32)$$

will as usual be pictured as the path integral of a classical theory in the (4+1)-d slab with finite extent β of the fifth dimension. Universality says that this classical theory is based on the 5-d gauge invariance only and therefore the low energy approximation to the theory in the slab will be the 5-d Abelian gauge theory. Since we are working on a lattice, we expect that the 5-d theory possesses a strong coupling phase at small β . It should also have a phase transition at some finite β_c to a Coulomb phase at weak coupling where the continuum limit of 5-d free photons can be taken. Therefore, when the slab extent β exceeds the critical value, the correlation length grows to infinity and we can describe the low energy excitations of the 5-d Coulomb phase with the 5-d Abelian gauge theory action

$$S[A_\mu] = \int_0^\beta dx_5 \int d^4x \frac{1}{4e^2} \left[F_{\mu\nu} F_{\mu\nu} + \frac{1}{c^2} \partial_5 A_\mu \partial_5 A_\mu \right]. \quad (9.33)$$

The 5-d theory has the dimensionful gauge coupling e and velocity of light in fifth direction c . Given the infinite correlation length in the Coulomb phase, the finite extent of the fifth direction becomes insignificant and the theory appears dimensionally

reduced to a 4-d theory. Once more we can imagine this reduction as the result of a renormalization group transformation which averages the 5-d photon field over the hypercube where it is strongly correlated. This hypercube has extent β in the fifth direction and βc in the other four directions. The result is the fixed-point action for the standard lattice gauge theory on a 4-d lattice of spacing $a' = \beta c$. The continuum limit of this theory results from the 5-d theory (9.33) if the fifth direction dependence of the fields is ignored, i.e. $\partial_5 A_\mu(x, x_5) = 0$. We can then perform the x_5 integration and get the reduced theory

$$S[A_\mu] \longrightarrow \int d^4 x \frac{1}{4g^2} F_{\mu\nu} F_{\mu\nu} \quad (9.34)$$

with effective coupling

$$\frac{1}{g^2} = \frac{\beta}{e^2}. \quad (9.35)$$

We therefore understand that the quantum link model for $\beta > \beta_c$ dimensionally reduces to the Coulomb phase of the standard lattice theory. Further, as β approaches β_c , the correlation length grows large. Due to dimensional reduction, the correlation length grows large with the same exponent as the correlation length of the Wilson theory near its critical coupling and therefore the nature of the phase transition will be the same as the transition in the Wilson theory. We conclude that the physics of the standard lattice theory formulated with the compact $U(1)$ gauge fields can also be described via dimensional reduction of the collective excitations of discrete variables in five dimensions.

Notice that similar to the non-Abelian quantum link formulation, we have not imposed the Gauss law $G_x|\Psi\rangle = 0$ on the states of the theory contributing to the trace (9.32). It is well known that in the path integral formulation the Gauss law results in a non-trivial Polyakov line of the gauge field in the time direction. This is because the time component of the gauge field appears as the Lagrange multiplier field which enforces the constraint. In the quantum link model the Gauss law constraint

would induce a component $A_5(\mathbf{x}, x_5)$. After dimensional reduction the Polyakov line

$$P(\mathbf{x}) = \exp \left(i \int_0^\beta dx_5 A_5(\mathbf{x}, x_5) \right) \quad (9.36)$$

would appear after as a scalar field in the 4-d reduced theory. We would like to avoid this field since we do not know its effect on the phase structure of the reduced theory. For this reason we do not impose the Gauss law and therefore the 5-d theory (9.33) is written in the gauge $A_5 = 0$. This choice breaks the 5-d gauge symmetry for finite time β but the physical 4-d gauge symmetry is intact in (9.33). The existence of the 5-d Coulomb phase should not be affected by this modification. Adding gauge-variant states which propagate in the fifth direction does not influence the massless excitations right above the ground state of the system. The physical spectrum information is in the correlation functions of operators in the physical time coordinate which is part of the 4-d lattice. Compactifying this direction would naturally lead to the quantum link formulation of the finite temperature gauge theory.

Chapter 10

Strong Coupling Expansions in U(1) Gauge Theory

10.1 Confinement at Strong Coupling

In this chapter we are going to demonstrate analytically properties of the $U(1)$ quantum link theory at strong coupling. Recall that the quantum partition function is

$$Z = \text{Tr} \exp \left(\beta J \sum_P (U_P + U_P^\dagger) \right) \quad (10.1)$$

where P runs over all the plaquettes of the lattice with $U_P = U_1 U_2 U_3^\dagger U_4^\dagger$ the plaquette operator made out of the 4 links in counterclockwise fashion around the plaquette. Consider that we work with a 4-d lattice with dimensions $L_1 \times L_2 \times L_3 \times L_4$. The trace is over the Hilbert space of the $N_L = 4L_1 L_2 L_3 L_4$ links of the lattice. The strong coupling expansion assumes that $\beta J \ll 1$ and therefore we can expand the exponential of the Hamiltonian in a Taylor series around $\beta J = 0$ and truncate to the first few terms, which should be a good approximation. The name is motivated by the Wilson theory where the expansion parameter is $1/g^2$. Expanding (10.1) we get

$$Z = \sum_{n=0}^{\infty} \frac{(\beta J)^n}{n!} \sum_{N_1} \sum_{N_2} \cdots \sum_{N_n} \text{Tr} \left[(U_{N_1} + U_{N_1}^\dagger) (U_{N_2} + U_{N_2}^\dagger) \cdots (U_{N_n} + U_{N_n}^\dagger) \right] \quad (10.2)$$

where the N_i 's run over the set of the $N_P = 6L_1L_2L_3L_4$ plaquettes of the lattice. We will analyze the $j = 1/2$ quantization of the links in the following for which the quantum spins are $\vec{S}_{x,\mu} = \frac{1}{2}\vec{\sigma}_{x,\mu}$ and $\vec{\sigma}$ are the Pauli matrices

$$\sigma^1 = \begin{pmatrix} 0 & 1 \\ 1 & 0 \end{pmatrix}, \quad \sigma^2 = \begin{pmatrix} 0 & -i \\ i & 0 \end{pmatrix}, \quad \sigma^3 = \begin{pmatrix} 1 & 0 \\ 0 & -1 \end{pmatrix}. \quad (10.3)$$

The plaquette operator is

$$U_P = \sigma_1^+ \sigma_2^+ \sigma_3^- \sigma_4^- \quad (10.4)$$

where σ^\pm are the spin-1/2 raising and lowering operators

$$\sigma^+ = \begin{pmatrix} 0 & 1 \\ 0 & 0 \end{pmatrix}, \quad \sigma^- = \begin{pmatrix} 0 & 0 \\ 1 & 0 \end{pmatrix}. \quad (10.5)$$

Recall the properties

$$\sigma^+ \sigma^+ = \sigma^- \sigma^- = 0, \quad \sigma^+ \sigma^- = P^+, \quad \sigma^- \sigma^+ = P^-, \quad \text{Tr } \sigma^\pm = 0 \quad (10.6)$$

where P^\pm are the projection operators on the $|\pm\rangle$ states with the properties

$$P^+ P^- = P^- P^+ = 0, \quad P^+ P^+ = P^+, \quad P^- P^- = P^-, \quad \text{Tr } P^\pm = 1. \quad (10.7)$$

We therefore understand that in order to get a non-vanishing trace of a certain link, the unit operator or an even number of link operators should be traced, chained as $\sigma^+ \sigma^- \sigma^+ \sigma^- \dots \sigma^+ \sigma^-$ or $\sigma^- \sigma^+ \sigma^- \sigma^+ \dots \sigma^- \sigma^+$. Pictorially, this means that every time the flux is flipped in one direction, the next move should undo the flip. The same is true for the plaquette operator also, which satisfies

$$U_P U_P = U_P^\dagger U_P^\dagger = 0, \quad U_P U_P^\dagger = P_1^+ P_2^+ P_3^- P_4^-, \quad U_P^\dagger U_P = P_1^- P_2^- P_3^+ P_4^+, \quad (10.8)$$

and therefore a shift of flux around the plaquette due to U_P can be canceled from the antiplaquette U_P^\dagger . There are two ways to get contributions in the expansion (10.2).

First, for each plaquette U_P that appears in a term, the corresponding antiplaquette U_P^\dagger should also appear. In that way it is possible to neutralize the link operators with their conjugates. Second, for each plaquette U_P that appears in a term, neighboring plaquettes that share links with U_P should also appear exactly once in the same orientation so that the link operators are neutralized. An example of these terms is a cube made of six plaquettes in the proper orientation or some larger structure which is bounded by a 2-d orientable surface with no boundary. As long as the surface is orientable and has no boundary we can tile it completely with plaquettes and get a non-vanishing trace. Another example valid on a periodic lattice with toroidal topology is the complete tiling of a plane with plaquettes, since it is a surface with no boundary on a periodic lattice. For example, tiling completely the 1 – 2 plane once gives a contribution at $\mathcal{O}(\beta^{L_1 L_2})$. A general term will consist of various disconnected surfaces. And of course pairs of plaquette-antiplaquettes can be overlaid anywhere on the surfaces as long as the ordering is allowed.

It is easy now to find the lowest order in β of the partition function (10.2). There is no $\mathcal{O}(\beta)$ term since it traces one plaquette only and the $\mathcal{O}(\beta^2)$ term requires the plaquette–antiplaquette term

$$\begin{aligned}
Z &\approx \text{Tr} \mathbb{1} + \frac{(\beta J)^2}{2} \sum_{N_1} \text{Tr} \left[(U_{N_1} + U_{N_1}^\dagger) (U_{N_1} + U_{N_1}^\dagger) \right] & (10.9) \\
&\approx 2^{N_L} + \frac{(\beta J)^2}{2} N_P 2^{N_L-4} \text{Tr} \left[P_1^+ P_2^+ P_3^- P_4^- + P_1^- P_2^- P_3^+ P_4^+ \right] \\
&= 2^{N_L} \left(1 + \frac{(\beta J)^2}{2} N_P \frac{2}{16} + \mathcal{O}((\beta J)^4) \right) .
\end{aligned}$$

A trivial lemma of the above analysis is that on a lattice with even L_1, L_2, L_3, L_4 the partition function contains only even powers of β . The energy density of the model can also be computed at lowest order

$$\mathcal{E} = \frac{\langle H \rangle}{V} = \frac{1}{V} \frac{\text{Tr} [H \exp(-\beta H)]}{\text{Tr} [\exp(-\beta H)]} = -\frac{1}{VZ} \frac{\partial Z}{\partial \beta} = -\frac{3\beta J^2}{4} + \mathcal{O}(\beta^3 J^4) . \quad (10.10)$$

Confinement in the strong coupling phase can be demonstrated if the Wilson loop expectation value exhibits the area law. Consider a planar rectangular Wilson loop

of dimension $L \times T$ embedded in a space-time plane of the lattice. The expectation value can again be expanded for small β

$$\begin{aligned} \langle W_{LT} \rangle &= \frac{1}{Z} \text{Tr} [W_{LT} \exp(-\beta H)] \\ &= \frac{1}{Z} \sum_{n=0}^{\infty} \frac{(\beta J)^n}{n!} \sum_{N_1} \sum_{N_2} \cdots \sum_{N_n} \text{Tr} [W_{LT} (U_{N_1} + U_{N_1}^\dagger) (U_{N_2} + U_{N_2}^\dagger) \cdots (U_{N_n} + U_{N_n}^\dagger)] \end{aligned} \quad (10.11)$$

Since the Wilson loop is a chain of operators

$$W_{LT} = \sigma_{l_1}^+ \cdots \sigma_{l_L}^+ \sigma_{t_1}^+ \cdots \sigma_{t_T}^+ \sigma_{l'_L}^- \cdots \sigma_{l'_1}^- \sigma_{t'_T}^- \cdots \sigma_{t'_1}^- \quad (10.12)$$

we will get contributions from the terms that can neutralize the link operators that live on the loop. In the light of the analysis we did earlier for the partition function, we see that this is possible if we tile an orientable surface, which is bounded by the Wilson loop, with plaquettes. The orientability of the surface guarantees that it can cancel exactly the oriented flux that goes around the loop. The lowest order in β to which this is possible requires the lowest number of plaquettes and therefore defines a minimal surface area problem with given boundary. The answer for the rectangular Wilson loop we work with is the planar surface defined by the rectangle. It requires LT antiplaquette operators to tile the rectangular and therefore the lowest order expectation value is

$$\begin{aligned} \langle W_{LT} \rangle &= \frac{1}{2^{NL}} \frac{(\beta J)^{LT}}{(LT)!} \sum_{N_1} \sum_{N_2} \cdots \sum_{N_{LT}} \text{Tr} [W_{LT} U_{N_1}^\dagger U_{N_2}^\dagger \cdots U_{N_{LT}}^\dagger] \\ &= \frac{(\beta J)^{LT}}{(LT)!} (LT)! \left(\frac{1}{2}\right)^{L(T+1)+T(L+1)} = \left(\frac{\beta J}{4}\right)^{LT} \left(\frac{1}{2}\right)^{L+T}. \end{aligned} \quad (10.13)$$

To lowest order, Z should be taken as the constant 2^{NL} . There is a factor $(LT)!$ from the permutations of the LT plaquettes that contribute. Any of these orderings uniquely fixes the state that contributes on the $L(T+1) + T(L+1)$ links that are involved in the rectangle and so they offer half of their Hilbert space to the trace.

Rewriting (10.13) as

$$\langle W_{LT} \rangle = \exp \left(-LT \ln \left(\frac{4}{\beta J} \right) - (L + T) \ln 2 \right) \quad (10.14)$$

we recognize the usual behavior of confining gauge theories with an area law for the Wilson loop followed by the perimeter term. We therefore establish linear confinement at small βJ in the $U(1)$ quantum link model with a lowest order string tension

$$\sigma = \ln \left(\frac{4}{\beta J} \right) . \quad (10.15)$$

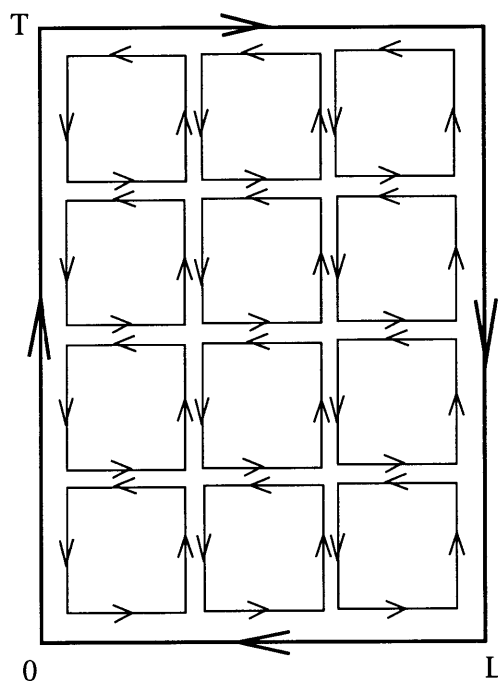


Figure 10-1: *Tiling a Wilson loop with plaquettes proves the area law in the strong coupling expansion.*

The next order contributions to (10.13) will come from excitations of the minimal surface that covers the rectangle. The lowest excitation is the attachment of a cube on the plane. This requires additional four plaquettes and can be attached on any of (LT) positions. We should not consider a disconnected plaquette-antiplaquette excitation which corrects at $\mathcal{O}(\beta^2)$ since this will be canceled by a corresponding

term in the denominator. Therefore the result (10.14) can be modified to

$$\langle W_{LT} \rangle \longrightarrow \langle W_{LT} \rangle [1 + \mathcal{O}((\beta J)^4 LT)] \approx \langle W_{LT} \rangle \exp(\mathcal{O}((\beta J)^4 LT)) \quad (10.16)$$

and the string tension will have the leading correction

$$\sigma = \ln\left(\frac{4}{\beta J}\right) + \mathcal{O}((\beta J)^4) . \quad (10.17)$$

Examining increasingly more complicated graphs we can derive higher order terms in this expansion. Nevertheless, these results will be valid only within the convergence radius of the expansion. The existence of a phase transition which means a non-analyticity in the partition function can never be determined in the series of βJ . In the series (10.11) an area law will appear at any order and we cannot deduce if a Coulomb phase exists at sufficiently small coupling. This requires non-perturbative methods which in most theories calls for a Monte Carlo simulation.

10.2 Some Comments

Having understood the nature of the strong coupling expansion of the $j = 1/2$ $U(1)$ quantum link model we can comment on some things.

First, the $U(1)$ theory with quantum links in a general j -representation is confining at strong coupling. This can be seen if we examine the expansions (10.2) and (10.11) for the partition function and the Wilson loop. The analysis we performed concerning the geometrical objects that contribute to both expansions remains the same simply because we should again match the number of times we raise the flux on each link with the number of times we lower the flux. The only difference is that more orderings of the operators are available since the flux space is larger and we can raise the flux more than once. To be more precise, a general j -representation state with flux m is transformed under raising and lowering as

$$U|j, m\rangle = c_{jm}^+ |j, m+1\rangle , \quad c_{jm}^+ = \sqrt{(j-m)(j+m+1)} , \quad (10.18)$$

$$U^\dagger |j, m\rangle = c_{jm}^- |j, m-1\rangle, \quad c_{jm}^- = \sqrt{(j+m)(j-m+1)},$$

$$U^{2j+1} = 0, \quad U^\dagger{}^{2j+1} = 0.$$

The trace on links with flux raising and lowering is

$$\begin{aligned} \text{Tr}UU^\dagger = \text{Tr}U^\dagger U &= \sum_{m=-j}^j \langle j, m | UU^\dagger | j, m \rangle = \sum_{m=-j}^j \langle j, m | U^\dagger U | j, m \rangle = \quad (10.19) \\ &= \sum_{m=-j}^j c_{jm}^{+2} = \sum_{m=-j}^j c_{jm}^{-2} = \frac{2j(j+1)(2j+1)}{3} \end{aligned}$$

Based on this, we can easily compute the lowest order contribution to $\langle W_{LT} \rangle$

$$\begin{aligned} \langle W_{LT} \rangle &= \frac{1}{(2j+1)^{N_L}} \frac{(\beta J)^{LT}}{(LT)!} \sum_{N_1} \sum_{N_2} \cdots \sum_{N_{LT}} \text{Tr} [W_{LT} U_{N_1}^\dagger U_{N_2}^\dagger \cdots U_{N_{LT}}^\dagger] \quad (10.20) \\ &= \frac{(\beta J)^{LT}}{(LT)!} (LT)! \left(\frac{1}{2j+1} \right)^{L(T+1)+T(L+1)} \left(\frac{2j(j+1)(2j+1)}{3} \right)^{L(T+1)+T(L+1)}. \end{aligned}$$

We should not forget that the transformations are rotating a quantum spin with magnitude $\sqrt{j(j+1)}$ and therefore we should divide each link operator U, U^\dagger by $\sqrt{j(j+1)}$ in order to approach the classical $U(1)$ results where a unit vector is rotated. With this normalization the Wilson loop expectation value

$$\langle W_{LT} \rangle = \left(\frac{4\beta J}{9} \right)^{LT} \left(\frac{2}{3} \right)^{L+T} = \exp \left(-LT \ln \left(\frac{9}{4\beta J} \right) - (L+T) \ln \left(\frac{3}{2} \right) \right) \quad (10.21)$$

shows an area law which again signals linear confinement at small βJ for any representation j .

A second comment concerns the non-Abelian quantum link models. It is well known that at strong coupling Wilson's non-Abelian gauge theories are confining. The lowest order contribution to the Wilson loop comes from completely tiling the minimal area stretched by the loop with plaquettes and tracing in the group space. This is based on the property that a group integration requires the link matrix and its conjugate in order to be non-zero. The same behavior carries over in the quantum link formulation. Here a link operator matrix element changes the colored flux in a

particular pattern and only the conjugate element can bring the state back. The group integration is replaced by the trace in the link Hilbert space and the strong coupling expansion will again get contributions from the orientable surfaces that are bounded by the Wilson loop operator and are tiled with plaquettes. The only difference is that some orderings of the operators will not be allowed but otherwise the Wilson loop will again show an area law. Therefore the non-Abelian quantum link models will be confining at small βJ . Due to dimensional reduction $\beta J \sim 1/g^2$ this is consistent with the strong coupling phase of the reduced Wilson theory.

Osterwalder and Seiler have proved [71] that the strong coupling expansion of any lattice gauge theory with a compact group in any dimension has a finite radius of convergence. Equivalently, there will always be a critical coupling $\beta_c > 0$ such that for $\beta < \beta_c$ the theory is in the confining phase. From what we have seen so far, the strong coupling expansion of the quantum link theories shows the same qualitative behavior as the classical theories and therefore it seems natural to conjecture that the Osterwalder-Seiler theorem holds also for all D -theory formulations of the gauge theories.

10.3 A Constraint on the Critical Coupling

The analysis of the strong coupling series for the partition function (10.2) and the Wilson loop (10.11) can be fully applied to the standard Wilson $U(1)$ theory. The link operators should be replaced by the corresponding phases and the trace of the Hilbert space by the $U(1)$ group integration

$$U_{x,\mu} \longrightarrow \exp(i\varphi_{x,\mu}), \quad \beta J \longrightarrow \frac{1}{2g^2}, \quad \text{Tr} \longrightarrow \int_{-\pi}^{\pi} \frac{d\varphi}{2\pi}. \quad (10.22)$$

Consider an arbitrary order n term in the expansion

$$Z = \sum_{n=0}^{\infty} \frac{(\beta J)^n}{n!} \sum_{N_1} \sum_{N_2} \cdots \sum_{N_n} \text{Tr} \left[(U_{N_1} + U_{N_1}^\dagger) (U_{N_2} + U_{N_2}^\dagger) \cdots (U_{N_n} + U_{N_n}^\dagger) \right] \quad (10.23)$$

Each of the selections N_1, N_2, \dots, N_n should tile exactly one or more closed surfaces and could further contain plaquette-antiplaquette terms in order to have a non-vanishing trace. This is the case for both the $j = 1/2$ quantum link and the Wilson theory. For each such selection there is one more contribution from its conjugate term. All such selections contribute to the Wilson expansion but only some of these selections contribute to the $j = 1/2$ quantum link model because the ordering of the operators matters since each raising of flux should be followed only by lowering of flux. Notice that all these terms appear with a plus sign in the expansion (10.23) and therefore the $(\beta J)^n$ coefficient gets a smaller contribution in the quantum link case. Furthermore, the tracing in the involved M_l links brings in a factor $(1/2)^{M_l}$ in the quantum case while it is a trivial integration with the measure (10.22) and result 1 in the classical case. Therefore the order $(\beta J)^n$ term always has a *smaller positive* coefficient than the classical term. The quantum link model therefore has a larger convergence radius than the classical model. If we assume that the radius of convergence of the series equals the critical coupling in both the classical and quantum link expansion, we can conclude that the critical β for the quantum link model will be *larger* than the corresponding critical value in the Wilson theory. Simulations of the Wilson theory show a critical value $1/g^2 = 1.01..$ and in the mapping (10.22) it is rescaled to $(\beta J)_c = 0.50..$ We can therefore constrain the critical value of the $j = 1/2$ quantum link model from below

$$(\beta J)_c > 0.50.. \tag{10.24}$$

The numerical results that we will present in the next chapter are consistent with this constraint. Finally we notice that the derivation of this inequality is independent of dimensionality. Since the classical Wilson theory in 3-d is strongly coupled at all β , we conclude that the 3-d $j = 1/2$ quantum link model will also remain strongly coupled for all β values.

Chapter 11

The Cluster Algorithm for Quantum Spins

11.1 Introduction

In chapter 5 we explained how classical spin systems can be simulated efficiently with the Wolff cluster algorithm. Now we turn to the quantum systems and extend our analysis to them. The Hamiltonian which defines the models can be diagonalized explicitly only for very small systems, therefore different strategies are needed. In fact, the Monte Carlo simulation is the only available method for accurate studies of the quantum spin dynamics. The loop-cluster algorithm was first presented in [72]. Since we deal with a Hamiltonian and our variables are spin operators in a certain representation, evolution in an extra time coordinate naturally emerges. In order to model the evolution in a numerically efficient way, we discretize the time interval and construct a path integral representation for the partition function, as we will show in section 2. The method of importance sampling can now be applied to this partition function. We expect that we can construct clusters of classical variables by joining interacting spins together with rules that obey detailed balance and ergodicity and update the system efficiently. In a more rigorous approach, we explain how the partition function can be mapped to the partition function for a random cluster model after a proper decomposition of the elementary transfer matrices. In section

3 we apply the method to the XY model and derive the rules needed for a cluster decomposition. We show the basis-independence of the cluster dynamics in section 4 and use it to measure Greens functions with improved estimators in section 5.

11.2 The Suzuki-Trotter decomposition

Let us consider the Hamilton operator for a spin model on a 2-d square lattice

$$H = \sum_{\mathbf{x}, \hat{\mu}} h_{\mathbf{x}, \hat{\mu}}, \quad (11.1)$$

where $h_{\mathbf{x}, \hat{\mu}}$ is a coupling of the spin operator at the site \mathbf{x} and its neighbor in direction $\hat{\mu} = 1, 2$. The structure is immediately generalizable to higher dimensions. The partition function is given by

$$Z = \text{Tr} \exp(-\beta H). \quad (11.2)$$

We now introduce the Suzuki-Trotter decomposition and imagine that H describes evolution in the compact time interval $[0, \beta]$. The trace implies periodic boundary conditions in time. We discretize time in small steps $\epsilon = \frac{\beta}{N}$ and rewrite Z as

$$Z = \text{Tr} \prod_{i=1}^N \exp(-\epsilon H) \quad (11.3)$$

In order to make the partition function accessible to numerical simulations we expand it further in a checker board pattern such that a minimal number of spins interact in a single time step. The Hamiltonian decomposes into

$$H = H_1 + H_2 + H_3 + H_4 \quad (11.4)$$

where the four terms are

$$H_1 = \sum_{x \in (2m, n)} h_{x, \hat{1}}, \quad H_2 = \sum_{x \in (m, 2n)} h_{x, \hat{2}}, \quad H_3 = \sum_{x \in (2m+1, n)} h_{x, \hat{1}}, \quad H_4 = \sum_{x \in (m, 2n+1)} h_{x, \hat{2}}. \quad (11.5)$$

Every H_i contains a sum of commuting operators, each of which represents a two-spin interaction. Thus $\exp(-\epsilon H_i)$ can be computed easily as a product of independent exponentiations of the two-spin interaction $h_{x, \hat{\mu}}$. The essence of the Suzuki-Trotter decomposition is the approximation

$$\exp(-\epsilon H) \simeq \exp(-\epsilon H_1) \exp(-\epsilon H_2) \exp(-\epsilon H_3) \exp(-\epsilon H_4) \quad (11.6)$$

which is valid for large N . The partition function is now expressed as a product of $4N$ operators. We introduce the unit operator as a sum over a complete set of states between the $4N$ exponentials. Each of these insertions defines a discrete time label $t = 1, 2, \dots, 4N$. The \pm sign which labels a spin state, e.g. as an eigenstate of σ_x^3 , becomes a classical, Ising-like spin living in a $(2+1)$ -d space. In this way we are left with a product of matrix elements of spins. In fact, since each H_i is a sum of commuting spin pairs, these matrix elements are independent products of the transfer matrix for the two-spin interaction which is defined as

$$T(s_1, s_2; s_3, s_4) = \langle s_3 s_4 | \exp(-\epsilon h_{x, \hat{\mu}}) | s_1 s_2 \rangle. \quad (11.7)$$

In this notation, the neighboring spin states s_1, s_2 , which live on a time slice t , are coupled to their images s_3, s_4 forwarded to the time slice $t+1$. What we have achieved is to reexpress a quantum partition function on a square lattice of dimension $L_1 \times L_2$ as an effective partition function for classical spins on a 3-d cubical lattice of dimension $4N \times L_1 \times L_2$,

$$Z = \prod_{x, t} \sum_{s_{x, t} = \pm 1/2} \exp(-S[s]). \quad (11.8)$$

The action $S[s]$ is a sum of contributions from the checker boarded plaquettes, each linking four spins into an effective interaction. The Boltzmann weight of each pla-

quette configuration is naturally given by the transfer matrix element between spin states

$$\exp(-S[s_{\mathbf{x},t}, s_{\mathbf{x}+\hat{\mu},t}; s_{\mathbf{x},t+1}, s_{\mathbf{x}+\hat{\mu},t+1}]) = T(s_{\mathbf{x},t}, s_{\mathbf{x}+\hat{\mu},t}; s_{\mathbf{x},t+1}, s_{\mathbf{x}+\hat{\mu},t+1}). \quad (11.9)$$

At this point we are ready to explore methods for an effective sampling of the configuration space of the (2+1)-d system that we constructed. The principle will be the same as in the classical spin systems that we have already explored. Namely, we would like to examine the interacting groups of spins and group them into clusters according to the weight of their configuration. The clusters constitute a complete decomposition of the (2+1)-d lattice and are flipped independently resulting in a much more efficient move through phase space. Of course the decomposition of the lattice into clusters must be done such that ergodicity and detailed balance are obeyed. In the way we have written the partition function as a product of independent plaquette interactions this is not a hard task. In fact, we have to examine the $4 \times 4 = 16$ states that can appear and construct flipping rules so that ergodicity and detailed balance for the plaquette phase space is obeyed. This is sufficient to guarantee that we will produce a Markov chain with this algorithm.

Actually, the decomposition of the plaquette can appear in a more natural way if we remember that the partition function can also be written in the form

$$Z = \text{Tr}\left(\prod_{p=1}^{N_p} T_p\right), \quad (11.10)$$

where we multiply in a time ordered fashion the $N_p = 2NL_1L_2$ transfer matrices. The trace and the multiplication of the matrices constitute exactly the summation over the spin states with periodic conditions in time. Each transfer matrix $T(s_1, s_2; s_3, s_4)$ can be rewritten as a sum over products of simpler tensors such as δ_{s_1, s_3} or σ_{s_1, s_2}^1 for example. In fact, as will be shown in the next section for the *XY* model, if we use tensors such that the plaquette is always decomposed into two groups of two spins each, the decomposition is unique and results in clusters which are loops of

spins. In that sense, the loop-cluster algorithm can also be pictured as following the worldlines of quantum spins in their (2+1)-d evolution. At the same time, as will be shown in detail in the next sections, this representation helps to reveal the basis-independence of the quantum cluster dynamics and consequently the construction of improved estimators for Green's functions.

11.3 Clustering the XY model

We apply the analysis of the previous section to the XY model which in the spin-1/2 representation is defined through the Hamilton operator

$$H = \sum_{\mathbf{x}, \hat{\mu}} h_{\mathbf{x}, \hat{\mu}} ; \quad h_{\mathbf{x}, \hat{\mu}} = -\frac{J}{2} \left(\sigma_{\mathbf{x}}^1 \sigma_{\mathbf{x}+\hat{\mu}}^1 + \sigma_{\mathbf{x}}^2 \sigma_{\mathbf{x}+\hat{\mu}}^2 \right) , \quad (11.11)$$

with a ferromagnetic coupling $J > 0$. Using the relations $\sigma^1 = \sigma^+ + \sigma^-$ and $\sigma^2 = -i(\sigma^+ - \sigma^-)$ we can express the transfer matrix as

$$T = \exp(-\epsilon h_{\mathbf{x}, \hat{\mu}}) = \exp(\epsilon J (\sigma_{\mathbf{x}}^+ \sigma_{\mathbf{x}+\hat{\mu}}^- + \sigma_{\mathbf{x}}^- \sigma_{\mathbf{x}+\hat{\mu}}^+)) . \quad (11.12)$$

It is easy to carry out the exponentiation if we remember that $\sigma^+ \sigma^+ = \sigma^- \sigma^- = 0$, $\sigma^+ \sigma^- = P^+$ and $\sigma^- \sigma^+ = P^-$, where P^\pm are the projection operators on the \pm eigenstates. Even and odd powers of ϵJ separate and the result is

$$T = \mathbb{1} + (\cosh(\epsilon J) - 1)(P_{\mathbf{x}}^+ P_{\mathbf{x}+\hat{\mu}}^- + P_{\mathbf{x}}^- P_{\mathbf{x}+\hat{\mu}}^+) + \sinh(\epsilon J)(\sigma_{\mathbf{x}}^+ \sigma_{\mathbf{x}+\hat{\mu}}^- + \sigma_{\mathbf{x}}^- \sigma_{\mathbf{x}+\hat{\mu}}^+) \quad (11.13)$$

Explicitly, the only non-zero matrix elements are

$$\begin{aligned} T(+ - ; + -) &= T(- + ; - +) = \cosh(\epsilon J) , & (11.14) \\ T(+ - ; - +) &= T(- + ; + -) = \sinh(\epsilon J) , \\ T(+ + ; + +) &= T(- - ; - -) = 1 . \end{aligned}$$

Now we notice that we can decompose this transfer matrix as a sum of simpler tensors. For the six non vanishing elements that we have, it is enough to use the diagonal operator $\delta_{s_1, s_3} \delta_{s_2, s_4}$, a cross-diagonal operator $\delta_{s_1, s_4} \delta_{s_2, s_3}$ and the operator $\sigma_{s_1, s_2}^1 \sigma_{s_3, s_4}^1$, which projects onto opposite spins on the same time slice. The decomposition can be written as

$$T(s_1, s_2; s_3, s_4) = w_1 \delta_{s_1, s_3} \delta_{s_2, s_4} + w_2 \delta_{s_1, s_4} \delta_{s_2, s_3} + w_3 \sigma_{s_1, s_2}^1 \sigma_{s_3, s_4}^1. \quad (11.15)$$

Matching the left and right matrix elements we get the equations

$$\begin{aligned} \cosh(\epsilon J) &= w_1 + w_3, \\ \sinh(\epsilon J) &= w_2 + w_3, \\ 1 &= w_1 + w_2 \end{aligned} \quad (11.16)$$

which give the solution

$$w_1 = \frac{1}{2}(1 + \exp(-\epsilon J)), \quad w_2 = \frac{1}{2}(1 - \exp(-\epsilon J)), \quad w_3 = \frac{1}{2}(\exp(\epsilon J) - 1). \quad (11.17)$$

Since we have $N_p = 2NL_1L_2$ plaquettes in the lattice and each one can offer three different tensors, the partition function can also be expressed as a sum over 3^{N_p} terms, each one being a unique product of the tensors weighted with the corresponding product of weights w_1, w_2 or w_3 . A choice of one of the tensors corresponds to a decomposition of the plaquette. For example, the tensor $\delta_{s_1, s_3} \delta_{s_2, s_4}$ corresponds to a configuration where the spins s_1, s_2 are in the same state with their forward neighbors in time. In that case, the spins s_1 and s_3 should be put in one cluster together while the spins s_2 and s_4 are joined into a different cluster. The tensor $\delta_{s_1, s_4} \delta_{s_2, s_3}$ is applied to states where s_1 equals s_4 and s_2 equals s_3 . It joins s_1 with s_4 and s_2 with s_3 . Finally, the tensor $\sigma_{s_1, s_2}^1 \sigma_{s_3, s_4}^1$ applies to states with s_1 opposite to its time slice neighbor s_2 and likely s_3 opposite to s_4 . It joins s_1 with s_2 into a cluster and s_3 with s_4 into a different cluster. As we have seen, each of the six plaquette configurations that have non-zero weight can be decomposed with two out of the three patterns. The

loop-cluster is simply following a given spin as various decompositions join it with neighboring spins in space or time. The evolution is traced forwards and backwards in time and due to the periodic boundary conditions, the worldline is going to form a loop. The spin is evolving keeping its orientation unless the loop joins it with a neighbor on the same time slice.

The probability for each plaquette decomposition appears naturally as the ratio of the decomposition factor w_1, w_2 or w_3 with the weight of the state. In this way we can prove easily that flipping a loop-cluster obeys detailed balance.

Let us examine the plaquette configurations

$$C_1 = (+-; +-) \text{ with weight } W[C_1] = \cosh(\epsilon J),$$

$$C_2 = (+-; -+) \text{ with weight } W[C_2] = \sinh(\epsilon J) \text{ and}$$

$$C_3 = (++; ++) \text{ with weight } W[C_3] = 1$$

and recall that total flips have the same weight.

Configuration C_1 can be decomposed with patterns w_1 or w_3 . After flipping the joined spins it will result in the configurations C_3 or C_2 . The corresponding probabilities are

$$\mathcal{P}(C_1 \rightarrow C_3) = w_1 / \cosh(\epsilon J) = [1 + \exp(-\epsilon J)] / [2 \cosh(\epsilon J)], \quad (11.18)$$

$$\mathcal{P}(C_1 \rightarrow C_2) = w_3 / \cosh(\epsilon J) = [\exp(\epsilon J) - 1] / [2 \cosh(\epsilon J)].$$

Configuration C_2 can be decomposed with patterns w_2 or w_3 . After flipping the joined spins it will result to the configurations C_3 or C_1 . The corresponding probabilities are

$$\mathcal{P}(C_2 \rightarrow C_3) = w_2 / \sinh(\epsilon J) = [1 - \exp(-\epsilon J)] / [2 \sinh(\epsilon J)], \quad (11.19)$$

$$\mathcal{P}(C_2 \rightarrow C_1) = w_3 / \sinh(\epsilon J) = [\exp(\epsilon J) - 1] / [2 \sinh(\epsilon J)].$$

Configuration C_3 can be decomposed with patterns w_1 or w_2 . After flipping the joined spins it will result to the configurations C_1 or C_2 . The corresponding probabilities

are

$$\begin{aligned} \mathcal{P}(C_3 \rightarrow C_1) &= w_1 = \frac{1}{2}(1 + \exp(-\epsilon J)), \\ \mathcal{P}(C_3 \rightarrow C_2) &= w_2 = \frac{1}{2}(1 - \exp(-\epsilon J)). \end{aligned} \quad (11.20)$$

We can see that detailed balance is satisfied automatically for any pair of configurations

$$W[C_i] \mathcal{P}(C_i \rightarrow C_j) = W[C_j] \mathcal{P}(C_j \rightarrow C_i). \quad (11.21)$$

Finally, notice that any plaquette configuration can decay to any other, therefore the constructed algorithm will also be ergodic.

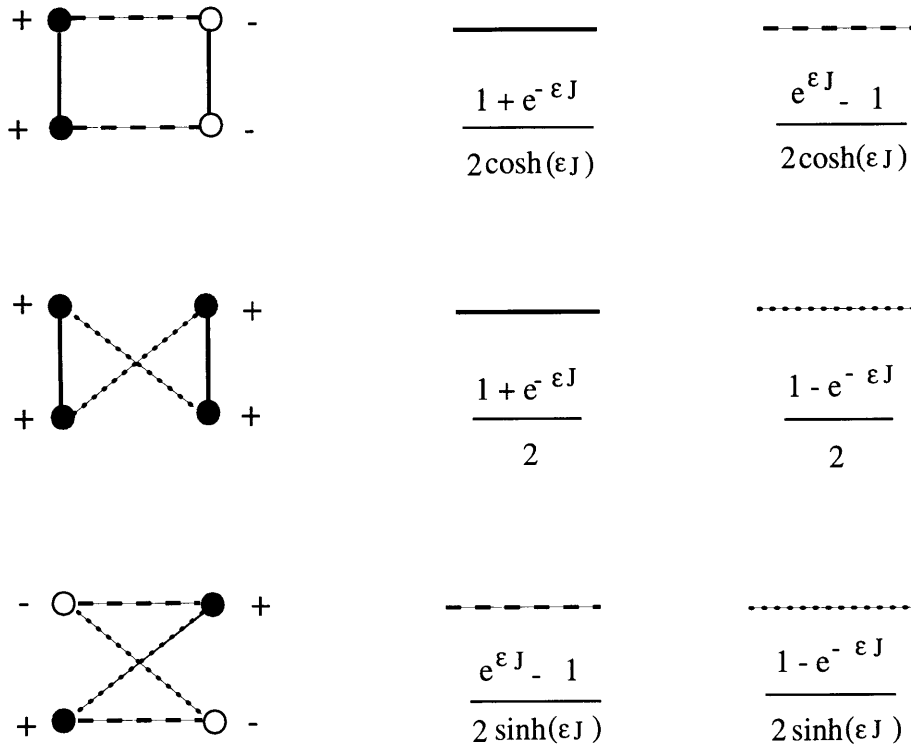


Figure 11-1: *The plaquette decomposition probabilities in the quantum XY model.*

The analysis can be easily repeated for the Heisenberg ferromagnets or antiferromagnets or any other spin model. In fact, the loop-cluster algorithm that we just developed has proved a very efficient tool for the simulation of all the spin models.

It can operate either as a single cluster algorithm where one constructs a single loop and flips it or as a multi cluster decomposition of the lattice where one would flip the clusters independently with a 50 – 50 probability.

11.4 Basis-Independence of the Clusters

In this section we are going to pursue further the understanding of the cluster decomposition of the (2+1)-d lattice. We recall that the partition function has been rewritten as

$$Z = \text{Tr}\left(\prod_{p=1}^{N_p} T_p\right) = \sum_{\mathcal{S}} W[\mathcal{s}_i], \quad (11.22)$$

Each configuration of spins \mathcal{S} appears with a probability $\mathcal{P}[\mathcal{s}_i] = W[\mathcal{s}_i]/Z$.

Now we recall that each plaquette transfer matrix T_p can be written as a sum of three decompositions which we denote as $\{n_p\} = \{1, 2, 3\}$. Therefore the partition function can be written as

$$Z = \text{Tr}\left(\prod_{p=1}^{N_p} \sum_{n_p=\{1,2,3\}} w_{n_p} \mathcal{M}_{n_p}\right) = \sum_{G=\{n_p\}} \text{Tr}\left(\prod_{p=1}^{N_p} w_{n_p} \mathcal{M}_{n_p}\right). \quad (11.23)$$

Here G denotes a unique choice of plaquette decompositions for the whole lattice, which is actually a connected graph of a complete decomposition of the lattice into loops. For convenience we name the tensors

$$\mathcal{M}_1 = \delta_{s_1, s_3} \delta_{s_2, s_4} \quad \mathcal{M}_2 = \delta_{s_1, s_4} \delta_{s_2, s_3} \quad \mathcal{M}_3 = \sigma_{s_1, s_2}^1 \sigma_{s_3, s_4}^1. \quad (11.24)$$

Let us now define the weight $W_G = \prod_{p=1}^{N_p} w_{n_p}$ for a certain graph G and the time ordered operator $\mathcal{M}_G = \prod_{p=1}^{N_p} \mathcal{M}_{n_p}$.

The partition function can now be written as

$$Z = \sum_G W_G \text{Tr}[\mathcal{M}_G], \quad (11.25)$$

which suggests an interesting interpretation. It describes a *random cluster model* in

the sense that the phase space now consists of the graphs containing loops that cover completely a (2+1)-d lattice. The associated Boltzmann weight is W_G while $\text{Tr}[\mathcal{M}_G]$ represents an internal quantum number assigned to the graph. It is very important to notice that W_G and $\text{Tr}[\mathcal{M}_G]$ are *independent* of the basis used to represent the spin operators. This means that the clusters are dynamical objects with geometrical properties of their own. The choice of a particular representation only changes the rules according to which the plaquettes are decomposed and therefore the way the loops are grown without affecting the Boltzmann weight that their length, shape e.t.c. is associated with.

11.5 Measurement of Green's Functions

The expectation value for an operator \mathcal{O}_x at site x is given by

$$\langle \mathcal{O}_x \rangle = \frac{1}{Z} \text{Tr}[\mathcal{O}_x \exp(-\beta H)]. \quad (11.26)$$

We would like to have an expression that would allow us to measure this expectation value. Therefore we again decompose H as in eq.(11.4) and insert $4N$ time slices to define a path integral. We immediately see that in order to recover the same (2+1)-d Boltzmann weight, \mathcal{O}_x has to be diagonal in the representation we are working in. If this is the case, we simply measure its value on an arbitrary time slice and we can determine its expectation value. If \mathcal{O}_x is not diagonal, then it appears as a defect in the effective interaction on some time slice. This means that a different path integral has to be generated in order to measure $\langle \mathcal{O}_x \rangle$. Still, the observable in that case would be the modified partition function itself divided by the unmodified partition function, and it appears extremely hard to measure such a thing with the available algorithmic processes.

The problem seemed intractable until it was realized recently [73] that precisely the cluster algorithm itself provides a way out. Recall that the partition function is a trace of time-ordered T -matrices. Now the presence of \mathcal{O}_x implies an insertion of

the matrix $\mathcal{O}_{s_{x,t},\tilde{s}_{x,t}}$ between some $T(\dots s_{x,t})$ matrix coupling $t-1$ and t slice bond, and a $T(\tilde{s}_{x,t}\dots)$ matrix acting between t and $t+1$ slices in the multiplicative scheme

$$\dots[\sum_{s_{x,t},\tilde{s}_{x,t}} T(\dots s_{x,t})\mathcal{O}_{s_{x,t},\tilde{s}_{x,t}}T(\tilde{s}_{x,t}\dots)]\dots \quad (11.27)$$

Since every T -matrix has been decomposed as $T = w_1 \mathcal{M}_1 + w_2 \mathcal{M}_2 + w_3 \mathcal{M}_3$, \mathcal{O}_x will be inserted in each of the 3^{N_p} decompositions of the lattice between the \mathcal{M}_{n_p} operators

$$\langle \mathcal{O}_x \rangle = \frac{1}{Z} \text{Tr}[\prod_{p=1}^{N_p} \sum_{n_p=\{1,2,3\}} w_{n_p}(\mathcal{O}_x \mathcal{M}_{n_p})] = \frac{1}{Z} \sum_{G=\{n_p\}} \text{Tr}[\prod_{p=1}^{N_p} w_{n_p}(\mathcal{O}_x \mathcal{M}_{n_p})] \quad (11.28)$$

and we recover an expression in the random cluster model

$$\langle \mathcal{O}_x \rangle = \frac{1}{Z} \sum_G W_G \text{Tr}[\mathcal{O}_x \mathcal{M}_G] = \langle \frac{\text{Tr}[\mathcal{O}_x \mathcal{M}_G]}{\text{Tr}[\mathcal{M}_G]} \rangle_G . \quad (11.29)$$

The numerical evaluation of this expression is an easy task with the cluster algorithm. After generating a graph G in a Markov chain with probability

$$\mathcal{P}(G) = \frac{1}{Z} W_G \text{Tr}[\mathcal{M}_G] \quad (11.30)$$

we have to examine the clusters of the graph and count if they contribute to the quantity $\text{Tr}[\mathcal{O}_x \mathcal{M}_G]$.

Let us demonstrate how this works with a concrete application to the XY model. Suppose we are interested in the expectation value of the operator σ_x^1 . The graph G consists of N_G clusters, \mathcal{C}_i ($i = 1, 2, \dots, N_G$) and since they do not intersect, the traces decompose into independent traces of the clusters

$$\text{Tr}[\mathcal{M}_G] = \prod_{i=1}^{N_G} \text{Tr}[\mathcal{M}_{\mathcal{C}_i}] , \quad \text{Tr}[\mathcal{O}_x \mathcal{M}_G] = \prod_{i=1}^{N_G} \text{Tr}[\mathcal{O}_x \mathcal{M}_{\mathcal{C}_i}] . \quad (11.31)$$

Therefore $\langle \sigma_x^1 \rangle = \langle \text{Tr}[\sigma_x^1 \mathcal{M}_G] \rangle_G$. But now remember that given a spin on the loop, all the other spin states are automatically determined from the clustering rules. This

gives $\text{Tr}\mathcal{M}_C = 2$. Furthermore, the operator σ_x^1 is the flipping operator $\sigma_x^1|\pm\rangle = |\mp\rangle$ and therefore causes an inconsistent flip within the loop. Therefore $\text{Tr}[\sigma_x^1\mathcal{M}_C] = 0$ and $\langle\sigma_x^1\rangle = 0$.

Now we proceed to the more interesting two-point function $\text{Re}\langle\sigma_x^+\sigma_y^-\rangle$ from which the correlation length is extracted. Since $\sigma^+ = (\sigma^1 + i\sigma^2)/2$ and $\sigma^- = (\sigma^1 - i\sigma^2)/2$, it follows that $\text{Re}\langle\sigma_x^+\sigma_y^-\rangle = (\langle\sigma_x^1\sigma_y^1\rangle + \langle\sigma_x^2\sigma_y^2\rangle)/4$. The $O(2)$ invariance of the model implies further that $\langle\sigma_x^1\sigma_y^1\rangle = \langle\sigma_x^2\sigma_y^2\rangle$ after a rotation by $\pi/2$ in the X - Y plane. Therefore $\langle\sigma_x^1\sigma_y^1\rangle$ suffices for reconstructing all physical results.

In order to get a contribution to $\langle\sigma_x^1\sigma_y^1\rangle$ we need to have *both* points x and y on the same loop. In this case, the second flip repairs the inconsistency created from the first and $\text{Tr}[\sigma_x^1\sigma_y^1\mathcal{M}_C]$ gets always the contribution 2. The loop appears as being cut at the sites x and y and half of it is flipped. Therefore, the improved estimator for the two-point function $\text{Re}\langle\sigma_x^+\sigma_y^-\rangle$ gets a positive contribution 1/2 for any pair of points in an examined loop. The translational invariance of the Hamiltonian guarantees that all the pairs are contributing equally to a correlation function which at the end depends only on the distance vector $x - y$.

Notice that on a given loop, we can get a non-zero contribution only if we put an even number of operators σ^1 or σ^2 . The operator σ^2 also behaves like a flipping operator up to phases, since $\sigma^2|\pm\rangle = \pm i|\mp\rangle$. A general $2n$ -point function of σ^1 's and σ^2 's will get a non-zero contribution if all the points live on a loop or are split in always even subsets that live on different loops. As a lemma, we realize that any $2n+1$ -point function is always zero, a result that we anticipated based on the reflection symmetry $\vec{S} \rightarrow -\vec{S}$ of the model.

The reason we managed to extract information about Green's functions previously thought unreachable can be traced precisely to the basis independence of the cluster dynamics. Since the geometrical properties of the clusters themselves are basis independent — recall that the graph weights W_G are basis independent — we can imagine that we work in a basis in which the operator \mathcal{O}_x is diagonal. In that case, the same clusters would be grown under different rules and we could go on and measure immediately the value of \mathcal{O}_x from the generated configuration. The basis independence of

the cluster dynamics can be checked explicitly in the XY model as in fact has been demonstrated in [73]. Suppose we are interested in $\langle \sigma_x^2 \sigma_y^2 \rangle_{XY}$. We can choose to work in the representation in which σ^2 is diagonal. This can be achieved formally if we rotate \vec{S} by $\pi/2$ in the 2–3 plane with the unitary operator $U = \prod_x \exp(-i\pi\sigma_x^1/4)$ which takes $\sigma_x^2 \rightarrow \sigma_x^3$ and $\sigma_x^3 \rightarrow -\sigma_x^2$. The transformation effectively maps the XY model to the XZ model which is defined through the Hamiltonian

$$H_{XZ} = -\frac{J}{2} \sum_{x,\hat{\mu}} \left(\sigma_x^1 \sigma_{x+\hat{\mu}}^1 + \sigma_x^3 \sigma_{x+\hat{\mu}}^3 \right) \quad (11.32)$$

Due to this rotation we have $\langle \sigma_x^2 \sigma_y^2 \rangle_{XY} = \langle \sigma_x^3 \sigma_y^3 \rangle_{XZ}$. Now, the plaquette decomposition rules for the XZ can be easily extracted from the rotated transfer matrix

$$\mathcal{T}_{XZ} = \exp(i\pi\sigma_x^1/4) \exp(i\pi\sigma_{x+\hat{\mu}}^1/4) \mathcal{T}_{XY} \exp(-i\pi\sigma_x^1/4) \exp(-i\pi\sigma_{x+\hat{\mu}}^1/4), \quad (11.33)$$

which again in the σ^3 basis is

$$\mathcal{T}_{XZ}(s_1, s_2; s_3, s_4) = \sum_{s'_1, s'_2, s'_3, s'_4} U_{s_3, s'_3}^\dagger U_{s_4, s'_4}^\dagger \mathcal{T}_{XY}(s'_1, s'_2; s'_3, s'_4) U_{s_1, s'_1} U_{s_2, s'_2}. \quad (11.34)$$

Using eq.(11.15) for \mathcal{T}_{XY} along with

$$U_{s_i, s'_i} = \frac{1}{\sqrt{2}} (\delta_{s_i, s'_i} - i\sigma_{s_i, s'_i}^1), \quad U_{s_i, s'_i}^\dagger = \frac{1}{\sqrt{2}} (\delta_{s_i, s'_i} + i\sigma_{s_i, s'_i}^1), \quad (11.35)$$

we get

$$\begin{aligned} \mathcal{T}_{XZ}(s_1, s_2; s_3, s_4) &= \frac{1}{4} \sum_{s'_1, s'_2, s'_3, s'_4} \left\{ (\delta_{s_3, s'_3} + i\sigma_{s_3, s'_3}^1) (\delta_{s_4, s'_4} + i\sigma_{s_4, s'_4}^1) \right. \\ &\quad \left. (w_1 \delta_{s'_1, s'_3} \delta_{s'_2, s'_4} + w_2 \delta_{s'_1, s'_4} \delta_{s'_2, s'_3} + w_3 \sigma_{s'_1, s'_2}^1 \sigma_{s'_3, s'_4}^1) (\delta_{s_1, s'_1} - i\sigma_{s_1, s'_1}^1) (\delta_{s_2, s'_2} - i\sigma_{s_2, s'_2}^1) \right\}. \end{aligned} \quad (11.36)$$

It requires a long but straightforward calculation to show that

$$\mathcal{T}_{XZ}(s_1, s_2; s_3, s_4) = w_1 \delta_{s_1, s_3} \delta_{s_2, s_4} + w_2 \delta_{s_1, s_4} \delta_{s_2, s_3} + w_3 \delta_{s_1, s_2} \delta_{s_3, s_4}. \quad (11.37)$$

We see that the three patterns which decompose the plaquette remain the same and in fact appear with the same weights w_1, w_2, w_3 . Therefore, both XY and XZ models are mapped to the same random cluster model. Nevertheless, one crucial difference has appeared. All the tensors are now δ -functions which means that the loops for the XZ contain spins of the *same orientation only*. What can we learn about correlation functions in the XZ in the σ^3 basis? First, notice that $\text{Tr}[\vec{\sigma}_x \mathcal{M}_{c_i}] = 0$. This is true since again σ^1 and σ^2 cause inconsistent flips around the loop and σ^3 gets $+1$ and -1 contribution from the spin states. Second, $\text{Tr}[\sigma_x^1 \sigma_y^1 \mathcal{M}_{c_i}]$ gets a contribution $+1$ if the pair x, y belongs to the same loop. From this we conclude that $\langle \sigma_x^1 \sigma_y^1 \rangle_{XZ} = \langle \sigma_x^1 \sigma_y^1 \rangle_{XY}$. Since the spins in a loop are all in the same state, we learn also that $\text{Tr}[\sigma_x^3 \sigma_y^3 \mathcal{M}_{c_i}] = \text{Tr}[\mathcal{M}_{c_i}] = 2$. Therefore, we also get a $+1$ contribution to $\langle \sigma_x^3 \sigma_y^3 \rangle_{XZ}$ and conclude the following interesting chain of equalities

$$\langle \sigma_x^1 \sigma_y^1 \rangle_{XY} = \langle \sigma_x^2 \sigma_y^2 \rangle_{XY} = \langle \sigma_x^1 \sigma_y^1 \rangle_{XZ} = \langle \sigma_x^3 \sigma_y^3 \rangle_{XZ} . \quad (11.38)$$

Using this methodology interesting relations can appear between higher n -point functions in the XY and the XZ spin models.

Chapter 12

The Flux-Cluster Algorithm

12.1 Introduction

In this chapter we are going to develop a cluster algorithm for the spin-1/2 $U(1)$ QLM . We are going to follow step-by-step the methodology applied to the Abelian spin model. In section 2 we are going to perform the Suzuki-Trotter decomposition and construct the (4+1)-d path integral with a discrete fifth direction. We therefore expect that the importance sampling of this partition function can be achieved by forming clusters of links and updating the system. We show in section 3 that rules for joining interacting links such that detailed balance and ergodicity are respected can be found. In section 4 we demonstrate that the cluster algorithm provides improved estimators for the measurement of Wilson loop expectation values. We finally show in section 5 that the discreteness of the Hilbert space allows the simulation of the model directly in the continuum of the fifth direction.

12.2 Suzuki-Trotter decomposition

Let us recall the $U(1)$ Hamiltonian

$$H = -J \sum_{\mathbf{x}, \mu < \nu} [U_{\mathbf{x}, \mu} U_{\mathbf{x}+\hat{\mu}, \nu} U_{\mathbf{x}+\hat{\nu}, \mu}^\dagger U_{\mathbf{x}, \nu}^\dagger + U_{\mathbf{x}, \nu} U_{\mathbf{x}+\hat{\nu}, \mu} U_{\mathbf{x}+\hat{\mu}, \nu}^\dagger U_{\mathbf{x}, \mu}^\dagger], \quad (12.1)$$

where in the spin-1/2 representation the link operators and the Gauss law generator are given by

$$U_{x,\mu} = \sigma_{x,\mu}^+ , \quad U_{x,\mu}^\dagger = \sigma_{x,\mu}^- , \quad G_x = \frac{1}{2} \sum_{\mu} (\sigma_{x,\mu}^3 - \sigma_{x-\hat{\mu},\mu}^3) . \quad (12.2)$$

Since $S_{x,\mu}^3$ corresponds to the electric field vector defined on the link, a natural basis to work with is diagonal in the electric field. Therefore, the $|\pm\rangle$ eigenstates of $\sigma_{x,\mu}^3$ correspond to the quantized electric flux living on the link (x, μ) and the cluster algorithm that is to be presented will be naturally named *flux-cluster algorithm*.

We start the Suzuki-Trotter decomposition by dissecting the compact interval $[0, \beta]$ into N small steps $\beta = \epsilon N$,

$$Z = \text{Tr} \prod_{i=1}^N \exp(-\epsilon H) . \quad (12.3)$$

In four dimensions, there are six planes in which the plaquette operators live. Searching for the maximal sets containing commuting operators we realize that we have to perform a checker board decomposition for each plane ($\mu < \nu$)

$$H_{\mu\nu} = H_{\mu\nu}^{(white)} + H_{\mu\nu}^{(black)} , \quad (12.4)$$

$$H_{\mu\nu}^{(white)} = -J \sum_{x | x_\mu + x_\nu = 2n} [U_{x,\mu} U_{x+\hat{\mu},\nu} U_{x+\hat{\nu},\mu}^\dagger U_{x,\nu}^\dagger + U_{x,\nu} U_{x+\hat{\nu},\mu} U_{x+\hat{\mu},\nu}^\dagger U_{x,\mu}^\dagger] , \quad (12.5)$$

$$H_{\mu\nu}^{(black)} = -J \sum_{x | x_\mu + x_\nu = 2n+1} [U_{x,\mu} U_{x+\hat{\mu},\nu} U_{x+\hat{\nu},\mu}^\dagger U_{x,\nu}^\dagger + U_{x,\nu} U_{x+\hat{\nu},\mu} U_{x+\hat{\mu},\nu}^\dagger U_{x,\mu}^\dagger] . \quad (12.6)$$

$H_{\mu\nu}^{(white)}$ and $H_{\mu\nu}^{(black)}$ are both sets of mutually commuting plaquette Hamiltonians. Furthermore, for each plane $(\mu\nu)$ there is an orthogonal plane $(\kappa\lambda)$ with all $\mu, \nu, \kappa, \lambda$ different from each other. We can therefore decompose H into six maximal sets of commuting plaquette operators

$$H = H_1 + H_2 + H_3 + H_4 + H_5 + H_6 , \quad (12.7)$$

$$H_1 = H_{12}^{(white)} + H_{34}^{(white)} , \quad H_2 = H_{12}^{(black)} + H_{34}^{(black)} , \quad (12.8)$$

$$H_3 = H_{13}^{(white)} + H_{24}^{(white)} \quad , \quad H_4 = H_{13}^{(black)} + H_{24}^{(black)} \quad , \quad (12.9)$$

$$H_5 = H_{14}^{(white)} + H_{23}^{(white)} \quad , \quad H_6 = H_{14}^{(black)} + H_{23}^{(black)} \quad . \quad (12.10)$$

For large N we approximate

$$\exp(-\epsilon H) \simeq \exp(-\epsilon H_1) \exp(-\epsilon H_2) \exp(-\epsilon H_3) \exp(-\epsilon H_4) \exp(-\epsilon H_5) \exp(-\epsilon H_6) \quad , \quad (12.11)$$

and inserting complete sets of flux states between the $6N$ exponentials, we recover a path integral for a 5-d partition function with $6N$ time slices between $t = 0$ and $t = \beta$,

$$Z = \prod_{\mathbf{x}, \mu, t} \sum_{e_{\mathbf{x}, \mu, t} = \pm \frac{1}{2}} \exp(-S[e]) \quad . \quad (12.12)$$

The classical fields are now the electric flux configurations $e_{\mathbf{x}, \mu, t}$ living on each t -slice copy of the 4-d lattice. Each plaquette transfer matrix

$$\mathcal{T} = \exp \left(\epsilon J \left[\sigma_{\mathbf{x}, \mu}^+ \sigma_{\mathbf{x}+\hat{\mu}, \nu}^+ \sigma_{\mathbf{x}+\hat{\nu}, \mu}^- \sigma_{\mathbf{x}, \nu}^- + \sigma_{\mathbf{x}, \mu}^- \sigma_{\mathbf{x}+\hat{\mu}, \nu}^- \sigma_{\mathbf{x}+\hat{\nu}, \mu}^+ \sigma_{\mathbf{x}, \nu}^+ \right] \right) \quad (12.13)$$

defines an effective cubic interaction between a plaquette and its image in the next slice. The classical action $S[e]$ appears as a sum of the individual cubic terms. For simplicity let us rename the flux states of a cube as

$$\begin{aligned} e_{\mathbf{x}, \mu, t} &= e_1 \quad , \quad e_{\mathbf{x}+\hat{\mu}, \nu, t} = e_2 \quad , \quad e_{\mathbf{x}+\hat{\nu}, \mu, t} = e_3 \quad , \quad e_{\mathbf{x}, \nu, t} = e_4 \quad , \\ e_{\mathbf{x}, \mu, t+1} &= e'_1 \quad , \quad e_{\mathbf{x}+\hat{\mu}, \nu, t+1} = e'_2 \quad , \quad e_{\mathbf{x}+\hat{\nu}, \mu, t+1} = e'_3 \quad , \quad e_{\mathbf{x}, \nu, t+1} = e'_4 \quad . \end{aligned} \quad (12.14)$$

Each cube appears with a Boltzmann weight

$$\begin{aligned} W[e_1, e_2, e_3, e_4 ; e'_1, e'_2, e'_3, e'_4] &= \exp(-S[e_1, e_2, e_3, e_4 ; e'_1, e'_2, e'_3, e'_4]) \quad (12.15) \\ &= \langle e'_1 e'_2 e'_3 e'_4 | \mathcal{T} | e_1 e_2 e_3 e_4 \rangle \quad . \end{aligned}$$

The exponentiation of \mathcal{T} is easy to carry out; in fact, it gives the same series as the

XY model, only with the addition of more diagonal states

$$\begin{aligned} \mathcal{T} = \mathbb{1} &+ (\cosh(\epsilon J) - 1)(P_{x,\mu}^+ P_{x+\hat{\mu},\nu}^+ P_{x+\hat{\nu},\mu}^- P_{x,\nu}^- + P_{x,\mu}^- P_{x+\hat{\mu},\nu}^- P_{x+\hat{\nu},\mu}^+ P_{x,\nu}^+) \\ &+ \sinh(\epsilon J)(\sigma_{x,\mu}^+ \sigma_{x+\hat{\mu},\nu}^+ \sigma_{x+\hat{\nu},\mu}^- \sigma_{x,\nu}^- + \sigma_{x,\mu}^- \sigma_{x+\hat{\mu},\nu}^- \sigma_{x+\hat{\nu},\mu}^+ \sigma_{x,\nu}^+) . \end{aligned} \quad (12.16)$$

From the 16×16 matrix elements, only 18 are non-vanishing:

The diagonal $\langle ++-- | \mathcal{T} | ++-- \rangle = \langle --++ | \mathcal{T} | --++ \rangle = \cosh(\epsilon J)$, the rest of the diagonals with weight 1 and the non-diagonal $\langle ++-- | \mathcal{T} | --++ \rangle = \langle --++ | \mathcal{T} | ++-- \rangle = \sinh(\epsilon J)$.

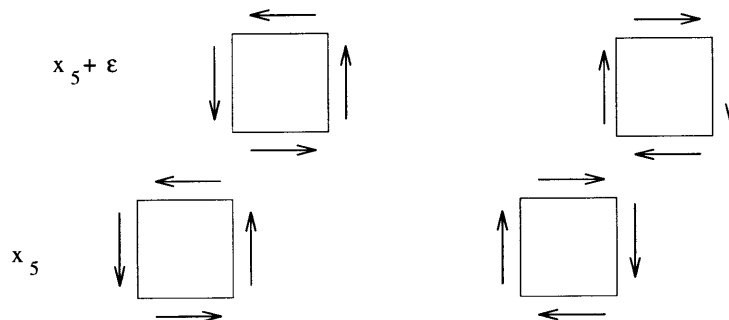
12.3 The Discrete Time Algorithm

The flux cluster algorithm is equivalent to a choice of decomposing the eight links of the elementary interacting cube into clusters in such a way that if one of the groups is flipped, a new state is obtained while detailed balance and ergodicity are always obeyed.

In contrast to the spin models, this problem appears too complicated to be handled transparently with the algebraic decomposition of \mathcal{T} in simpler tensors. Therefore, we are going to work in a more pictorial way in order to present the general choices of cluster rules for the elementary cube. We are going to examine the cube configurations with non-zero weight and simply examine the possibilities for decomposition patterns. Then, we are going to assign probabilities to each pattern such that detailed balance and ergodicity are obeyed. We will find that we have many options for an algorithm and, in fact, parameterize the space of possible algorithms. Different choices will in general have different degrees of efficiency.

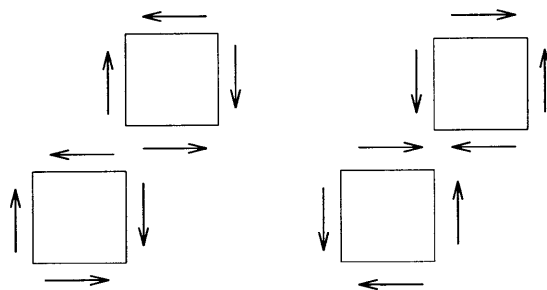
Examining the cube states we should first remember that the \pm flux state denotes the electric field orientation, which in the following graphs is going to be represented by an arrow. Second, note that the Hamiltonian is invariant under rotations and reflections and therefore our cluster rules should respect that. We are going to define classes of cube configurations related by these symmetries and treat them identically.

Class 1 contains the diagonal states $(++-- ; ++--)$ and $(--++ ; --++)$ with non-trivial weight $\cosh(\epsilon J)$. They are characterized by the fact that the flux flows continuously around the plaquettes.



Class 1

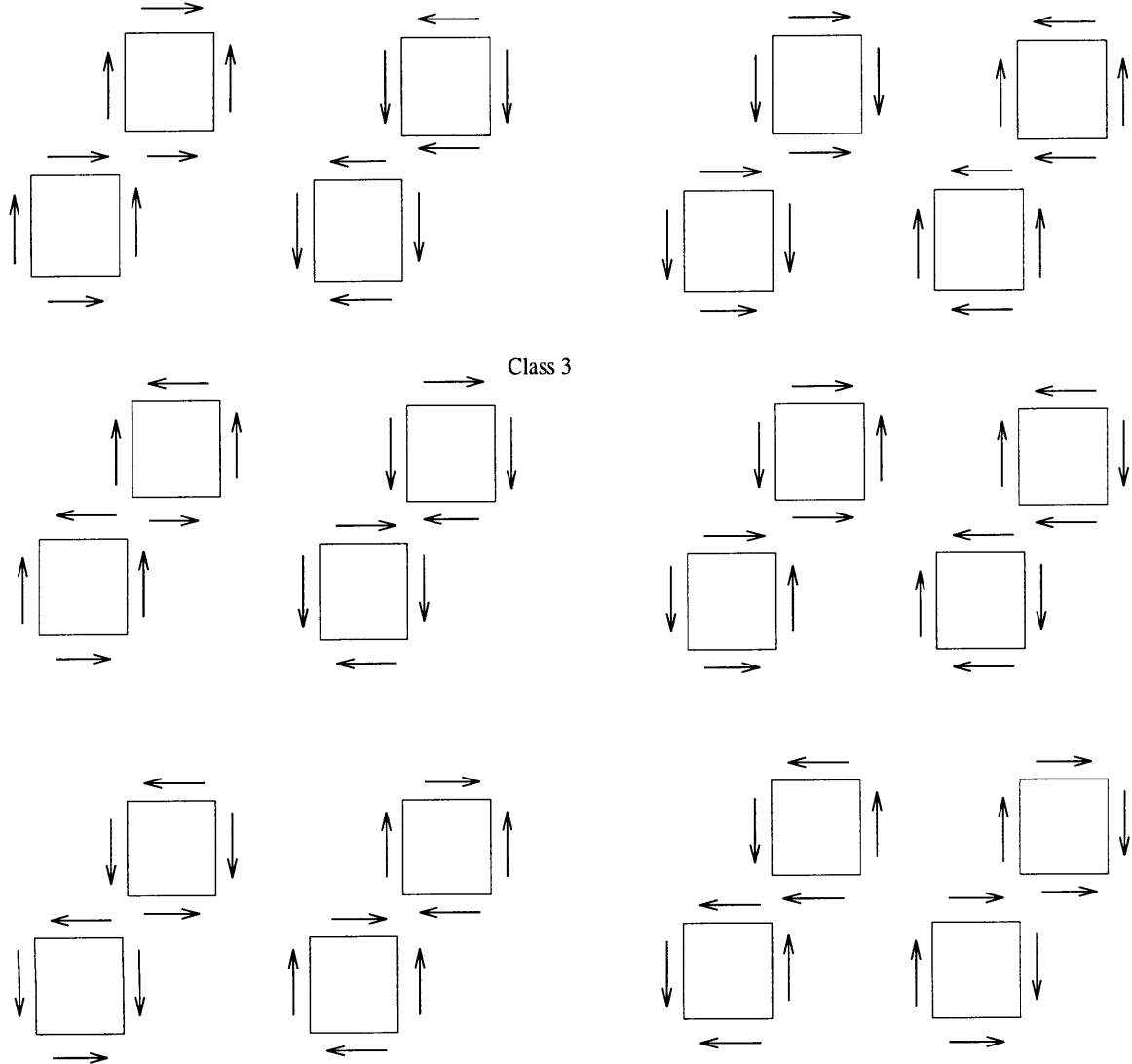
Class 2 contains the diagonal states $(+--+ ; +--+)$ and $(-+-+ ; -+-+)$ with weight 1. The flux flow for these states is interrupted at all four corners of the plaquette.



Class 2

Class 3 contains the diagonal states $(++++ ; +++)$, $(---- ; ----)$ and $(+-+- ; +-+-)$, $(-+-+ ; -+-+)$ of weight 1. These states have violation of the flux flow at two diagonally opposite sites of the plaquette.

Class 4 contains the diagonal states $(++-+ ; ++-+)$, $(+++- ; +++-)$, $(+--- ; +---)$, $(-+--- ; -+---)$ and their flipped partners $(--+- ; --+-)$, $(---+ ; ---+)$, $(-+++ ; -+++)$ and $(+-++ ; +-++)$. All these states have weight 1 and their characteristic is that one link flux is against the flow of the rest three on the plaquette.

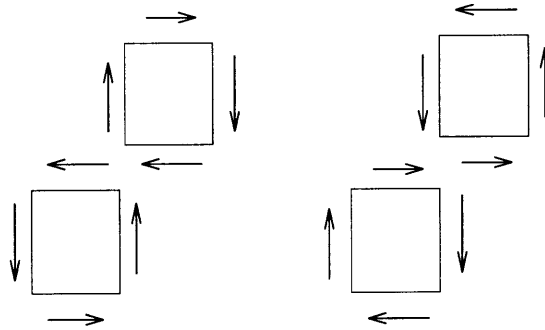


Class 3

Class 4

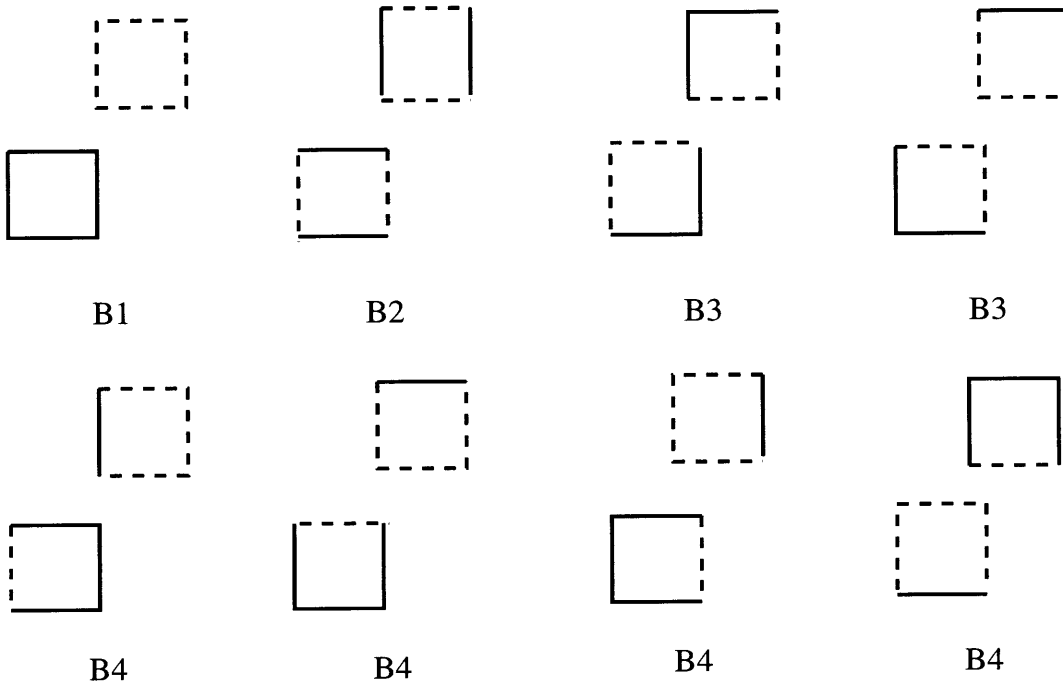
Class 5 contains the only non diagonal states $(++--; --++)$ and $(--++; ++--)$ which have weight $\sinh(\epsilon J)$. These states have a continuous flux flow on both plaquettes but in opposite directions. We will refer to these states as transition cubes.

We start by looking for decomposition patterns that would make a transition cube decay to one of the 16 diagonal states. We will refer to the decomposition patterns generally as “cube breakups”. Since each link on the transition cube has opposite flux from its t -forward neighbor, a cluster flip that can take it to a diagonal state needs to flip exactly four links and no pair of them should be t -forward neighbors.



Class 5

Therefore, the transition cube breakups decompose the cube into two clusters of 4 links each and as we see easily there are 8 patterns to do that. Each pattern has the meaning of a projection operator on a certain state as we will specify later. We identify rotationally connected breakups into patterns B1-B4.



Transition Breakups

The other class of breakups would after flipping take a diagonal state to a diagonal state. In order to respect that, these breakups should include t -forward neighboring links in the same cluster. There are several ways to perform these diagonal breakups, again identifying rotationally related patterns.

One way (D1) is to assign all four pairs to independent clusters.

A second way is to join two pairs in one cluster and the other two pairs in a different cluster. There are two classes that achieve this, depending on if the joined pairs are opposite (D2) or adjacent (D3) to each other in the plaquette.

A third way is to join three pairs into a cluster and the last pair to a different one (D4).

Finally, a fourth way is to join two of those pairs to a cluster and assign the other two pairs to independent clusters. Rotational symmetry distinguishes two classes in this way according to if the two independent pairs are adjacent (D5) or opposite (D6) to each other in the cube. We are not considering the possibility to join all 8 links to a cluster since such a move would not induce an interesting update.

The breakup types that we have pictorially presented above actually represent projection operators made out of appropriate tensors that decompose the transfer matrix as we have already seen in the spin models. This pictorial decomposition is not yet complete since we have not specified what configurations live on the links that are joined with these graphs. We are going to assign such a specification now. We are going to demand that links on the same time slice that are going to be included in a cluster should keep the flux flow around the plaquette. This will be essential, as we will see later, for the existence of improved estimators for Wilson loops. Each projection operator, which is one of the graphs above, is assigned a coefficient in the decomposition of the transfer matrix. We call these coefficients $B_1 - B_4$ and $D_1 - D_6$ according to the patterns.

Following this specification, each of the five classes of transfer matrix elements is decomposed uniquely into the patterns B1-B4 and D1-D6. For example, a class 1 configuration can decay to a transition cube (class 5) through the pattern B1 only. It can also decay to the diagonal class 4 through pattern D1, to class 2 through pattern D2, to class 3 through both of the patterns D3, to class 4 through the four patterns D4, to class 3 through two of the patterns D5 and to class 4 through the other two patterns D5 and finally to class 2 through one of the D6 patterns and to class 4 through the other D6 pattern.

A class 2 configuration can decay to the transition cube only through pattern B2.

The diagonal patterns that are allowed are only D1, D2 and D6. The rest violate the flux continuation restriction we imposed. It can therefore decay through D1 to class 4, through pattern D2 to class 1 and through one pattern D6 to a class 1 state and through the other pattern D6 to a class 4 state. Similarly we can find pictorially the decays for the other states. The pictorial decomposition of the transfer matrix gives the equations

$$\begin{aligned}
\cosh(\epsilon J) &= B_1 + D_1 + D_2 + 2D_3 + 4D_4 + 4D_5 + 2D_6, & (12.17) \\
1 &= B_2 + D_1 + D_2 + 2D_6, \\
1 &= B_3 + D_1 + D_3 + 2D_5, \\
1 &= B_4 + D_1 + D_4 + 2D_5 + D_6, \\
\sinh(\epsilon J) &= B_1 + B_2 + 2B_3 + 4B_4.
\end{aligned}$$

Each cube has a probability to decay to another cube given by the coefficient of the decay pattern that connects the two cubes divided by the weight of the first cube. In this way the detailed balance is automatically guaranteed — recall the discussion for the XY cluster algorithm. The coefficients $B_1 - B_4$ and $D_1 - D_6$ are therefore positive numbers between 0 and 1. Further, we see that only D_1 is an $\mathcal{O}(1)$ number while the rest are small $\mathcal{O}(\epsilon J)$ numbers. There are five parameters left undetermined from (12.17). Each allowed choice of these parameters constitutes a flux-cluster algorithm for the $j = 1/2$ $U(1)$ QLM which will automatically have improved estimators for Wilson loops. Ergodicity has to be checked individually for each selection. We can select $D_2 - D_6$ as free parameters. The rest of the coefficients are then determined

$$\begin{aligned}
D_1 &= \frac{7 + e^{-\epsilon J}}{8} - \frac{1}{4}D_2 - \frac{1}{2}D_3 - D_4 - 2D_5 - D_6, & (12.18) \\
B_1 &= \frac{4e^{\epsilon J} + 3e^{-\epsilon J} - 7}{8} - \frac{3}{4}D_2 - \frac{3}{2}D_3 - 3D_4 - 2D_5 - D_6, \\
B_2 &= \frac{1 - e^{-\epsilon J}}{8} - \frac{3}{4}D_2 + \frac{1}{2}D_3 + D_4 + 2D_5 - D_6, \\
B_3 &= \frac{1 - e^{-\epsilon J}}{8} + \frac{1}{4}D_2 - \frac{1}{2}D_3 + D_4 + D_6,
\end{aligned}$$

$$B_4 = \frac{1 - e^{-\epsilon J}}{8} + \frac{1}{4}D_2 + \frac{1}{2}D_3 .$$

A simple choice for an algorithm is $D_2 = D_3 = D_4 = D_5 = D_6 = 0$. This is an ergodic choice and is the algorithm that has been used for the numerical results presented in chapter 14.

12.4 Measuring Wilson Loops

The algorithm we presented above joins links carrying electric flux in a continuous flow and follows their evolution in the fifth Euclidean direction. Therefore the cluster which is generated is a two-dimensional surface embedded in the (4+1)-d lattice of the *QLM*. Physically this surface is the world-sheet of electric flux strings. Since we do not enforce the Gauss law constraint in the *QLM* Hilbert space, these electric flux strings can be oriented closed or open strings. A closed string carrying oriented flux does not change the charge anywhere after it is flipped and therefore respects the Gauss law constraint. An open string, on the other hand, is an electric field line from one point to another, and after it is flipped it will generate violations of the electric charge at its endpoints. The cluster which is the string world-sheet will therefore be an orientable surface of arbitrary topology and in general we can picture it as a union of both closed and open 2-d patches.

Following the quantum *XY* development, we would anticipate that the partition function can be rewritten as a *quantum random surface model*. Indeed the partition function is

$$Z = \text{Tr} \left(\prod_{c=1}^{N_c} \mathcal{T}_c \right) = \sum_{\{e\}} W[e] \quad (12.19)$$

with the transfer matrices in a fifth direction ordered product. Each transfer matrix of the N_c cubes has been expressed as a sum of the projection operator-patterns $B_1 - B_4$ and $D_1 - D_6$ with corresponding coefficients $B_1 - B_4$, $D_1 - D_6$. There are in total $8 + 14 = 22$ decompositions. Let us denote all these decompositions $n_c = 1, 2, \dots, 22$

with corresponding operators \mathcal{M}_{n_c} and coefficients w_{n_c} . Then

$$Z = \text{Tr}\left(\prod_{c=1}^{N_c} \sum_{n_c=1}^{22} w_{n_c} \mathcal{M}_{n_c}\right) = \sum_{G=\{n_c\}} \text{Tr}\left(\prod_{c=1}^{N_c} w_{n_c} \mathcal{M}_{n_c}\right) \quad (12.20)$$

where G is a graph representing a unique choice of breakup $\{n_c\}$ for each of the (4+1)-d lattice cubes. We can define the fifth direction ordered decomposition operator for each graph $\mathcal{M}_G = \prod_{c=1}^{N_c} \mathcal{M}_{n_c}$, which has the weight $W_G = \prod_{c=1}^{N_c} w_{n_c}$. Each graph G is a unique and complete decomposition of the (4+1)-d lattice into 2-d surfaces. The partition function then becomes

$$Z = \sum_G W_G \text{Tr} \mathcal{M}_G, \quad (12.21)$$

which is the partition function for a random surface model. Notice that this expression is independent of the basis chosen to describe the Hilbert space. The surfaces that fill the volume are dynamical objects generated with the Boltzmann weight W_G and an associated internal quantum number $\text{Tr} \mathcal{M}_G$. For a given βJ their shapes, topology e.t.c. is independent of the basis chosen to describe the system.

The order parameter of the model is the expectation value of the Wilson loop operator

$$\langle \hat{W}_C \rangle = \frac{1}{Z} \text{Tr}[U_1 U_2 \dots U_{\ell-1}^\dagger U_\ell^\dagger \exp(-\beta H)], \quad (12.22)$$

for a loop C with length ℓ . Since it is a non-diagonal operator, we cannot measure its value by simply looking at the (4+1)-d configuration. In fact, it corresponds to a different partition function than Z , namely one with a defect loop inserted on a certain time-slice t_0 which flips the electric flux along the loop. But we can again realize that the flux-cluster algorithm provides the solution. This is because the flux-cluster algorithm generates objects that occasionally contribute to both the numerator and denominator of (12.22). These objects are the 2-d surfaces which contain the Wilson loop under examination on the time-slice t_0 . Further, they should contribute to both traces in (12.22). Given the flux on a link, all the other link states are immediately defined from the growth rules of the cluster. The Wilson loop flips the electric flux

on the surface as it crosses the time-slice t_0 . In order to get a contribution to the numerator, it should therefore be possible to flip the flux on half of the cluster or in other words cutting the cluster along the loop on time-slice t_0 should produce two *disconnected* components. We see that clusters that grow forward and backwards from time-slice t_0 so that eventually the two sides join through the periodic fifth direction boundary cannot fall into two pieces and they will hence not contribute to the Wilson loop expectation value. Using the transfer matrix decomposition patterns we can express (12.22) as

$$\begin{aligned} \langle \hat{W}_c \rangle &= \frac{1}{Z} \text{Tr} \left[\prod_{c=1}^{N_c} \sum_{n_c=1}^{22} w_{n_c} (\hat{W}_c \mathcal{M}_{n_c}) \right] = \frac{1}{Z} \sum_{G=\{n_c\}} \text{Tr} \left[\prod_{c=1}^{N_c} w_{n_c} (\hat{W}_c \mathcal{M}_{n_c}) \right] \quad (12.23) \\ &= \frac{1}{Z} \sum_G W_G \text{Tr} [\hat{W}_c \mathcal{M}_G] = \left\langle \frac{\text{Tr} [\hat{W}_c \mathcal{M}_G]}{\text{Tr} [\mathcal{M}_G]} \right\rangle_G, \end{aligned}$$

where all the operators are inserted in the fifth direction ordered fashion. If the graph G contains N_G connected surfaces and one of them allows the Wilson loop cut, then $\text{Tr} [\mathcal{M}_G] = \text{Tr} [\hat{W}_c \mathcal{M}_G] = 2^{N_G}$ and we see that we always get the contribution 1 to (12.22). We have therefore realized an *improved estimator* for the order parameter. In the numerical simulations, after a cluster is generated we should examine all possible Wilson loop cuts on various time-slices and record which ones contribute. In this way we can collect rapidly a lot of information on Wilson loops of various sizes.

We should finally emphasize that the algorithm provides us with this improved estimator because of the flux continuation on each time-slice requirement. Only in this way the Wilson loop, which is an oriented product of raising and lowering operators, is able to match with the electric flux on the path and reverse it. Therefore the improved estimator is guaranteed to exist for any of the algorithm choices in (12.18).

12.5 The Continuous Time Algorithm

The standard approach for recovering a path-integral formulation for a field theory, given its Hamiltonian formulation, is based on the fine discretization of the time dimension and the introduction of a copy of a complete set of states at each time-slice.

The path integral weight is then recovered from the transfer matrix element between two consecutive time-slices. The expression becomes exact only as the discretization interval approaches zero. Farhi and Gutmann realized [74] that this is necessary only if the field basis is continuous. This is because the fields can fluctuate infinitesimally even in very small time intervals and we should therefore be able to include these fluctuations in the path integral. On the other hand, if the field basis is discrete the picture is different, namely a basis state evolves for finite time segments before the sporadic jump to a different state. Any path then can be reconstructed exactly from an enumerable set of data which are the initial state and the time-values when the field jumps to a different state. It was shown in [74] how to construct a measure for the finite time segments per state and the transition matrix between states so that the exact path integral is recovered.

This idea finds excellent application to the numerical simulations of quantum spin and link systems. The cluster algorithms can be implemented directly in the continuum of the Euclidean time. There are two major advantages compared to the discrete time implementations. The first is the complete elimination of the $\mathcal{O}(\epsilon)$ Trotter error of the observables in a simulation. Furthermore, no repetitive runs for various ϵ values are required in order to establish a reliable $\epsilon \rightarrow 0$ limit. The second advantage lies in the reduction of storage. Only the times of the sporadic transition for each spin need to be recorded and this constitutes a substantial decrease in the computer storage space that is required.

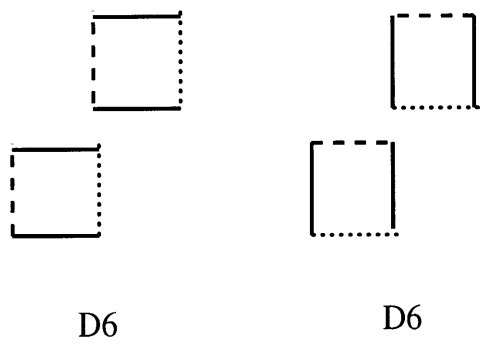
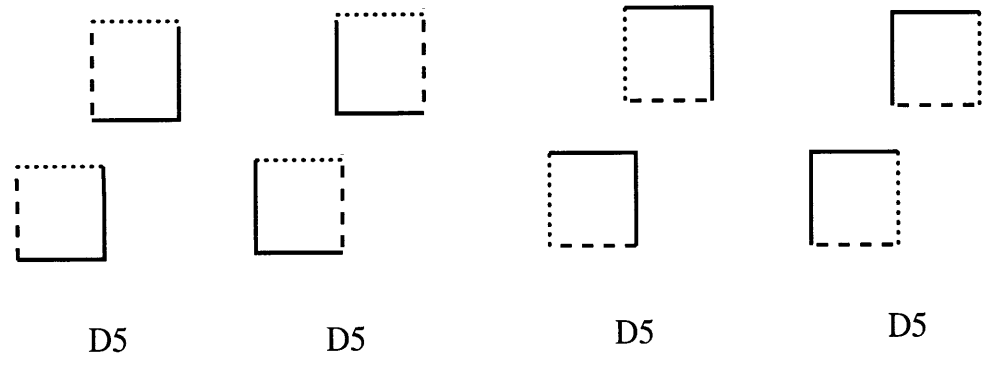
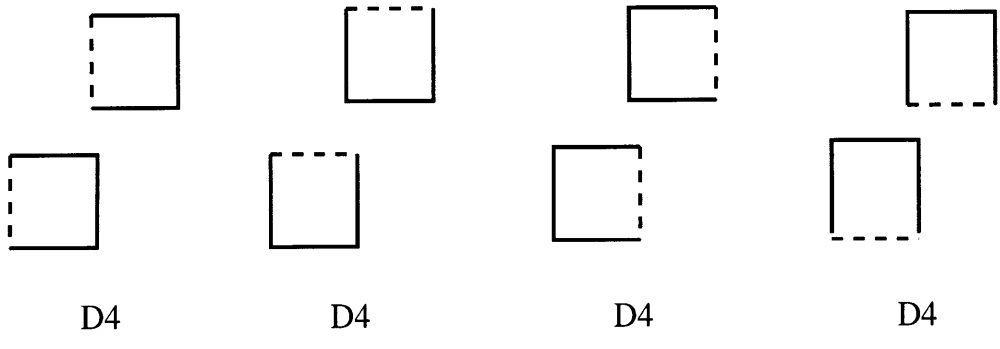
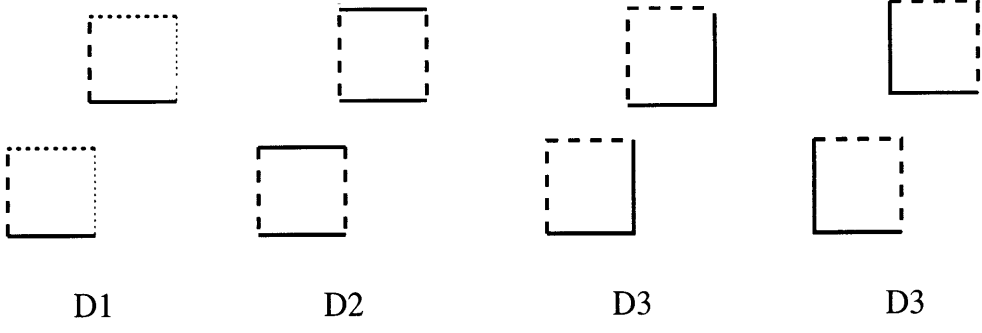
The discrete-time flux-cluster rules (12.18) indicate what should be done in the continuum. Taking $\epsilon \rightarrow 0$ we get $D_1 = 1$ which simply states that each link state evolves in time as is. The rest of the parameters are $\mathcal{O}(\epsilon)$ numbers and become uniform probability densities. Dividing by ϵ , the parameters $B_1 - B_4$ become probabilities per unit time for a plaquette with clockwise or counterclockwise flux to have a transition on any of the links it comprises. This is pictured as a new segment of the flux-cluster starting on the transition links according to the patterns $B_1 - B_4$. The parameters $D_2 - D_4$ divided by ϵ are the probabilities per unit time for a link to be joined with a neighboring link on a common plaquette. This amounts into joining an

existing cluster segment with another segment on the neighboring link at the time of the transition according to the patterns $D1 - D4$. The continuous time probability densities $\tilde{B}_1 - \tilde{B}_4$ and $\tilde{D}_2 - \tilde{D}_6$ satisfy

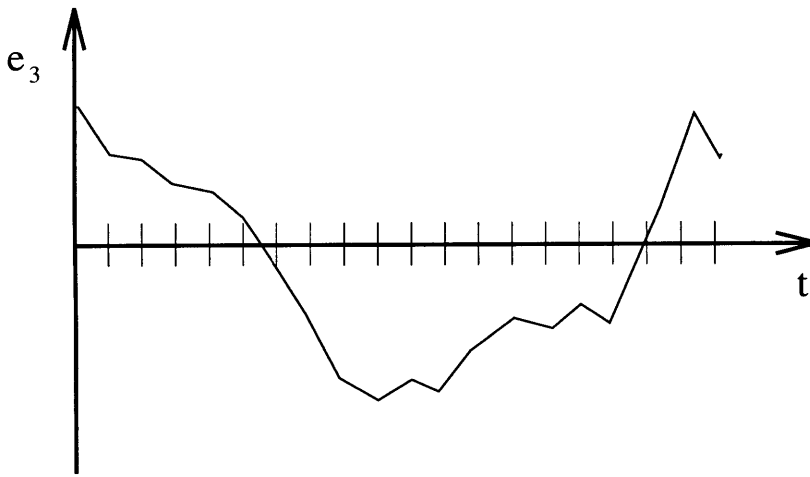
$$\begin{aligned}
\tilde{B}_1 &= \frac{J}{8} - \frac{3}{4}\tilde{D}_2 - \frac{3}{2}\tilde{D}_3 - 3\tilde{D}_4 - 2\tilde{D}_5 - \tilde{D}_6, \\
\tilde{B}_2 &= \frac{J}{8} - \frac{3}{4}\tilde{D}_2 + \frac{1}{2}\tilde{D}_3 + \tilde{D}_4 + 2\tilde{D}_5 - \tilde{D}_6, \\
\tilde{B}_3 &= \frac{J}{8} + \frac{1}{4}\tilde{D}_2 - \frac{1}{2}\tilde{D}_3 + \tilde{D}_4 + \tilde{D}_6, \\
\tilde{B}_4 &= \frac{J}{8} + \frac{1}{4}\tilde{D}_2 + \frac{1}{2}\tilde{D}_3,
\end{aligned} \tag{12.24}$$

for the allowable $\tilde{D}_2 - \tilde{D}_6$ choices.

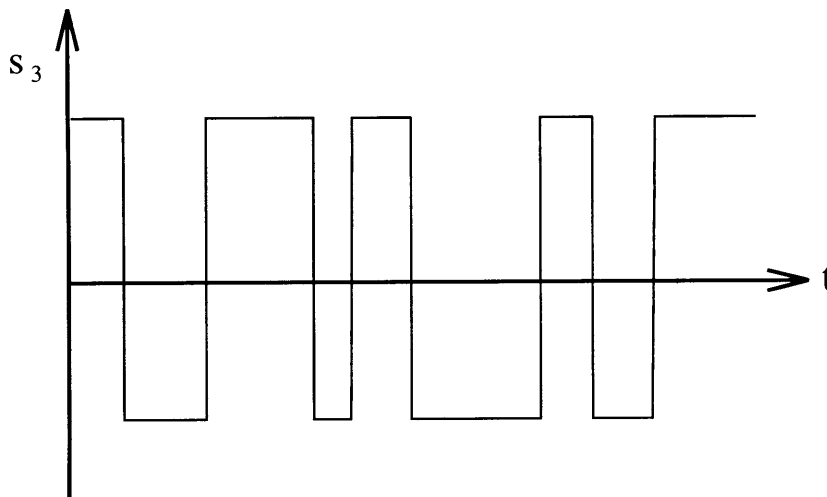
Finally we note that if the fields take values on a continuous but also compact manifold the continuous time path integral can be constructed. This is because the state space in the momentum representation is discrete. For some standard manifolds like toruses and spheres the momentum representation is known since it requires solving the Laplace problem on them. For an $O(2)$ spin or a compact $U(1)$ gauge field for example the momentum space basis is labeled by the integers. It is therefore feasible that, if cluster algorithms are found in the Hamiltonian formulation of Wilson gauge theories, they could operate in the continuum of the time coordinate. It would be expected to be advantageous, especially when the fields do not fluctuate much.



Diagonal Breakups



Path of a classical spin



Path of a quantum spin

Figure 12-1: *Typical paths for the third component of a classical spin e_3 and a quantum spin-1/2 state s_3 . The random motion of the classical spin requires time discretization while the sporadic flips of the spin-1/2 state require only the recording of the transition time.*

Chapter 13

The Winding Number

In this chapter we are going to discuss a very interesting quantity that can be defined in the $U(1)$ spin and gauge theories at finite volumes. We refer to this quantity as winding number because it turns out that it is a non-local quantity connected with the topological properties of the field configuration. In particular, it reflects the dependence of the theory in a finite volume on the boundary conditions. It requires large correlations in the theory in order to feel the effect of the boundary and therefore the winding number can be used as a probe for the existence of a massless phase. We will study the behavior of the winding number in connection with the transitions to the ordered phases of the 2-d XY model and the 4-d Abelian gauge theory. Since we also have the D -theory formulations of these models, we are going to study the winding number in the quantum spin and link models and discuss how it can be measured with the cluster algorithms.

13.1 Winding number in the XY model

Consider the classical XY model in a 2-d volume $L_1 \times L_2$. Instead of the usual periodic boundary conditions, we are going to apply the “twisted” boundary condition

$$\varphi(x_1 + L_1, x_2) = \varphi(x_1, x_2) + \theta_1, \quad \varphi(x_1, x_2 + L_2) = \varphi(x_1, x_2) + \theta_2 \quad (13.1)$$

which amounts to rotating all the spins on the boundary in direction 1 by a constant angle θ_1 and all the spins on the boundary in direction 2 by θ_2 . This is expected to change the ground state of the system since we can no longer align all spins in order to get the minimal energy solution. In order to understand qualitatively the change in the ground state energy consider the classical equation of motion

$$\partial_\mu \partial_\mu \varphi(x) = 0 \quad (13.2)$$

subject to the boundary condition (13.1). Due to the second order derivative, the field has a first order dependence in x as

$$\varphi_{cl}(x) = \frac{x_1 \theta_1}{L_1} + \frac{x_2 \theta_2}{L_2} + \text{constant} , \quad (13.3)$$

and a classical action

$$S_{\theta_\mu}[\varphi_{cl}] = \frac{1}{2g} \int_0^{L_1} dx_1 \int_0^{L_2} dx_2 (\partial_\mu \varphi_{cl})^2 = \frac{1}{2g} \int_0^{L_1} dx_1 \int_0^{L_2} dx_2 \left[\left(\frac{\theta_1}{L_1} \right)^2 + \left(\frac{\theta_2}{L_2} \right)^2 \right] \quad (13.4)$$

which for a square lattice $L_1 = L_2$ has no volume dependence

$$S_{\theta_\mu}[\varphi_{cl}] = \frac{1}{2g} \theta_\mu \theta_\mu . \quad (13.5)$$

In the saddle point approximation the partition function will be

$$Z_{\theta_\mu} \approx \exp(-S_{\theta_\mu}[\varphi_{cl}]) \approx \exp\left(-\frac{1}{2g} \theta_\mu \theta_\mu\right) . \quad (13.6)$$

Consider then the expression

$$-\frac{1}{Z_{\theta_\mu}} \sum_{\mu=1,2} \frac{d^2 Z_{\theta_\mu}}{d\theta_\mu^2} \Big|_{\theta_\mu=0} = \frac{2}{g} \quad (13.7)$$

from which the renormalized coupling g can be found. It is not realistic to measure numerically the partition function for varying twist angles θ_μ around 0. Instead,

consider the Fourier transformed partition function

$$Z_{\theta_\mu} = \sum_{W_\mu \in \mathbb{Z}} Z_{W_\mu} \exp(i\theta_\mu W_\mu) \quad (13.8)$$

where we passed to a description in terms of the integer winding number W_μ . The result (13.7) then becomes

$$-\frac{1}{Z_{\theta_\mu}} \sum_{\mu=1,2} \frac{d^2 Z_{\theta_\mu}}{d\theta_\mu^2} \Big|_{\theta_\mu=0} = \frac{\sum_{W_\mu \in \mathbb{Z}} W_\mu W_\mu Z_{W_\mu}}{\sum_{W_\mu \in \mathbb{Z}} Z_{W_\mu}} = \langle W_\mu W_\mu \rangle = \frac{2}{g} \quad (13.9)$$

from which we understand that the renormalized coupling equals the statistical average of the squared winding number — called the *helicity modulus* — measured in a simulation with untwisted boundary condition but with varying winding number. The winding number squared of a field configuration is proportional to the energy stored in the spin bonds that pass through the boundary. From the derivation (13.9) we expect that the helicity modulus is sensitive to the large correlations of the system. In fact it is an order parameter for the KT transition. At high temperatures there are short correlations and therefore the helicity modulus vanishes in the infinite volume limit. At the critical coupling the correlation length grows large and the helicity modulus obtains a non-zero value, connected to the renormalized coupling through (13.9). Everywhere in the ordered phase the average winding number has a non-zero distribution which can be qualitatively estimated from (13.6)

$$Z_{W_\mu} \approx \int d\theta_\mu \exp\left(-\frac{1}{2g}\theta_\mu\theta_\mu\right) \exp(i\theta_\mu W_\mu) \approx \exp\left(-\frac{g}{2}W_\mu W_\mu\right). \quad (13.10)$$

As argued before, it will be sharply peaked at zero for large couplings while it will become broader in the weak coupling phase.

We can now extend the study to the quantum XY model. We introduce the twisted boundary condition by rotating the quantum spin operators

$$\begin{aligned} \vec{S}_{x_1+L_1, x_2} &= \exp(i\theta_1 S_{x_1, x_2}^3) \vec{S}_{x_1, x_2} \exp(-i\theta_1 S_{x_1, x_2}^3), \\ \vec{S}_{x_1, x_2+L_2} &= \exp(i\theta_2 S_{x_1, x_2}^3) \vec{S}_{x_1, x_2} \exp(-i\theta_2 S_{x_1, x_2}^3), \end{aligned} \quad (13.11)$$

which transforms the spin raising and lowering operators on the boundary to

$$S_{L_1, x_2}^\pm \longrightarrow \exp(\pm i\theta_1) S_{L_1, x_2}^\pm, \quad S_{x_1, L_2}^\pm \longrightarrow \exp(\pm i\theta_2) S_{x_1, L_2}^\pm \quad (13.12)$$

and leaves the S^3 components invariant. The Hamiltonian of the model is therefore modified by extra phases on the spin bonds that cross the boundaries. The model is now described from the modified quantum partition function

$$Z_{\theta_\mu} = \text{Tr} \exp(-\beta H_{\theta_\mu}). \quad (13.13)$$

As we have already discussed in chapter 8, evolution in the Euclidean time extent β defines an effective (2+1)-d theory which, as long as $\beta > \beta_c$, is a free spin-wave phase with the low-energy effective action

$$S[\varphi] = \int_0^\beta dt \int_0^{L_1} dx_1 \int_0^{L_2} dx_2 \frac{\rho_s}{2} [(\partial_\mu \varphi)^2 + \frac{1}{c^2} (\partial_t \varphi)^2] \quad (13.14)$$

subject to the twisted boundary condition

$$\varphi(x_1 + L_1, x_2, t) = \varphi(x_1, x_2, t) + \theta_1, \quad \varphi(x_1, x_2 + L_2, t) = \varphi(x_1, x_2, t) + \theta_2 \quad (13.15)$$

Due to the large correlation length and as long as the dimensions L_1 and L_2 are much larger than βc , the spin-wave will dimensionally reduce to the 2-d spin-wave (13.3) described by the classical XY action with coupling

$$\frac{1}{g} = \beta \rho_s. \quad (13.16)$$

We can therefore repeat the steps (13.4) – (13.9) and connect again the helicity modulus in the quantum XY model to the renormalized coupling or spin stiffness

$$-\frac{1}{Z_{\theta_\mu}} \sum_{\mu=1,2} \frac{d^2 Z_{\theta_\mu}}{d\theta_\mu^2} \Big|_{\theta_\mu=0} = \frac{\sum_{W_\mu \in \mathbb{Z}} W_\mu W_\mu Z_{W_\mu}}{\sum_{W_\mu \in \mathbb{Z}} Z_{W_\mu}} = \langle W_\mu W_\mu \rangle = 2\beta \rho_s. \quad (13.17)$$

The helicity modulus is again an order parameter for the quantum XY model KT

phase transition. In the ordered phase the winding number is expected to have a broad distribution with a non-zero helicity modulus while it is very suppressed in the high temperature phase. The jump in the value of the helicity modulus at the KT temperature is a universal quantity of various 2-d critical theories. It determines the value of quantities like the renormalized charge, superfluid density, spin stiffness and other depending on the microscopic theory in question.

The winding number in the quantum XY model can be measured accurately with the loop-cluster algorithm. The transfer matrix for the modified bonds that touch the boundary is

$$\begin{aligned} \mathcal{T}_{\theta_\mu} = \exp \left(\epsilon J (e^{i\theta_\mu} \sigma_x^+ \sigma_{x+\hat{\mu}}^- + e^{-i\theta_\mu} \sigma_x^- \sigma_{x+\hat{\mu}}^+) \right) = \quad (13.18) \\ \mathbb{1} + (\cosh(\epsilon J) - 1)(P_x^+ P_{x+\hat{\mu}}^- + P_x^- P_{x+\hat{\mu}}^+) + \sinh(\epsilon J)(e^{i\theta_\mu} \sigma_x^+ \sigma_{x+\hat{\mu}}^- + e^{-i\theta_\mu} \sigma_x^- \sigma_{x+\hat{\mu}}^+) \end{aligned}$$

and we see that the effective plaquette interaction with weight $\sinh(\epsilon J)$ gets modified. Recall that this plaquette is always decomposed such that the loop crosses the boundary. Every time the cluster passes through the boundary we will record a θ_μ -dependent change in the plaquette energy after the flip. The quantity

$$-\frac{1}{Z_{\theta_\mu}} \frac{d^2 Z_{\theta_\mu}}{d\theta_\mu^2} \Big|_{\theta_\mu=0} \quad (13.19)$$

exactly measures the energy stored in the boundary bonds which equals the squared winding number. We see that a loop-cluster that crosses the boundary-1 W_1 times and the boundary-2 W_2 times induces after its flip a change in the winding number $\Delta W_\mu = (W_1, W_2)$. We therefore see that the loop-cluster algorithm provides a clear way to measure the winding number which can in turn be used for an accurate study of the KT phase transition in the quantum XY model [64].

13.2 Winding number in the $U(1)$ gauge theory

A winding number can be introduced in the finite volume $U(1)$ gauge theory also. Consider the theory in a volume $L_1 \times L_2 \times L_3 \times L_4$ and allow periodicity for the gauge

field $A_\mu(\mathbf{x})$ up to a gauge transformation as it passes the boundary in a transverse direction ν

$$A_\mu(\mathbf{x} + L_\nu \hat{\nu}) = A_\mu(\mathbf{x}) + \partial_\mu \Lambda^{(\nu)}(\mathbf{x}) . \quad (13.20)$$

Translating to another point by passing boundaries in ν and ρ directions in different order

$$\begin{aligned} A_\mu(\mathbf{x} + L_\nu \hat{\nu} + L_\rho \hat{\rho}) &= A_\mu(\mathbf{x} + L_\nu \hat{\nu}) + \partial_\mu \Lambda^{(\rho)}(\mathbf{x} + L_\nu \hat{\nu}) & (13.21) \\ &= A_\mu(\mathbf{x}) + \partial_\mu \Lambda^{(\nu)}(\mathbf{x}) + \partial_\mu \Lambda^{(\rho)}(\mathbf{x} + L_\nu \hat{\nu}) , \\ A_\mu(\mathbf{x} + L_\nu \hat{\nu} + L_\rho \hat{\rho}) &= A_\mu(\mathbf{x} + L_\rho \hat{\rho}) + \partial_\mu \Lambda^{(\nu)}(\mathbf{x} + L_\rho \hat{\rho}) \\ &= A_\mu(\mathbf{x}) + \partial_\mu \Lambda^{(\rho)}(\mathbf{x}) + \partial_\mu \Lambda^{(\nu)}(\mathbf{x} + L_\rho \hat{\rho}) , \end{aligned}$$

generates a constraint on $\Lambda^{(\nu)}(\mathbf{x})$

$$\partial_\mu \left[\Lambda^{(\nu)}(\mathbf{x} + L_\rho \hat{\rho}) - \Lambda^{(\nu)}(\mathbf{x}) - (\nu \leftrightarrow \rho) \right] = 0 , \quad (13.22)$$

from which we deduce the non-periodic boundary condition on the gauge transformations

$$\Lambda^{(\nu)}(\mathbf{x} + L_\rho \hat{\rho}) = \Lambda^{(\nu)}(\mathbf{x}) + \theta_{\nu\rho} , \quad (13.23)$$

with $\theta_{\nu\rho}$ an antisymmetric constant. We dropped the symmetric piece as we will see that it does not affect the physical $F_{\nu\rho}$. The smoothest transformation satisfying (13.23) for general indices is

$$\Lambda^{(\nu)}(\mathbf{x}) = \sum_\rho \frac{\theta_{\nu\rho} x_\rho}{L_\rho} \quad (13.24)$$

which implies the boundary condition on the gauge field

$$A_\mu(\mathbf{x} + L_\nu \hat{\nu}) = A_\mu(\mathbf{x}) + \partial_\mu \Lambda^{(\nu)}(\mathbf{x}) = A_\mu(\mathbf{x}) - \frac{\theta_{\mu\nu}}{L_\mu} . \quad (13.25)$$

From this we get the classical solution for the gauge field and the corresponding field strength

$$A_\mu^{cl}(x) = -\sum_\rho \frac{\theta_{\mu\rho} x_\rho}{L_\mu L_\rho}, \quad F_{\mu\nu}^{cl}(x) = (\partial_\mu A_\nu - \partial_\nu A_\mu)(x) = \frac{2\theta_{\mu\nu}}{L_\mu L_\nu}. \quad (13.26)$$

We therefore understand that introducing the non-periodic gauge transformations has the physical effect of introducing a constant background field strength in the bulk of the theory. Discretizing the bulk on a lattice with spacing a compactifies the gauge field and the gauge transformation to angles in $[0, 2\pi]$. From (13.23) we see that $\theta_{\mu\nu}$ also becomes an angle. The links in the Wilson theory obey the lattice version of (13.25)

$$u_{x+L_\nu \hat{\nu}, \mu} = u_{x, \mu} \exp\left(-ia \frac{\theta_{\mu\nu}}{L_\mu}\right) \quad (13.27)$$

which implies the minimal action plaquette

$$\vartheta_{x, \mu\nu}^{cl} = a^2 \frac{2\theta_{\mu\nu}}{L_\mu L_\nu}. \quad (13.28)$$

The physical effect remains the same. The minimal action is

$$S_{\theta_{\mu\nu}}^{cl} = \frac{1}{4g^2} \int d^4x F_{\mu\nu}^{cl} F_{\mu\nu}^{cl} = \frac{2}{g^2} \sum_{\substack{\mu < \nu \\ \mu \neq \nu \neq \rho \neq \sigma}} \theta_{\mu\nu}^2 \frac{L_\rho L_\sigma}{L_\mu L_\nu} \quad (13.29)$$

which for the lattice with $L_1 = L_2 = L_3 = L_4$ is volume independent. The semiclassical approximation to the partition function in that case is

$$Z_{\theta_{\mu\nu}} \approx \exp\left(-\frac{2}{g^2} \sum_{\mu < \nu} \theta_{\mu\nu}^2\right) \quad (13.30)$$

with the renormalized charge due to quantum effects. We can again pass to the Fourier space description with integer winding number $W_{\mu\nu}$

$$Z_{\theta_{\mu\nu}} = \sum_{W_{\mu\nu} \in \mathbb{Z}} Z_{W_{\mu\nu}} \exp(i\theta_{\mu\nu} W_{\mu\nu}) \quad (13.31)$$

and connect the renormalized charge to the helicity modulus

$$-\frac{1}{Z_{\theta_{\mu\nu}}} \sum_{\mu \neq \nu} \frac{d^2 Z_{\theta_{\mu\nu}}}{d\theta_{\mu\nu}^2} \Big|_{\theta_{\mu\nu}=0} = \frac{\sum_{W_{\mu\nu} \in \mathbb{Z}} W_{\mu\nu} W_{\mu\nu} Z_{W_{\mu\nu}}}{\sum_{W_{\mu\nu} \in \mathbb{Z}} Z_{W_{\mu\nu}}} = \langle W_{\mu\nu} W_{\mu\nu} \rangle = \frac{48}{g^2}. \quad (13.32)$$

In complete analogy to the XY model we expect the helicity modulus to be an order parameter for the 4-d Abelian lattice theory. The infinite correlation length in the Coulomb phase can feel the boundary of the system and consequently a non-zero value for the helicity modulus is to be expected. The winding number has a broad distribution in this phase which qualitatively is the Fourier transform of (13.30)

$$Z_{W_{\mu\nu}} \approx \exp \left(-\frac{g^2}{8} \sum_{\mu < \nu} W_{\mu\nu}^2 \right). \quad (13.33)$$

In the strongly coupled phase we expect the winding number to be largely suppressed and the helicity modulus to drop to zero. The value of the helicity modulus jump at the critical coupling is then expected to define the renormalized electric charge of the theory.

We can define the winding number in the quantum link formulation also. We impose the boundary condition (13.27) on the quantum links by rotating the link operators

$$U_{\mathbf{x}+L_\nu \hat{\nu}, \mu} = \exp \left(-ia \frac{\theta_{\mu\nu}}{L_\mu} S_{\mathbf{x}, \mu}^3 \right) U_{\mathbf{x}, \mu} \exp \left(ia \frac{\theta_{\mu\nu}}{L_\mu} S_{\mathbf{x}, \mu}^3 \right) \quad (13.34)$$

which therefore modifies the quantum link operators by extra phases on the boundaries of the system and consequently modifies the plaquette operators of the Hamiltonian that touch the boundaries. The modified quantum partition function

$$Z_{\theta_{\mu\nu}} = \text{Tr} \exp(-\beta H_{\theta_{\mu\nu}}) \quad (13.35)$$

is also the path integral for the evolution of the system in the fifth periodic direction with extent β . As long as $\beta > \beta_c$ the 5-d effective theory is the Abelian gauge theory

in the gauge $A_5 = 0$

$$S[A_\mu] = \int_0^\beta dx_5 \int d^4x \frac{1}{4e^2} \left[F_{\mu\nu} F_{\mu\nu} + \frac{1}{c^2} \partial_5 A_\mu \partial_5 A_\mu \right], \quad (13.36)$$

but now subject to the non-periodic boundary condition

$$A_\mu(x + L_\nu \hat{\nu}, x_5) = A_\mu(x, x_5) - \frac{\theta_{\mu\nu}}{L_\mu}. \quad (13.37)$$

Due to the infinite correlation length, dimensional reduction to 4-d is going to take place. We require $L_{1,2,3,4} \gg \beta c$ and therefore the reduced theory will be the finite volume Abelian gauge theory with the non-periodic boundary condition (13.25) and coupling

$$\frac{1}{g^2} = \frac{\beta}{e^2}. \quad (13.38)$$

We can therefore again connect the helicity modulus in the quantum link model with the effective coupling

$$-\frac{1}{Z_{\theta_{\mu\nu}}} \sum_{\mu \neq \nu} \frac{d^2 Z_{\theta_{\mu\nu}}}{d\theta_{\mu\nu}^2} \Big|_{\theta_{\mu\nu}=0} = \frac{\sum_{W_{\mu\nu} \in \mathbb{Z}} W_{\mu\nu} W_{\mu\nu} Z_{W_{\mu\nu}}}{\sum_{W_{\mu\nu} \in \mathbb{Z}} Z_{W_{\mu\nu}}} = \langle W_{\mu\nu} W_{\mu\nu} \rangle = \frac{48\beta}{e^2}. \quad (13.39)$$

The helicity modulus in the quantum link model is an order parameter for the phase transition to the Coulomb phase, which due to the dimensional reduction is the same as the Wilson theory transition. It is expected to have a universal jump with a broad winding number distribution in the Coulomb phase $\beta > \beta_c$.

The winding number in the quantum link model can be measured with the flux-cluster algorithm. The transfer matrix for the modified plaquettes is

$$\begin{aligned} \mathcal{T} &= \exp \left(\epsilon J \left[e^{i\frac{\theta_{\mu\nu}}{L_\mu}} \sigma_{x,\mu}^+ \sigma_{x+\hat{\mu},\nu}^+ \sigma_{x+\hat{\nu},\mu}^- \sigma_{x,\nu}^- + e^{-i\frac{\theta_{\mu\nu}}{L_\mu}} \sigma_{x,\mu}^- \sigma_{x+\hat{\mu},\nu}^- \sigma_{x+\hat{\nu},\mu}^+ \sigma_{x,\nu}^+ \right] \right) \quad (13.40) \\ &= \mathbb{1} + (\cosh(\epsilon J) - 1) \left(P_{x,\mu}^+ P_{x+\hat{\mu},\nu}^+ P_{x+\hat{\nu},\mu}^- P_{x,\nu}^- + P_{x,\mu}^- P_{x+\hat{\mu},\nu}^- P_{x+\hat{\nu},\mu}^+ P_{x,\nu}^+ \right) \\ &+ \sinh(\epsilon J) \left(e^{i\frac{\theta_{\mu\nu}}{L_\mu}} \sigma_{x,\mu}^+ \sigma_{x+\hat{\mu},\nu}^+ \sigma_{x+\hat{\nu},\mu}^- \sigma_{x,\nu}^- + e^{-i\frac{\theta_{\mu\nu}}{L_\mu}} \sigma_{x,\mu}^- \sigma_{x+\hat{\mu},\nu}^- \sigma_{x+\hat{\nu},\mu}^+ \sigma_{x,\nu}^+ \right), \end{aligned}$$

and we see that only the transition cubes with weight $\sinh(\epsilon J)$ get modified. In the

Trotter decomposition of chapter 12 the partition function gets modified by the extra phases. Each clockwise transition cube $(++--; --++)$ contributes $+1$ to the winding number while each counterclockwise cube $(--++; ++--)$ contributes -1 . Each plaquette of the 4-d QLM evolves in time and the net number of its clockwise minus its counterclockwise transitions is its contribution to the winding number. In order to determine the winding number $W_{\mu\nu}$ we examine a plaquette in the $(\mu\nu)$ plane that touches the boundary and measure the net number of its transitions as it evolves in the fifth direction. We further examine all the translations of this plaquette in the two transverse directions and the total net number of transitions is the winding number $W_{\mu\nu}$. Due to the gauge symmetry, this number is the same for any plaquette in the $(\mu\nu)$ plane. This is because the phase modifications on the boundary can become equal phase modifications on any plaquette in the $(\mu\nu)$ plane using appropriate gauge transformations. This is reflected in eq.(13.26) where a uniform background field appeared due to the modified boundary conditions. We see that the winding number is a clear and easy quantity to measure directly on a QLM configuration.

In the $j = 1/2$ (3+1)-d and (4+1)-d QLM simulations it turns out that the winding number is not updated efficiently. The algorithm is exploring a part of the phase space with the winding number staying practically fixed for all the Monte Carlo updates. It is unfortunate that we cannot learn anything about the phases of the QLM through the helicity modulus which has been proved very useful for the quantum XY phase transition. Nevertheless, in a higher representation QLM simulation it would still be a very prominent probe for the phase structure of the theory.

Chapter 14

Simulations of the U(1) Quantum Link Model

14.1 Local Observables

We have run extensive simulations of the $j = 1/2$ *QLM* in (3+1)-d and (4+1)-d. The reason we are interested in the (3+1)-d theory also is that this model should dimensionally reduce to the 3-d Abelian lattice theory which is confining at all couplings. This model should not possess any phase transition and it is instructive to look for the qualitative differences of various observables between three and four dimensions. We used the continuous time flux-cluster algorithm and we studied the behavior of the cluster size per volume along with local observables like the energy density and the specific heat of the model looking for a singular behavior.

In figures (14-1) and (14-2) we present the behavior of the cluster area per volume for the (4+1)-d and (3+1)-d *QLM*. In the spin models we can prove that the cluster size is connected to the squared magnetization of the system and is therefore a physical quantity which shows a singular behavior at the critical point. We have not managed to connect the cluster area in the *QLM* with a physical quantity but we nevertheless find these graphs very interesting and possibly indicating a connection with the correlation length in the models. The (4+1)-d *QLM* cluster area seems to have a transition at $\beta \approx 0.65$ from a small finite value to a value that increases with

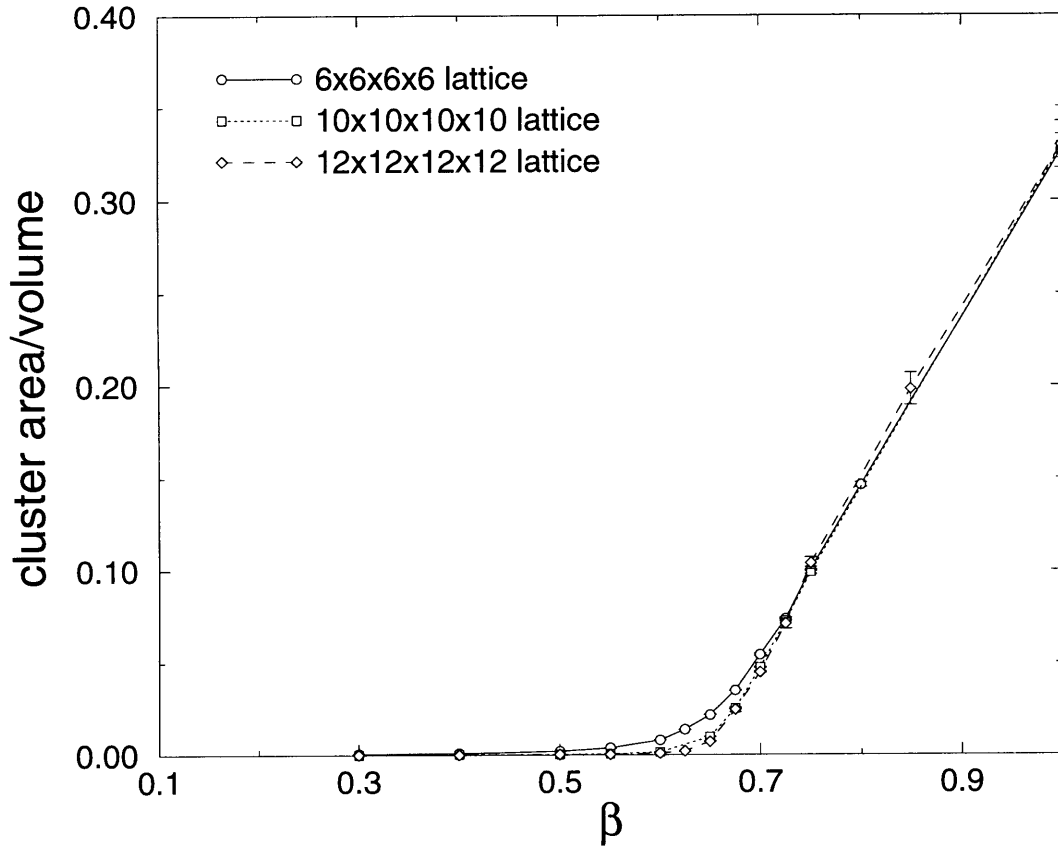


Figure 14-1: *Cluster area per 5-d volume in the (4+1)-d U(1) quantum link model.*

the volume. If the cluster area is connected to the correlation length, this indicates an infinite correlation length above $\beta \approx 0.65$ and therefore a Coulomb phase. The (3+1)-d *QLM* cluster area is plotted in the same scale and does not seem to increase with the volume but instead stays finite for all couplings. The fact that the cluster area becomes also large here is a finite volume effect and will go away as long as the correlation length can fit in the volume.

The energy density of the system is

$$\mathcal{E} = \frac{1}{VZ} \text{Tr} [H \exp(-\beta H)] = -\frac{1}{VZ} \frac{\partial Z}{\partial \beta}, \quad (14.1)$$

where $V = \beta L_1 L_2 L_3 L_4$ is the 5-d volume of the theory. After the Suzuki-Trotter

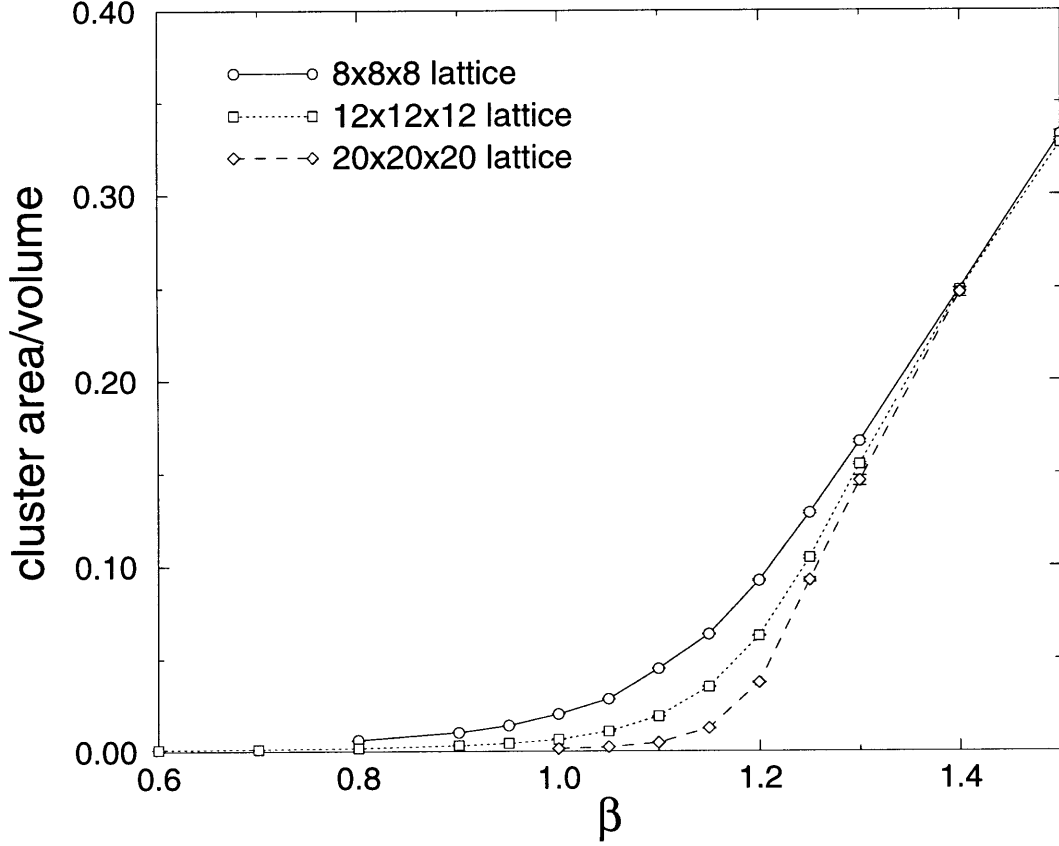


Figure 14-2: Cluster area per 4-d volume in the (3+1)-d $U(1)$ quantum link model.

decomposition, the 5-d effective action is written in terms of cubic interactions

$$Z = \prod_{\mathbf{x}, \mu, t} \sum_{e_{\mathbf{x}, \mu, t} = \pm \frac{1}{2}} \exp(-S[e]). \quad (14.2)$$

A 5-d configuration has N_1 cubes with weight $e^{-S_1} = \cosh(\epsilon J)$, N_2 cubes with weight $e^{-S_2} = \sinh(\epsilon J)$, N_3 cubes with weight $e^{-S_3} = 1$ and action $S = N_1 S_1 + N_2 S_2$. From this we find

$$\begin{aligned} \mathcal{E} &= -\frac{1}{VZ} \prod_{\mathbf{x}, \mu, t} \sum_{e_{\mathbf{x}, \mu, t} = \pm \frac{1}{2}} \frac{\partial e^{-S}}{\partial \beta} = \frac{1}{VZ} \prod_{\mathbf{x}, \mu, t} \sum_{e_{\mathbf{x}, \mu, t} = \pm \frac{1}{2}} \frac{\partial S}{\partial \beta} e^{-S} \\ &= \frac{1}{V} \sum_{i=1}^2 \left\langle N_i \frac{\partial S_i}{\partial \beta} \right\rangle = -\frac{1}{V} \left[\frac{\epsilon J}{\beta} \tanh(\epsilon J) \langle N_1 \rangle + \frac{\epsilon J}{\beta} \coth(\epsilon J) \langle N_2 \rangle \right], \end{aligned} \quad (14.3)$$

which is easy to measure with the discrete time algorithm from the Monte Carlo averages of cubes with non-trivial weight. The continuum limit of the energy density is taken as $\epsilon \rightarrow 0$

$$\mathcal{E} = -\frac{1}{\beta V} \langle N_2 \rangle, \quad (14.4)$$

and the continuous time algorithm measures the energy density by averaging the number of transition plaquettes. In figures (14-3) and (14-4) we present measurements of the energy density of the *QLM*. Examination of the energy histograms for various volumes for the (4+1)-d *QLM* has not revealed any signal of a phase transition. The explosion of the cluster area at $\beta \approx 0.65$ is not escorted by a critical behavior in the energy or the higher moments of the energy examined.

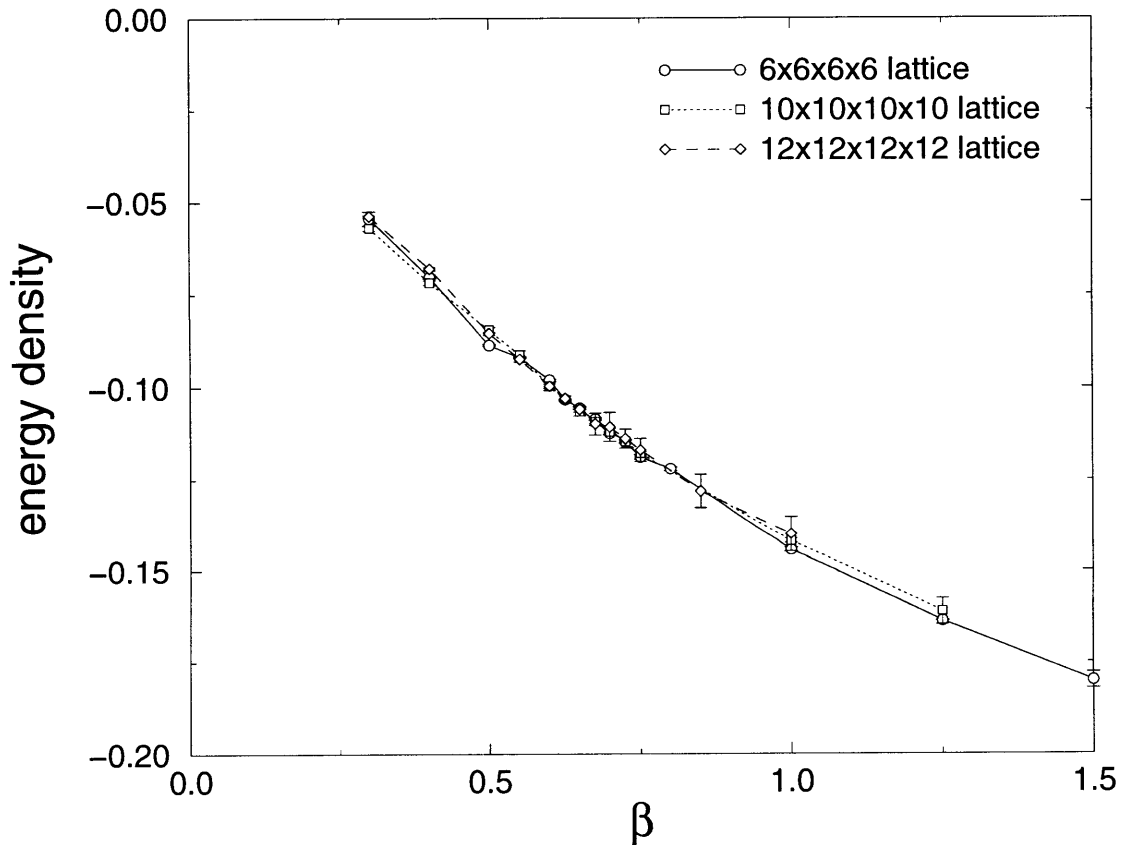


Figure 14-3: *Energy density of the (4+1)-d U(1) quantum link model.*

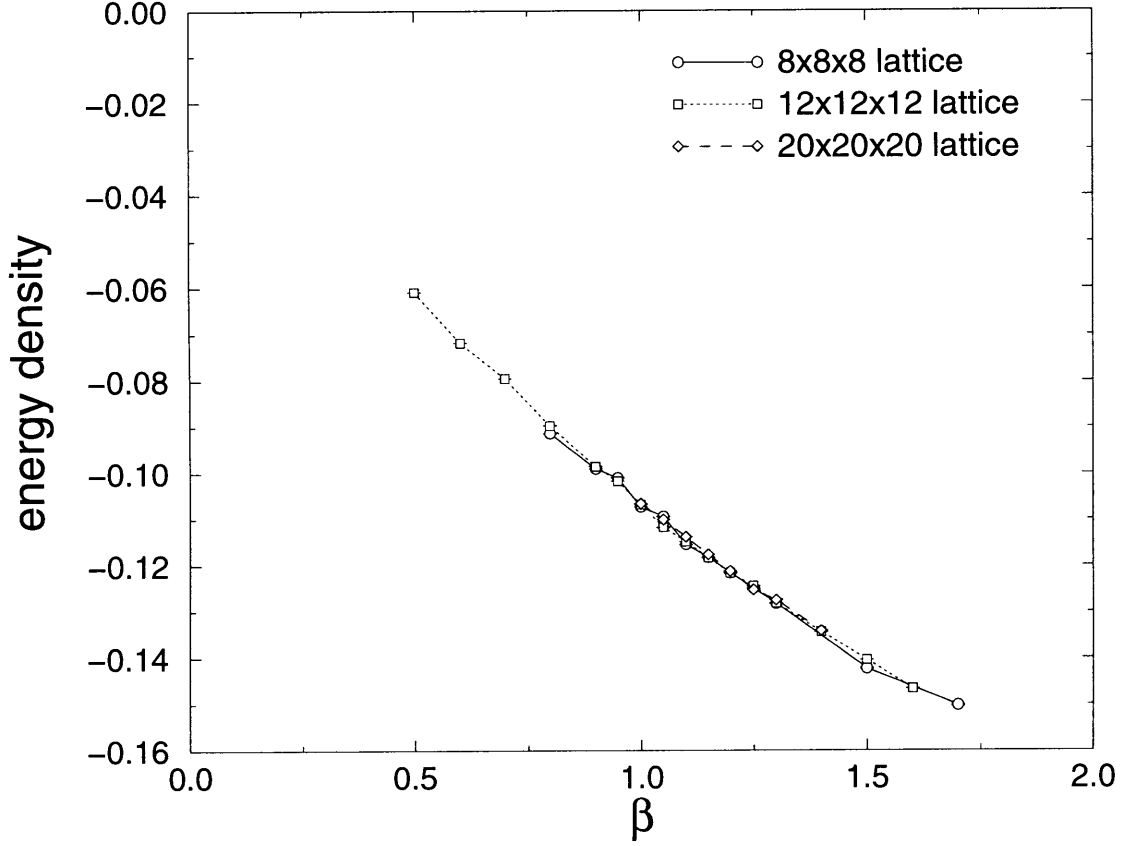


Figure 14-4: *Energy density of the (3+1)-d U(1) quantum link model.*

The specific heat of the system can be derived similarly

$$c = \frac{\partial \mathcal{E}}{\partial T} = -\beta^2 \frac{\partial \mathcal{E}}{\partial \beta} = \frac{\beta^2}{V} \frac{\partial}{\partial \beta} \left(\frac{1}{Z} \frac{\partial Z}{\partial \beta} \right) = \frac{\beta^2}{V} \left[\frac{1}{Z} \frac{\partial^2 Z}{\partial \beta^2} - \left(\frac{1}{Z} \frac{\partial Z}{\partial \beta} \right)^2 \right]. \quad (14.5)$$

Using (14.2) and (14.1) we find the discrete time formula

$$\begin{aligned} c &= \frac{\beta^2}{VZ} \prod_{\mathbf{x}, \mu, t} \sum_{e_{\mathbf{x}, \mu, t} = \pm \frac{1}{2}} \frac{\partial^2}{\partial \beta^2} e^{-S} - \beta^2 \mathcal{E}^2 V \\ &= \frac{\beta^2}{VZ} \prod_{\mathbf{x}, \mu, t} \sum_{e_{\mathbf{x}, \mu, t} = \pm \frac{1}{2}} \left[\left(\frac{\partial S}{\partial \beta} \right)^2 - \frac{\partial^2 S}{\partial \beta^2} \right] e^{-S} - \beta^2 \mathcal{E}^2 V \\ &= \frac{\beta^2}{V} \left\langle \left(\frac{\partial S}{\partial \beta} \right)^2 - \frac{\partial^2 S}{\partial \beta^2} \right\rangle - \beta^2 \mathcal{E}^2 V \end{aligned} \quad (14.6)$$

$$\begin{aligned}
&= \frac{(\epsilon J)^2}{V} \left\{ \left(\langle N_1^2 \rangle - \langle N_1 \rangle^2 \right) \tanh^2(\epsilon J) + \left(\langle N_2^2 \rangle - \langle N_2 \rangle^2 \right) \coth^2(\epsilon J) \right. \\
&\quad \left. + 2 \left(\langle N_1 N_2 \rangle - \langle N_1 \rangle \langle N_2 \rangle \right) + \langle N_1 \rangle \frac{1}{\cosh^2(\epsilon J)} - \langle N_2 \rangle \frac{1}{\sinh^2(\epsilon J)} \right\}.
\end{aligned}$$

The continuous time limit of this expression is

$$C = \frac{1}{V} \left[\langle N_2^2 \rangle - \langle N_2 \rangle^2 - \langle N_2 \rangle \right], \quad (14.7)$$

and therefore the continuous time algorithm evaluates easily the specific heat from the average number of transitions and its variance. We observed that the specific heat has strong fluctuations and does not give useful information about a critical point in the theory.

14.2 Higgsing the U(1) Theory

It is interesting to examine a modification of the *QLM* where the gauge symmetry is broken. Typically in order to break the gauge symmetry we employ the Higgs mechanism which minimally couples the gauge fields to the Higgs scalars and forces the symmetry breaking through a quartic potential. The result is a mass term for the gauge bosons and therefore short correlation lengths in the theory. In order to break the $U(1)$ symmetry we consider first the minimal coupling of the classical $U(1)$ links to a classical Higgs complex scalar. We then select the unitary gauge which eliminates the Higgs field from the action and quantize the links resulting in the Higgsed $U(1)$ Hamiltonian

$$H = -J \sum_P (U_P + U_P^\dagger) - \frac{\kappa}{2} \sum_{x,\mu} (U_{x,\mu} + U_{x,\mu}^\dagger). \quad (14.8)$$

Notice that the charge conjugation $U_{x,\mu} \leftrightarrow U_{x,\mu}^\dagger$ is still a symmetry of the theory. At $\kappa = 0$ the theory is expected to have the confining and the Coulomb phase separated at some critical β . At positive κ we expect a line of transitions to extent in the $\beta - \kappa$ plane separating the confining from the Coulomb phase. At large enough κ the Higgs phase should appear with short correlation length corresponding to a massive

photon. Expanding the classical link $u_{x,\mu} \sim \exp(iA_\mu(x))$ we estimate the photon mass as $m = \sqrt{\kappa}$. A line of transitions will separate the Higgs from the Coulomb phase at finite κ for any β above the critical value. The confining and the Higgs phases are analytically connected.

The model (14.8) is easy to simulate with the flux-cluster algorithm we already have. In the $j = 1/2$ *QLM* the breaking term is $\kappa\sigma_{x,\mu}^1$ and is therefore a flux flipping operator on each link. We perform the Suzuki–Trotter decomposition by introducing an extra time-slice for the breaking term. The transfer matrix for the breaking term assigns an $\mathcal{O}(\epsilon\kappa)$ probability to each link to flip its state when it passes to the next time-slice. In the flux-cluster algorithm this assigns an $\mathcal{O}(\epsilon\kappa)$ probability for each link of the cluster to terminate its propagation in fifth-time when it is in the special time-slice. The $U(1)$ breaking interaction can be easily incorporated in the continuous time flux cluster algorithm also. Here each link propagates for finite time intervals and is assigned the $\mathcal{O}(\kappa)$ probability per unit time to flip uniformly in the $[0, \beta)$ interval.

We have simulated this model in (4+1)-d at small volumes 4^4 and 6^4 with the discrete time algorithm. We simulated at β between 1.0 – 3.0 (we always set $J=1$) and various κ from 0.01 up to 5.0. We measure the cluster size and the energy of the system due to the gauge invariant plaquette term and the breaking term separately. In this β range without the breaking term the cluster size is very large. As the breaking term is turned on, the cluster size decreases very fast. This is what we expect physically. Although we have not succeeded to connect the large cluster size with an infinite correlation length, in the Higgs phase where the correlation length is definitely short the cluster size should definitely be short also. Indeed, at $\kappa \sim 1 - 2$ the cluster size has dropped substantially indicating a massive photon in the theory. Also the energy of the system is transferred from the plaquette term to the breaking term and at $\kappa \sim 1 - 2$ the breaking term already dominates the system.

In our preliminary study we have not observed signals of a phase transition in the energy of the model as we vary κ . Typically it is seen that Higgs phases are separated from Coulomb phases with first order transitions. We instead see a crossover from the Higgs phase to the strongly coupled phase of the model. While we cannot exclude that

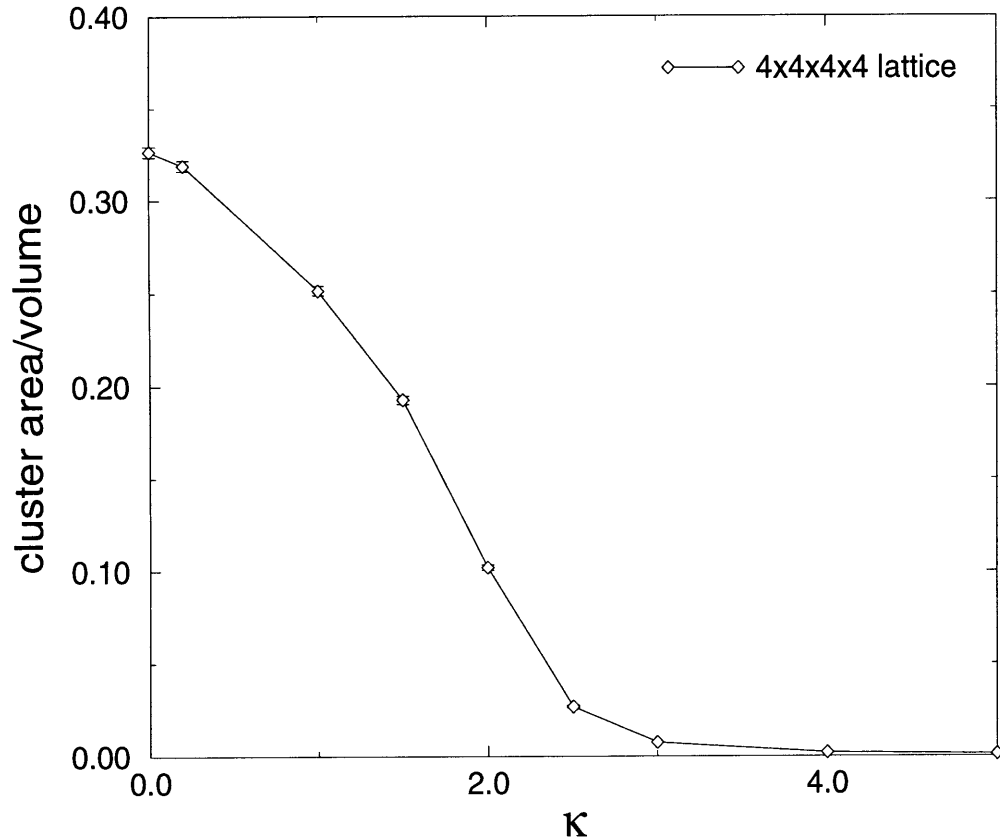


Figure 14-5: *Cluster area per 5-d volume in the Higgsed (4+1)-d U(1) quantum link model at $\beta = 1.0$. The cluster area decreases fast with the Higgs parameter κ since the correlation length becomes short.*

a high-statistics study of the Higgsed model at large volumes might reveal the phase transition to a Coulomb phase, it does not seem very plausible with the results we already have. This may be due to the inability of the algorithm to move efficiently in the phase space, thus hiding the true dynamics of the model in the region of couplings explored.

14.3 Final Comments

In this work we have presented a new non-perturbative formulation for gauge theories which follows the general framework of D -theory. We showed that by quantizing a

classical spin or gauge theory in d dimensions we may obtain the dynamics of the original theory formulated with classical fields. This is possible if the $(d+1)$ -dimensional theory has massless excitations. The extra dimension in that case becomes insignificant compared to the correlation length of the theory. The collective excitations of the discrete variables build the classical fields which after dimensional reduction interact through the original classical theory. In that sense, we saw that the 2-d quantum Heisenberg antiferromagnetic magnons at low temperatures describe the physics of the 2-d $O(3)$ non-linear σ -model fields at weak coupling while the KT phase transition of the 2-d $O(2)$ model can be studied via the critical point of the 2-d quantum XY model. We utilized the Coulomb phases of 5-d Abelian and non-Abelian gauge theories to show that quantum link formulations of gauge theories also exist.

A discrete variable formulation is not simply an academic matter. The loop-cluster algorithm can be constructed for the quantum spin models resulting in very efficient simulations. An extra advantage due to the discreteness of the variables is that we can implement the algorithms directly in continuous time. We showed how a flux-cluster algorithm naturally exists for the spin-1/2 Abelian QLM . Further, the algorithm provides an improved estimator for the Wilson loop which is the order parameter of the theory. This alone is a major improvement compared to the traditional local algorithms applied to the study of gauge theories. It is very plausible that the flux-cluster algorithm can be generalized in non-Abelian quantum link models also.

The simulations have not identified with certainty a critical point in the $(4+1)$ -d model. The cluster area presents a qualitatively different behavior between $(3+1)$ -d and $(4+1)$ -d which would point to a phase transition to a Coulomb phase at $\beta \approx 0.65$ if a connection between the cluster area and the correlation length really exists. We have not been able to establish this connection. The energy of the model, on the other hand, and higher moments of it do not show any signal of a phase transition in this region of couplings. All we learn from strong coupling expansions is that the critical β is above 0.5, but this does not exclude that the model might not have a phase transition at all.

The Wilson loops in our simulations do not indicate a phase transition also. Al-

though the clusters become large above $\beta \approx 0.65$, we have found that most of the clusters do not contribute to the Wilson loop improved estimator. In fact, even at large β the clusters that contribute to the improved estimator have small area and the Wilson loops are therefore also small. This behavior is consistent with an area law and therefore confinement at all couplings *if* the algorithm is moving efficiently in the phase space. The algorithm we used becomes *de facto* inefficient for β above ~ 2 because the clusters fill the volume. Therefore we cannot conclude anything from our study about the model beyond $\beta \sim 2$.

The winding number is a very interesting topological quantity that can be defined and measured for both classical and quantum Abelian spin and link theories. In the quantum spin model it has proved an excellent probe for the KT phase transition. Unfortunately, the same is not true in the quantum link model with spin $1/2$. The flux-cluster algorithm does not update the winding number efficiently and we cannot learn anything from it. Maybe this is pointing to a general inefficiency of the algorithm. In any case the general algorithm has a large parameter space. Different choices of algorithms in this space will in general result in different efficiencies. It is certainly an interesting direction for future studies.

Another interesting direction for the understanding of the Abelian QLM is to study the model at a higher representation. Already at spin-1 the model presents an interesting qualitative difference from spin- $1/2$. A spin-1 quantum link contains spin-0 besides the ± 1 states and therefore it is possible to construct a state with zero flux everywhere. This is encouraging because the classical ground state of the Wilson theory also has zero flux everywhere. In the spin- $1/2$ quantization on the other hand this is not possible and this could be a reason for the presence of frustration in the system which eventually alters the expected behavior. The spin-1 quantization appears as a more reasonable truncation of the electric flux space and deserves investigation. The cluster algorithms can be extended to higher spin quantizations. The method for spin- j is to introduce $2j$ spin- $1/2$ states on each site/link and enforce the projection to the spin- j states. The transfer matrix appears as a sum of interactions between various spin- $1/2$ quantum spins and therefore cluster rules can again be found. The

update is the flipping of the spin-1/2 states that belong to the cluster. A continuous time loop-cluster algorithm for the general spin 2-d Heisenberg quantum antiferromagnet has already been constructed and it is clear that the same can be achieved for the Abelian QLM .

In summary, a lot of experience has been gained from the numerical investigations of the spin-1/2 Abelian QLM with the flux-cluster algorithm. Based on this experience and the new tools that have become available the long standing problems of lattice gauge theory can be attacked.

Appendix A

An Ultralocal Perfect Action in One Dimension

The expression for the perfect free massive propagator in 1-d

$$\Delta(p; m) = \sum_{l \in \mathbb{Z}} \frac{1}{(p + 2\pi l)^2 + m^2} \frac{4 \sin^2(p/2)}{(p + 2\pi l)^2} + \alpha \quad (\text{A.1})$$

with $p \in] - \pi, \pi]$ can be computed analytically using the formula

$$\sum_{l \in \mathbb{Z}} F(l) = - \sum_{\{z_i\}} \text{Residua of } \left\{ \pi \cot(\pi z) F(z) \right\}_{z_i} \quad (\text{A.2})$$

where $\{z_i\}$ are the poles of the function $F(z)$ in the complex plane with the requirement that none of the poles is in \mathbb{Z} . This formula is valid if $F(z)$ vanishes as $|z| \rightarrow \infty$. A complex contour integration of $\pi \cot(\pi z) F(z)$ around the boundary of the complex plane will vanish and therefore the sum of the residua of the poles in the plane will be zero. A straightforward computation of the residua of $\pi \cot(\pi z) F(z)$ at the first order poles of $\cot(\pi z)$ which are all in \mathbb{Z} verifies (A.2).

Define

$$F(z) = \frac{1}{(p/2\pi + z)^2 + (m/2\pi)^2} \frac{1}{(p/2\pi + z)^2} \quad (\text{A.3})$$

which has the second order pole $z_0 = -p/2\pi$ and the first order poles $z_1 = -p/2\pi + im/2\pi$ and $\bar{z}_1 = -p/2\pi - im/2\pi$.

The residua at the poles are

$$\begin{aligned}
R(z_0) &\equiv \text{Residue of } \left\{ \cot(\pi z) F(z) \right\}_{z_0} = \frac{d}{dz} \left[\frac{\cot(\pi z)(z - z_0)^2}{(z - z_0)^2(z - z_1)(z - \bar{z}_1)} \right]_{z=z_0} \quad (\text{A.4}) \\
&= -\frac{\pi}{\sin^2(\pi z_0)} \frac{1}{(z_0 - z_1)(z_0 - \bar{z}_1)} - \frac{\cot(\pi z_0)}{(z_0 - z_1)^2(z_0 - \bar{z}_1)} - \frac{\cot(\pi z_0)}{(z_0 - z_1)(z_0 - \bar{z}_1)^2} \\
&= -\frac{4\pi^3}{m^2} \frac{1}{\sin^2(p/2)}
\end{aligned}$$

$$\begin{aligned}
R(z_1) &\equiv \text{Residue of } \left\{ \cot(\pi z) F(z) \right\}_{z_1} = \left[\frac{\cot(\pi z)(z - z_1)}{(z - z_0)^2(z - z_1)(z - \bar{z}_1)} \right]_{z=z_1} \quad (\text{A.5}) \\
&= i \frac{4\pi^3}{m^3} \cot(-p/2 + im/2)
\end{aligned}$$

$$\begin{aligned}
R(\bar{z}_1) &\equiv \text{Residue of } \left\{ \cot(\pi z) F(z) \right\}_{\bar{z}_1} = \left[\frac{\cot(\pi z)(z - \bar{z}_1)}{(z - z_0)^2(z - z_1)(z - \bar{z}_1)} \right]_{z=\bar{z}_1} \quad (\text{A.6}) \\
&= -i \frac{4\pi^3}{m^3} \cot(-p/2 - im/2)
\end{aligned}$$

and from these after some trigonometric algebra we get

$$\begin{aligned}
\sum_{l \in \mathbb{Z}} F(l) &= -\pi [R(z_0) + R(z_1) + R(\bar{z}_1)] \quad (\text{A.7}) \\
&= \frac{4\pi^4}{m^2} \frac{1}{\sin^2(p/2)} - \frac{4\pi^4}{m^3} \frac{\sinh m}{\sin^2(p/2) + \sinh^2(m/2)}.
\end{aligned}$$

The propagator is

$$\begin{aligned}
\Delta(p; m) &= \frac{4 \sin^2(p/2)}{16\pi^4} \sum_{l \in \mathbb{Z}} F(l) + \alpha \quad (\text{A.8}) \\
&= \frac{1}{m^2} - \frac{\sinh m}{m^3} + \frac{8 \sinh^3(m/2) \cosh(m/2)}{m^3 [4 \sin^2(p/2) + 4 \sinh^2(m/2)]} + \alpha.
\end{aligned}$$

We can ultralocalize the 1-d perfect propagator to the standard nearest-neighbor

propagator if we choose the RG transformation parameter

$$\alpha = \frac{\sinh m}{m^3} - \frac{1}{m^2}. \quad (\text{A.9})$$

We also learn that the standard propagator $[4 \sin^2(p/2) + \mu^2]^{-1}$ can become a perfect propagator in 1-d with the physical mass m given from $2 \sinh(m/2) = \mu$ and the wave-function renormalization factor $8 \sinh^3(m/2) \cosh(m/2)/m^3$. At the limit $m \rightarrow 0$ we get $\alpha = 1/6$ in agreement with the value in [14] that optimizes also the 2-d FP action. We noticed also that formula (A.2) cannot be applied successively to perform the higher-dimensional summations. The structure of the poles is such that the second summation residua reintroduce the infinite summations.

Bibliography

Books in lattice gauge theory

- M. Creutz, *Quarks, Gluons and Lattices*, Cambridge University Press, 1983.
- H. J. Rothe, *Lattice Gauge Theories, An Introduction*, World Scientific, 1992.
- I. Montvay and G. Münster, *Quantum Fields on a Lattice*, Cambridge University Press, 1994.

- [1] A. M. Polyakov, Phys. Lett. 59B (1975) 79.
- [2] M. Peskin and D. Schroeder, *An Introduction to Quantum Field Theory*, Addison-Wesley, 1995.
- [3] N. D. Mermin and H. Wagner, Phys. Rev. Lett. 17 (1966) 1133;
S. Coleman, Commun. Math. Phys. 31 (1973) 259.
- [4] T. Bell and K. Wilson, Phys. Rev. B11 (1975) 3431.
- [5] K. Pohlmeyer, Comm. Math. Phys. 46 (1976) 207;
M. Lüscher and K. Pohlmeyer, Nucl. Phys. B137 (1978) 46.
- [6] A. B. Zamolodchikov and Al. B. Zamolodchikov, Ann. Phys. 120 (1979) 253.
- [7] P. Hasenfratz, M. Maggiore and F. Niedermayer, Phys. Lett. B245 (1990) 522;
P. Hasenfratz and F. Niedermayer, Phys. Lett. B245 (1990) 529.
- [8] S. Coleman, *Aspects of Symmetry*, Cambridge University Press, 1985.

- [9] H. Flyvbjerg, Phys. Lett. B219 (1989) 323;
H. Flyvbjerg and S. Varsted, Nucl. Phys. B344 (1990) 646;
H. Flyvbjerg and F. Larsen, Phys. Lett. B266 (1991) 92;
H. Flyvbjerg, Nucl. Phys. B348 (1991) 714.
- [10] K. Symanzik, Nucl. Phys. B226 (1983) 187, 205.
- [11] M. Lüscher and P. Weisz, Comm. Math. Phys. 97 (1985) 59.
- [12] K. Wilson and J. Kogut, Phys. Rep. C12 (1974) 75;
K. Wilson, Rev. Mod. Phys. 47 (1975)773; *ibid.* 55 (1983) 583
- [13] K. Wilson, *in* Recent developments of gauge theories, ed. G.'t Hooft et al.
(Plenum, New York,1980).
- [14] P. Hasenfratz and F. Niedermayer, Nucl. Phys. B414 (1994) 785.
- [15] M. Lüscher, P. Weisz and U. Wolff, Nucl. Phys. B359 (1991) 221.
- [16] M. Lüscher, Phys. Lett. B118 (1982) 391.
- [17] M. Lüscher, hep-ph/9711205.
- [18] R. Sommer, hep-ph/9711243.
- [19] LATTICE 96 Proceedings, Nucl. Phys. B (Proc. Suppl.) 53 (1997).
- [20] LATTICE 97 Proceedings, Nucl. Phys. B (Proc. Suppl.) 63 (1998).
- [21] M. D'Elia, F. Farchioni and A. Papa, Nucl. Phys. B456 (1995) 313.
- [22] M. Blatter, R. Burkhalter, P. Hasenfratz and F. Niedermayer, Phys. Rev. D53
(1996) 923.
- [23] U. Wolff, Phys. Rev. Lett. 62 (1989) 361.
- [24] F. Niedermayer, Phys. Rev. Lett. 61 (1988) 2026.
- [25] A. Tsapalis and U.-J. Wiese, Nucl. Phys. B (Proc. Suppl.) 53 (1997) 948.

- [26] W. Bietenholz and U.-J. Wiese, Nucl. Phys. B464 (1996) 319.
- [27] A. Gottlob, M. Hasenbusch and K. Pinn, Phys. Rev. D54 (1996) 1736.
- [28] S. Caracciolo, A. Montanari and A. Pelissetto, Nucl. Phys. B (Proc. Suppl.) 63 (1998) 916.
- [29] F. Niedermayer, Nucl. Phys. B (Proc. Suppl.) 53 (1997) 56.
- [30] P. Hasenfratz, Nucl. Phys. B (Proc. Suppl.) 63 (1998) 53.
- [31] U.-J. Wiese, Phys. Lett. B315 (1993) 417.
- [32] W. Bietenholz and U.-J. Wiese, Phys. Lett. B378 (1996) 222.
- [33] W. Bietenholz, R. Brower, S. Chandrasekharan and U.-J. Wiese, Nucl. Phys. B (Proc. Suppl.) 53 (1997) 921.
- [34] N. Metropolis, A. Rosenbluth, M. Rosenbluth, A. Teller and E. Teller, J. Chem. Phys. 21 (1953) 1087.
- [35] R. Swendsen and J.-S. Wang, Phys. Rev. Lett. 58 (1987) 86.
- [36] P. Kasteleyn and C. Fortuin, J. Phys. Soc. Jpn. Suppl. 26s (1969) 11;
C. Fortuin and P. Kasteleyn, Physica (Utrecht) 57 (1972) 536.
- [37] U. Wolff, Nucl. Phys. B334 (1990) 581.
- [38] M. Greven et al., Phys. Rev. Lett. 72 (1994) 1096; Z. Phys. B96 (1995) 465.
- [39] T. Barnes, Int. J. Mod. Phys. C2 (1991) 659.
- [40] U.-J. Wiese and H.-P. Ying, Z. Phys. B93 (1994) 147.
- [41] B. B. Beard and U.-J. Wiese, Phys. Rev. Lett. 77 (1996) 5130.
- [42] P. Hasenfratz and H. Leutwyler, Nucl. Phys. B343 (1990) 241.
- [43] P. Hasenfratz and F. Niedermayer, Phys. Lett. B268 (1991) 231.

- [44] K. Nakajima et al., Z. Phys. B96 (1995) 479.
- [45] S. Chakravarty, B. I. Halperin and D. R. Nelson, Phys. Rev. B39 (1989) 2344.
- [46] B. B. Beard, R. J. Birgeneau, M. Greven and U.-J. Wiese, Phys. Rev. Lett. 80 (1998) 1742.
- [47] S. Caracciolo et al., Phys. Rev. Lett. 75 (1995) 1891.
- [48] J. K. Kim, Phys. Rev. Lett. 70 (1993) 1735; Phys. Rev. D50 (1994) 4663.
- [49] G.'t Hooft in High energy physics, ed. A. Zichichi (Editorie Compositori, Bologna, 1976).
- [50] S. Mandelstam, Phys. Rep. 23C (1976) 245.
- [51] N. Seiberg and E. Witten, Nucl. Phys. B426 (1994) 19; Nucl. Phys. B431 (1994) 484.
- [52] K. Wilson, Phys. Rev. D10 (1974) 2445.
- [53] Y. Shamir, Nucl. Phys. B406 (1993) 90.
- [54] D. B. Kaplan, Phys. Lett. B288 (1992) 342.
- [55] V. Furman and Y. Shamir, Nucl. Phys. 439 (1995) 54.
- [56] S. Chandrasekharan and U.-J. Wiese, Nucl. Phys. B492 (1997) 455.
- [57] R. Brower, S. Chandrasekharan and U.-J. Wiese, hep-th/9704106.
- [58] P. Orland and D. Rohrlich, Nucl. Phys. B338 (1990) 647.
- [59] A. M. Polyakov, *Gauge Fields and Strings*, 1987.
- [60] M. Creutz, Phys. Rev. Lett. 43 (1979) 553.
- [61] B. B. Beard, R. Brower, S. Chandrasekharan, D. Chen, A. Tsapalis and U.-J. Wiese, Nucl. Phys. B (Proc. Suppl.) 63 (1998) 775.

- [62] J. M. Kosterlitz and D. J. Thouless, *J. Phys. C*6 (1973) 1181.
- [63] H.-Q. Ding and M. S. Makivić, *Phys. Rev. B*42 (1990) 6827.
- [64] K. Harada and N. Kawashima, *cond-mat/9702081*.
- [65] A. Guth, *Phys. Rev. D*21 (1980) 2291.
- [66] T. Banks, J. Kogut and R. Myerson, *Nucl. Phys. B*129 (1977) 493.
- [67] L. Polley and U.-J. Wiese, *Nucl. Phys. B*356 (1991) 629.
- [68] A.M. Polyakov, *Phys. Lett. B*59 (1975) 82.
- [69] M. Göpfert and G. Mack, *Commun. Math. Phys.* 82 (1982) 545.
- [70] D. Horn, *Phys. Lett.* 100B (1981) 149.
- [71] K. Osterwalder and E. Seiler, *Ann. Phys. (N.Y.)* 110 (1978) 440.
- [72] H. G. Evertz, G. Lana and M. Marcu, *Phys. Rev. Lett.* 70 (1993).
- [73] R. Brower, S. Chandrasekharan and U.-J. Wiese, *cond-mat/9801003*.
- [74] E. Farhi and S. Gutmann, *Ann. Phys.* 213 (1992) 182.